Spring 5-15-2023

Development of Myelin in Wolfram Syndrome

Olga Reine Neyman

WASHINGTON UNIVERSITY IN ST. LOUIS

Division of Biology and Biomedical Sciences
Neurosciences

Dissertation Examination Committee:
Tamara Hershey, Chair
Deanna Barch
Nico Dosenbach
Joshua Shimony
Fumihiko Urano

Development of Myelin in Wolfram Syndrome

by
Olga Reine Neyman

A dissertation presented to
Washington University in St. Louis
in partial fulfillment of the
requirements for the degree
of Doctor of Philosophy

May 2023
St. Louis, Missouri

Table of Contents

List of Figures

List of Tables

Acknowledgments

I would like to thank everyone who has made my time at Washington University School of Medicine as great as it has been, along with everyone who has helped me get here. I would particularly like to thank my mentor, Tamara Hershey, for incredible guidance and support throughout my years as a graduate student. Thank you for teaching me how to approach science and for all your pearls of wisdom related not just to my project, buy my career and life in general. I would like to thank my thesis committee, Deanna Barch, Joshua Shimony, Nico Dosenbach, and Fumihiko Urano for always being available to talk and help steer me down more productive paths.

I could have not finished this work without all the support and assistance I received from my fellow lab members and all the wonderful people at the NIL. I also owe my sanity to my friends who have always had my back with pep talks, commiseration, and plans for adventures. Finally, I would like to thank my parents who taught me the value of hard work and curiosity and have always done everything they could to help me achieve my dreams.

Olga Reine Neyman

Washington University in St. Louis

May 2023

ABSTRACT OF THE DISSERTATION

Development of Myelin in Wolfram Syndrome

By

Olga Neyman

Doctor of Philosophy in Biology and Biomedical Sciences

Neurosciences

Washington University in St. Louis, 2023

Professor Tamara Hershey, Chair

Wolfram syndrome is a rare, autosomal recessive disease traditionally characterized by juvenile onset insulin dependent diabetes, optic atrophy, deafness, and neurodegeneration often beginning in childhood and adolescence. The disease is caused by mutations in *WFS1*, which encodes for the protein wolframin and is associated with endoplasmic (ER) stress-mediated apoptosis. ER stress-related dysfunction may inhibit production of myelin during neurodevelopment in Wolfram syndrome, as active and developing oligodendrocytes are more vulnerable to ER stress than mature ones. It is known that white matter tracts are compromised in the disease, but many questions related to the vulnerability of myelin and its impact on the disease remain. Here we characterize the developmental trajectory of myelin in both white and gray matter and examine how differences in myelin in Wolfram syndrome correlate to disease presentation. We also examine a novel mouse model of the disease to see how well any myelin pathology in the model mirrors what is seen in humans.

The human studies determined that a decreased rate of myelination in Wolfram syndrome as compared to controls throughout most of the brain, with a divergence in myelin integrity in early adulthood. However, tracts associated with visual processing were clearly hypomyelinated in early childhood followed by a normal rate of increased myelination over age. On the other hand, gray matter myelin was found to be largely conserved in the disease. Symptom severity was correlated to whole brain white matter myelin integrity markers in the brain, but lacked specificity, i.e. visual acuity was not correlated with markers in the optic radiations. The mouse model analysis found some differences in myelin integrity in regions such as the optic tracts, but was overall found to not be a sufficiently good model of the neuronal phenotype on Wolfram syndrome.

Together, these studies confirm the strong involvement of white matter integrity in the pathology of the disease. They suggest a regionally specific pattern of vulnerability in the timing and rate of myelin development, and a broad relationship between the level of myelin integrity and severity of disease. These findings are crucial for the betterment of our understanding of this severe disease and will facilitate the identification of therapeutic targets and biomarkers to evaluate the efficacy of potential treatments.

Chapter 1: Introduction

1.1 Overview of Dissertation

Wolfram syndrome in a rare genetic disease which generally presents with optic atrophy, insulin-dependent diabetes, diabetes insipidus, and deafness, and can be accompanied by numerous other neurological symptoms. One of the most pronounced aspects of the Wolfram phenotype is either the dysmyelination within the brain. While the involvement of myelin is easily discernible through clinical radiology, the extent and progression of this involvement has not been well characterized, and will thus be the focus of this dissertation.

After an introduction covering the basics of the disease, myelin development, and how it may be studied, the dissertation examines the development of myelin in white matter tracts in Wolfram syndrome using state-of-the art diffusion tensor imaging analysis. The goals of this analysis are to describe the progression of the involvement of myelin and discern any regional differences in development. This chapter also explores how any differences in myelin integrity in Wolfram syndrome correlates to the severity of symptoms expressed.

Myelin is known to be impacted in white matter tracts in Wolfram, but myelin is also present in gray matter, albeit to a smaller degree. The next chapter thus explores whether myelin in the gray matter is also implicated in the disease. In order to do so, a technique called myelin mapping was applied. As this methodology provides a myelin index for the entire brain, myelin integrity in subcortical regions was also explored.

In order to develop a better understanding of the impact of Wolfram on a brain on a cellular level, animal models need to be used. To this time, no sufficiently translatable animal model, particularly for the neurophenotype of the disease, has been universally adopted. We complete this work by examining myelin and volumetric differences in an exon 5 knockout model to see how accurately it replicates the human phenotype.

1.2 Overview of Wolfram Syndrome `

Wolfram syndrome is a rare, autosomal recessive disease traditionally characterized by early-onset diabetes mellitus (DM), diabetes insipidus (DI), optic atrophy (OA) and sensorineural hearing loss (D), giving it the historic name DIDMOAD. After the finding of its causative genes (Inoue et al., 1998), the presentation of the disease was found to be more complex. Only two-third of patients will ultimately develop all symptoms of the classical presentation, but many will also develop a number of other neurologic abnormalities including bladder and bowel dysfunction, temperature dysregulation, gait abnormalities, loss of the senses of smell and taste, and psychiatric concerns (Samara et al., 2019).

The presentation and progression of Wolfram syndrome has proven to be complex, with a large degree of variability among patients. A seminal study of 45 patients in the UK provided a framework for the natural history of the disease. On average, the first symptom to be noticed was insulin-deficient diabetes mellitus (median age 6), followed by optic atrophy (median age 11), diabetes insipidus (second decade), sensorineural deafness (second decade), and renal abnormalities (third decade). Neurological abnormalities such as cerebellar ataxia and myoclonus were reported to appear in the fourth decade, and the median age for death was 30, ranging from 25-49, usually from central respiratory failure driven by brainstem atrophy (Barrett et al., 1995). However, neurological abnormalities have since been shown to present significantly earlier, with a different study bringing the median age for neurologic symptoms down to 15, observed as cerebellar ataxia, dysarthria, dysphagia, nystagmus, or peripheral neuropathy (Chaussenot et al., 2011), and life expectancy was found to be previously underestimated. The

median age of a specialized service for those with Wolfram syndrome in England was 37 years old, with their oldest patient being 62 years (Eljamel et al., 2019).

While optic atrophy and insulin-dependent diabetes are nearly universal symptoms, central diabetes insipidus affects approximately 70% of patients while sensorineural deafness affects 65%. Most patients (60-90%) will develop urinary tract problems such as obstruction of ducts between the kidneys and bladder, high capacity atonal bladder, disrupted urination, bladder sphincter dyssynergia, or difficulty in controlling low of urine. 60% of patients report neurological manifestations, with ataxia being the most common concern (Urano, 2016).

Numerous studies have looked more in depth at particular aspects of the disease presentation. For instance, studies of gait of patients with Wolfram showed that patients walk slower, take shorter and wider steps, and spend prolonged time in double support, even at early ages (Pickett, Duncan, Hoekel, et al., 2012). Deficits were found to be related to anticipatory transitions, postural responses, and sensory orientation subcomponents (Pickett, Duncan, Paciorkowski, et al., 2012). Explorations of optic deficits have described color vision deficits in 94%, visual field defects in 100%, optic disk pallor in 94%, abnormally large optic nerve cup:disk ratio in 33%, thinned RNFL in 100%, afferent pupillary defects in 61%, cataracts in 22%, nystagmus in 39%, and strabismus in 39% of subjects (Hoekel et al., 2014). A sleep study found that 29% of adult patients and 100% of young pediatric patients has obstructive sleep apnea (Licis, Davis, Eisenstein, Lugar, & Hershey, 2019). Olfactory problems have also been found to be prevalent (Bischoff et al., 2015), with deficits in smell identification rather than olfactory sensitivity. On the other hand, intensity of taste is decreased with conserved perception (Alfaro et al., 2020). A quarter of patients in a different study were found to have severe psychiatric symptoms that led to either suicidal attempts or psychiatric hospitalizations (Swift,

Perkins, Chase, Sadler, & Swift, 1991). Other commonly reported symptoms include headaches, hypogonadism, hyponatremia, and autotomic dysfunction including impaired thermoregulation, orthostatic hypotension, constipation and fecal impaction, diarrhea, and excessive sweating (Urano, 2016).

A few postmortem histopathological case studies of Wolfram syndrome have been reported in the literature. Most report on the atrophy of the hypothalamic nucleic and degeneration of the optic nerves, chiasm, and tract, along with the degeneration of the pons and cerebellum (Carson, Slager, & Steinberg, 1977; Genís, Dávalos, Molins, & Ferrer, 1997; Hilson, Merchant, Adams, & Joseph, 2009; Shannon, Becker, & Deck, 1999). More specifically, neurons in the paraventricular and supraoptic nuclei of the hypothalamus were decreased, along with. neurohypophyseal tissue in the pituitary gland. Loss of retinal ganglion neurons and lateral geniculate nuclei were found, along with loss of myelinated axons in the optic nerve, chiasm, and tract, and atrophy of the superior colliculus (Hilson et al., 2009). One study specifies that loss of neurons in the lateral geniculate nuclei mainly affected the small cell layers (Genís et al., 1997). Loss of fibers in the cochlear nerve, and loss of neurons in the cochlear nuclei and inferior colliculus, and atrophy of the stria vascularis were also found (Genís et al., 1997; Hilson et al., 2009). Other findings included decreased volume and loss of neurons in the pontine base and inferior olivary nucleus. Axonal dystrophy with axonal swellings were found in the optic radiations, hippocampal fornices, pontocerebellar tracts, and deep cerebral white matter (Shannon et al., 1999).

Brain imaging has allowed for the study of larger groups of patients at varied levels of disease severity along with following their progression. For the clinician, a multitude of

abnormalities are easily discernible on the MRI of a brain with Wolfram syndrome, particularly atrophy of the brainstem, cerebellum, middle cerebellar peduncle, optic tract and optic nerve and a lack of a posterior pituitary bright spot on a T1 (Barrett, Bundey, & Macleod, 1995; Ganie et al., 2011; Gocmen & Guler, 2014; Hadidy, Jarrah, Al-Till, El-Shanti, & Ajlouni, 2004; Ito, Sakakibara, & Hattori, 2007). Other abnormalities reported include cerebral atrophy, signal intensity changes in FLAIR (fluid attenuation inversion recovery) or T2 images of the periventricular white matter, ventral pons, and substania nigra as well as empty sella (Chaussenot et al., 2011; Samara et al., 2019).

The Washington University Wolfram Research Clinic has gathered the most comprehensible neuroimaging data on Wolfram syndrome on a longitudinal cohort of children and young adults. Patients with Wolfram syndrome were found to have smaller intracranial volumes overall, with smaller volumes of the brainstem (particularly the pons), gray matter in the cerebellum, white matter in the cerebellum, total cortical white matter, and total subcortical gray matter (Hershey et al., 2012; Lugar et al., 2016). Closer examination showed that cortical thickness was notably lower in the pre-central, lingual, and rostral middle frontal regions, as well as in the primary and secondary visual cortex. On the other hand, increased thickness and volumes were found in the primary and secondary auditory cortex and temporal lobe (Hershey et al., 2012; Lugar et al., 2016). An examination of the longitudinal volumetric changes in the brains showed atypical decreases in the brainstem – particularly in the ventral pons – thalamus, and cerebellar cortex. Cortical white matter volumes showed a lower rate of increase as compared to controls in select regions like the optic radiations (Lugar et al., 2019). Diffusion tensor imaging was used to study white matter integrity. Initial findings demonstrated decreased fractional anisotropy (FA) and mean diffusion (MD) in the cerebellum and optic radiations

(Hershey et al., 2012), while a more detailed analysis showed differences to be more diffuse, with decreased FA and increased radial diffusion (RD) in the optic radiations inferior fronto-occipital fasciculus, middle cerebellar peduncle, and acoustic radiations. Increased RD alone was found in the corpus callosum and decreased FA alone was found in the corticospinal tract (Lugar et al., 2016).

The disease is primarily caused by mutations in the *WFS1* gene which codes for the protein wolframin. Mutations have been described throughout the coding sequence of the gene, without obvious clustering in particular locations. Loss-of-function mutations, including stop, frame-shift, and splice site mutations, are common. Just over a third of mutations were missense mutations (Hofmann, Philbrook, Gerbitz, & Bauer, 2003). A small number of cases are caused by mutations in the *CISD2* gene, leading to Wolfram syndrome type 2. The latter is also characterized by optic atrophy and diabetes mellitus, but also presents with peptic ulcer disease defective platelet aggregation (Amr et al., 2007). In the following chapters, we will be largely focused on disease stemming from the *WFS1* mutation.

Wolframin is located primarily in the endoplasmic reticulum (Takeda et al., 2001). It is expressed throughout the body, with the highest levels found in the brain, pancreas, and heart, and muscle (Hofmann et al., 2003; West et al., 2014; Yu, Yu, Wang, Gao, & Chen, 2010). It is a transmembrane protein (Strom, 1998), which is associated with the regulation of intracellular calcium homeostasis, with increased levels of expression causing increased cytosolic calcium levels (Osman et al., 2003) by increasing the rate of calcium uptake (Takei et al., 2006). Wolframin has been found, at least in rats, to be a calmodulin binding protein, with mutations to

protein causing impaired binding of calmodulin, suggesting wolframin plays a role in a calcium signal transduction system (Yurimoto et al., 2009).

A study of the role of wolframin in pancreatic β cells found that downregulation of wolframin caused a decrease in β cell proliferation rate and altered morphological features, including a stellate appearance (McBain & Morgan, 2003). The defect in cell proliferation may explain the childhood onset of insulin dependent diabetes, rather than a natal onset. Further studies showed impaired stimulus-secretion coupling in β cells and a lower increase in cytosolic calcium upon stimulation with glucose (Ishihara et al., 2004). Ishihara also showed WFS1-deficient cells were more susceptible to apoptosis.

It has been suggested that wolframin also plays a role during pregnancy, with increased expression in the placenta during the first trimester of the pregnancy and moderate level during the third, suggesting that wolframin is needed to maintain normal levels of cytotrophoblast cell proliferation (Lucariello et al., 2014). This same study also looked at how expression changes in pregnant women with diabetes and found lower levels of expression during the third trimester, suggesting woframin also assists in physiologic glucose hemostasis in the placenta.

A primary hypothesized etiology for the symptoms of Wolfram syndrome has been increased endoplasmic reticular (ER) stress. Wolframin has been shown to negatively regulate ER stress by forming a stress-mediated complex with activating transcription factor 6α (ATF6α), which suppresses its activity. It also helps degrade regulates a key transcription factor involved in ER stress signaling, activating transcription factor 6α (ATF6α), through the ubiquitin-proteasome pathway (Fonseca et al., 2010). Without the ability to keep ER stress under control, cells are more vulnerable to apoptosis. The vulnerability to ER stress has also been seen in non-rodent animal models. Knocking down the Drosophila homolog of WFS1 has been shown to

cause increased susceptibility to oxidative stress-, excitotoxicity-, or tauopathy-induced behavioral deficits and neurodegeneration (Sakakibara, Sekiya, Fujisaki, Quan, & Iijima, 2018).

Mitochondrial dysfunction has also been hypothesized as a cause for Wolfram syndrome. Cagalinec et al. show that the downregulation of *WFS1* triggers ER stress associated with inositol 1,4,5-trisphosphate receptor dysfunction and thus altered intracellular calcium homeostasis. Higher cytosolic calcium was found at rest, but a lower maximal level was found under stimulated conditions. Altered calcium homeostasis was then found to cause the dysregulation of mitochondrial dynamics in neurons. The mitochondria were found to have altered fusion and fission rates as compared to wildtype mitochondria, and underwent mitophagy more frequently. PINK1 and Parkin proteins were suggested to involved in the mechanism explaining the link between *WFS1* Deficiency-related ER stress and impaired mitochondrial dynamics (Cagalinec et al., 2016).

1.3 Myelin and Oligodendrocytes

Concentric layers of myelin surround axons like insulation on a wire. Myelin's best known function is the facilitation of conduction along the axon, though myelin also plays a role in plasticity (Monje, 2018). Oligodendrocytes are responsible for myelin generation in the central nervous system, with each oligodendrocyte extending numerous processes to neighboring axon segments (Baumann & Pham-Dinh, 2001). Their progenitor cells are known as oligodendrocyte precursor cells (OPCs). OPCs first arise from the ventricular germinal zones of the embryonic neural tube and migrate to different areas of the brain before differentiating into oligodendrocytes (Bergles & Richardson, 2016). OPCs remain present into adulthood.

OPCs begin to differentiate into oligodendrocytes prenatally. In humans, myelination of the spinal cord occurs through the second half of gestation (Baumann & Pham-Dinh, 2001), though most myelination occurs during the first year of life (Snaidero & Simons, 2014). Myelination proceeds in a caudorostral direction in the brain, and rostralcaudually in the spinal cord. Motor roots are the first to be myelinated, followed by sensory, superior cerebellar peduncle, and optic radiations (Baumann & Pham-Dinh, 2001). Associative areas continue myelinating the longest, into the second decade of life.

1.4 Imaging Myelin

Most neuroimaging of myelin microstructure has taken advantage of diffusion tensor imaging (DTI). DTI estimates the rate and direction of the diffusion of water in the brain to draw conclusions about the architecture of axonal fibers and myelin (P. J. Basser, Mattiello, & LeBihan, 1994; Peter J Basser & Pierpaoli, 1996; Mori & Zhang, 2006). In standard DTI, diffusion within a voxel is modeled as an ellipsoid characterized by eigenvectors. The volume of this ellipsoid is defined at the mean diffusion (MD). Axial diffusion (AD) measures the diffusion along the long axis of the ellipsoid and represents diffusion along the axon. The eigenvectors orthogonal to the AD represent the radial diffusion (RD), or diffusion perpendicular to the axon. Fractional anisotropy (FA) describes the eccentricity of the ellipsoid. In a healthy, myelinated axon, water is expected to diffuse most readily along the length of the axon. One would thus expect a high AD, high FA, and low RD (Mori & Zhang, 2006).

Animal and histological studies have shown how these diffusion parameters changes with axonal and myelin injury. Decreases in AD correspond to axial degeneration, as fragmentation of the axon impedes water movement (Budde, Xie, Cross, & Song, 2009). Increases in RD correlate

with dysmyelination, as water is able to more easily diffuse perpendicularly without the protective sheath (Song et al., 2002).

Nevertheless, diffusion parameters do not always accurately and specifically reflect expected pathologies. Cuprizone mouse models have been well established for the study of demyelination (Torkildsen, Brunborg, Myhr, & Bø, 2008). Zhang et al. reported inconsistencies between *in vivo* and *ex vivo* imaging, with the former causing misleading diffusion anisotropy measurements (Zhang, Jones, McMahon, Mori, & Calabresi, 2012). Differences in AD have also been found to be more sensitive to acute axonal injury rather axonal atrophy that may be found in chronic injury (Aung, Mar, & Benzinger, 2013). Factors such as cell infiltration and partial volume effects can impact interpretation of diffusion parameters. It must be remembered that diffusion parameters describe just that – the diffusion of water, and do not allow for a precise view of how microstructures such as cytoskeletal lattices of neurofilaments and microtubules, axonal membranes, and myelin are directly influencing it (Beaulieu, 2009).

Numerous approaches have been taken to improve upon the results that can be gathered from DTI. The quality of the data itself has improved, due to the use of stronger MRI machines, collection more directions, improved standards for acceptable movement, and movement correction approaches.

Researchers have also developed more complicated diffusion models that expand on the original tensor model and provide new parameters to better characterize myelin microstructure. A few examples of these models include diffusion kurtosis imaging (DKI) (Arab, Wojna-Pelczar, Khairnar, Szabó, & Ruda-Kucerova, 2018), high angular resolution diffusion imaging (HARDI) (Özarslan & Mareci, 2003), generalized q-sampling imaging (GQI) (Jin et al., 2019), q-ball imaging (QBI) (Tuch, 2004), neurite orientation dispersion and density imaging (NODDI)

(Deligianni et al., 2016), and diffusion basis spectrum imaging (DBSI) (Cross & Song, 2017). Notably more advanced sequence protocols are required for the application of these models as compared to rudimentary DTI. DBSI is expanded on below due to the relevance for future chapters.

DBSI models the diffusion-weighted signal through a linear combination of multiple discrete anisotropic tensors and a spectrum of isotropic tensors (Cross & Song, 2017; X. Wang et al., 2014; Y. Wang et al., 2015, 2011). The component of the signal described by the anisotropic tensor is defined as the fiber fraction (FF). The anisotropy is further characterized as in standard DTI, providing values of MD, RD, AD, and FA. The isotropic components are subdivided into restricted and non-restricted components. Restricted diffusion is defined by an apparent diffusivity under 0.3 $\mu m^2/ms$. The amount of signal described by this level of diffusion is referred to as the restricted fraction (RF). This restricted diffusion has been shown to correlate with resident and infiltrating cellularity. The non-restricted component is defined by apparent diffusivity greater than 0.3 $\mu m^2/ms$., and also has a corresponding non-restricted fraction to quantify its prevalence in the signal. This component has been interpreted as extracellular space excluding cellularity. Occasionally, the non-restricted component is further divided into hindered fraction and water fraction, with the latter corresponding to larger values of the apparent diffusivity than the former. By adding these extra parameters, DBSI is better able to resolve effects of cellularity, from inflammation or otherwise, and vasogenic edema. The model also handles partial volume effects from cerebrospinal fluid and crossing fibers better than traditional DTI methods (Y. Wang et al., 2015).

Several tactics for estimating myelin content more directly, rather than relying on the diffusion of water, have been developed. These tactics can be categorized as methods utilizing

the magnetization transfer effect, myelin water imaging, susceptibility mapping, and relating the magnetic resonance (MR) signal to cortical myelination (Heath, Hurley, Johansen-Berg, & Sampaio-Baptista, 2018).

Magnetization transfer imaging assumes that most of the macromolecular content in the CNS is myelin (Brochet & Dousset, 1999). The concept relies on the fact that the MR signal from protons bound to large macromolecules in the body decays too quickly to be measured by conventional MR imaging (Grossman, Gomori, Ramer, Lexa, & Schnall, 1994). Resonant frequencies can be used to saturate the bound protons, but not those of the free water. This energy is then transferred to free water molecules as the system equilibrates, which attenuates the water signal that would be measured through standard MR imaging.

Myelin water fraction utilizes the concept that the T2 decay time depends upon its local environment. (Alonso-Ortiz, Levesque, & Pike, 2015; MacKay & Laule, 2016; Mackay et al., 1994). Water trapped within the layers of myelin has a significantly lower decay time than intra or extracellular water. When decay is plotted against signal amplitude, distinct distributions depending on the source of the water are observed. Myelin water fraction is thus the fraction of the signal from the myelin water distribution over the total water signal.

Susceptibility mapping relies on tissues having different magnetic susceptibility that influences the local signal magnitude and phase (Heath et al., 2018). Diamagnetic regions cause spins to precess at a lower frequency than paramagnetic regions. Tissues with different susceptibility values will have different accrual of phase, which can be detected with specialized sequences. Increased myelination has been found to correlate decreased susceptibility (more diamagnetic).

The above three categories of methods require specialized sequences for use. However, it has also been found that the ratio of a T1w image to T2w creates a topography that accurately follows the spatial distribution of myelin in the brain. The technique is known as myelin mapping (Glasser, Goyal, Preuss, Raichle, & Van Essen, 2014; Glasser & Van Essen, 2011).

1.5 References

Alfaro, R., Doty, T., Narayanan, A., Lugar, H., Hershey, T., & Pepino, M. Y. (2020). Taste and smell function in Wolfram syndrome. *Orphanet Journal of Rare Diseases*, *15*(1). https://doi.org/10.1186/s13023-020-1335-7

Alonso-Ortiz, E., Levesque, I. R., & Pike, G. B. (2015). MRI-based myelin water imaging: A technical review. *Magnetic Resonance in Medicine*, *73*(1), 70–81. https://doi.org/10.1002/mrm.25198

Amr, S., Heisey, C., Zhang, M., Xia, X. J., Shows, K. H., Ajlouni, K., … Shiang, R. (2007). A homozygous mutation in a novel zinc-finger protein, ERIS, is responsible for Wolfram syndrome 2. *American Journal of Human Genetics*, *81*(4), 673–683. https://doi.org/10.1086/520961

Arab, A., Wojna-Pelczar, A., Khairnar, A., Szabó, N., & Ruda-Kucerova, J. (2018, May 1). Principles of diffusion kurtosis imaging and its role in early diagnosis of neurodegenerative disorders. *Brain Research Bulletin*, Vol. 139, pp. 91–98. https://doi.org/10.1016/j.brainresbull.2018.01.015

Aung, W. Y., Mar, S., & Benzinger, T. L. (2013). Diffusion tensor MRI as a biomarker in axonal

and myelin damage. *Imaging in Medicine*, *5*(5), 427–440. https://doi.org/10.2217/iim.13.49

Barrett, T. ., Bundey, S. ., & Macleod, A. . (1995). Neurodegeneration and diabetes: UK nationwide study of Wolfram (DIDMOAD) syndrome. *The Lancet*, *346*(8988), 1458–1463. https://doi.org/10.1016/S0140-6736(95)92473-6

Basser, P. J., Mattiello, J., & LeBihan, D. (1994). MR diffusion tensor spectroscopy and imaging. *Biophysical Journal*, *66*(1), 259–267. https://doi.org/10.1016/S0006-3495(94)80775-1

Basser, Peter J, & Pierpaoli, C. (1996). Microstructural and Physiological Features of Tissues Elucidated by Quantitative-Diffusion-Tensor MRI. In *JOURNAL OF MAGNETIC RESONANCE, Series B* (Vol. 111).

Baumann, N., & Pham-Dinh, D. (2001). Biology of oligodendrocyte and myelin in the mammalian central nervous system. *Physiological Reviews*, Vol. 81, pp. 871–927. https://doi.org/10.1152/physrev.2001.81.2.871

Beaulieu, C. (2009). The biological basis of diffusion anisotropy. In *Diffusion MRI* (pp. 105–126). https://doi.org/10.1016/B978-0-12-374709-9.00006-7

Bergles, D. E., & Richardson, W. D. (2016). Oligodendrocyte development and plasticity. *Cold Spring Harbor Perspectives in Biology*, *8*(2). https://doi.org/10.1101/cshperspect.a020453

Bischoff, A. N., Reiersen, A. M., Buttlaire, A., Al-lozi, A., Doty, T., Marshall, B. A., … Washington University Wolfram Syndrome Research Group. (2015). Selective cognitive and psychiatric manifestations in Wolfram Syndrome. *Orphanet Journal of Rare Diseases*, *10*(1), 66. https://doi.org/10.1186/s13023-015-0282-1

Brochet, B., & Dousset, V. (1999). Pathological correlates of magnetization transfer imaging abnormalities in animal models and humans with multiple sclerosis. *Neurology*, *53*(SUPPL. 3). Retrieved from https://pubmed.ncbi.nlm.nih.gov/10496205/

Budde, M. D., Xie, M., Cross, A. H., & Song, S. K. (2009). Axial diffusivity is the primary correlate of axonal injury in the experimental autoimmune encephalomyelitis spinal cord: A quantitative pixelwise analysis. *Journal of Neuroscience*, *29*(9), 2805–2813. https://doi.org/10.1523/JNEUROSCI.4605-08.2009

Cagalinec, M., Liiv, M., Hodurova, Z., Hickey, M. A., Vaarmann, A., Mandel, M., … Kaasik, A. (2016). Role of Mitochondrial Dynamics in Neuronal Development: Mechanism for Wolfram Syndrome. *PLoS Biology*, *14*(7). https://doi.org/10.1371/journal.pbio.1002511

Carson, M. J., Slager, U. T., & Steinberg, R. M. (1977). Simultaneous Occurrence of Diabetes Mellitus, Diabetes Insipidus, and Optic Atrophy in a Brother and Sister. *American Journal of Diseases of Children*, *131*(12), 1382–1385. https://doi.org/10.1001/archpedi.1977.02120250064010

Chaussenot, A., Bannwarth, S., Rouzier, C., Vialettes, B., Mkadem, S. A. El, Chabrol, B., … Paquis-Flucklinger, V. (2011). Neurologic features and genotype-phenotype correlation in Wolfram syndrome. *Annals of Neurology*, *69*(3), 501–508. https://doi.org/10.1002/ana.22160

Cross, A. H., & Song, S. K. (2017). "A new imaging modality to non-invasively assess multiple sclerosis pathology." *Journal of Neuroimmunology*, *304*, 81–85. https://doi.org/10.1016/j.jneuroim.2016.10.002

Deligianni, F., Carmichael, D. W., Zhang, G. H., Clark, C. A., Clayden, J. D., Bihan, D. Le, …

Glover, G. (2016). NODDI and Tensor-Based Microstructural Indices as Predictors of Functional Connectivity. *PLOS ONE*, *11*(4), e0153404. https://doi.org/10.1371/journal.pone.0153404

Eljamel, S., Ghosh, W., De Stone, S., Griffiths, A., Barrett, T., & Thompson, R. (2019). A cost of illness study evaluating the burden of Wolfram syndrome in the United Kingdom. *Orphanet Journal of Rare Diseases*, *14*(1), 185. https://doi.org/10.1186/s13023-019-1149-7

Fonseca, S. G., Ishigaki, S., Oslowski, C. M., Lu, S., Lipson, K. L., Ghosh, R., … Urano, F. (2010). Wolfram syndrome 1 gene negatively regulates ER stress signaling in rodent and human cells. *The Journal of Clinical Investigation*, *120*(3), 744–755. https://doi.org/10.1172/JCI39678

Ganie, M. A., Laway, B. A., Nisar, S., Wani, M. M., Khurana, M. L., Ahmad, F., … Tufail, S. (2011). Presentation and clinical course of Wolfram (DIDMOAD) syndrome from North India. *Diabetic Medicine*, *28*(11), 1337–1342. https://doi.org/10.1111/j.1464-5491.2011.03377.x

Genís, D., Dávalos, A., Molins, A., & Ferrer, I. (1997). Wolfram syndrome: A neuropathological study. *Acta Neuropathologica*, *93*(4), 426–429. https://doi.org/10.1007/s004010050635

Glasser, M. F., Goyal, M. S., Preuss, T. M., Raichle, M. E., & Van Essen, D. C. (2014, June 1). Trends and properties of human cerebral cortex: Correlations with cortical myelin content. *NeuroImage*, Vol. 93, pp. 165–175. https://doi.org/10.1016/j.neuroimage.2013.03.060

Glasser, M. F., & Van Essen, D. C. (2011). Mapping human cortical areas in vivo based on myelin content as revealed by T1- and T2-weighted MRI. *The Journal of Neuroscience : The Official Journal of the Society for Neuroscience*, *31*(32), 11597–11616.

https://doi.org/10.1523/JNEUROSCI.2180-11.2011

Gocmen, R., & Guler, E. (2014). Teaching NeuroImages: MRI of brain findings of Wolfram (DIDMOAD) syndrome. *Neurology*, *83*(24), e213–e214. https://doi.org/10.1212/WNL.0000000000001082

Grossman, R. I., Gomori, J. M., Ramer, K. N., Lexa, F. J., & Schnall, M. D. (1994). Magnetization transfer: theory and clinical applications in neuroradiology. *Radiographics : A Review Publication of the Radiological Society of North America, Inc*, *14*(2), 279–290. https://doi.org/10.1148/radiographics.14.2.8190954

Hadidy, A. M., Jarrah, N. S., Al-Till, M. I., El-Shanti, H. E., & Ajlouni, K. M. (2004). Radiological findings in Wolfram syndrome. *Saudi Medical Journal*, *25*(5), 638–641. Retrieved from https://pubmed.ncbi.nlm.nih.gov/15138533/

Heath, F., Hurley, S. A., Johansen-Berg, H., & Sampaio-Baptista, C. (2018, February 1). Advances in noninvasive myelin imaging. *Developmental Neurobiology*, Vol. 78, pp. 136–151. https://doi.org/10.1002/dneu.22552

Hershey, T., Lugar, H. M., Shimony, J. S., Rutlin, J., Koller, J. M., Perantie, D. C., … Washington University Wolfram Study Group. (2012). Early brain vulnerability in Wolfram syndrome. *PloS One*, *7*(7), e40604. https://doi.org/10.1371/journal.pone.0040604

Hilson, J. B., Merchant, S. N., Adams, J. C., & Joseph, J. T. (2009). Wolfram syndrome: a clinicopathologic correlation. *Acta Neuropathologica*, *118*(3), 415–428. https://doi.org/10.1007/s00401-009-0546-8

Hoekel, J., Chisholm, S. A., Al-Lozi, A., Hershey, T., Earhart, G., Hullar, T., … Wasson, J.

(2014). Ophthalmologic correlates of disease severity in children and adolescents with Wolfram syndrome. *Journal of AAPOS, 18*(5), 461-465.e1. https://doi.org/10.1016/j.jaapos.2014.07.162

Hofmann, S., Philbrook, C., Gerbitz, K. D., & Bauer, M. F. (2003). Wolfram syndrome: Structural and functional analyses of mutant and wild-type wolframin, the WFS1 gene product. *Human Molecular Genetics*, *12*(16), 2003–2012. https://doi.org/10.1093/hmg/ddg214

Inoue, H., Tanizawa, Y., Wasson, J., Behn, P., Kalidas, K., Bernal-Mizrachi, E., … Permutt, M. A. (1998). A gene encoding a transmembrane protein is mutated in patients with diabetes mellitus and optic atrophy (Wolfram syndrome). *Nature Genetics*, *20*(2), 143–148. https://doi.org/10.1038/2441

Ishihara, H., Takeda, S., Tamura, A., Takahashi, R., Yamaguchi, S., Takei, D., … Oka, Y. (2004). Disruption of the WFS1 gene in mice causes progressive β-cell loss and impaired stimulus - Secretion coupling in insulin secretion. *Human Molecular Genetics*, *13*(11), 1159–1170. https://doi.org/10.1093/hmg/ddh125

Ito, S., Sakakibara, R., & Hattori, T. (2007). Wolfram Syndrome Presenting Marked Brain MR Imaging Abnormalities with Few Neurologic Abnormalities. *AJNR Am. J. Neuroradiol.*, *28*(2), 305–306. Retrieved from http://www.ajnr.org/content/28/2/305.long

Jin, Z., Bao, Y., Wang, Y., Li, Z., Zheng, X., Long, S., & Wang, Y. (2019). Differences between generalized Q-sampling imaging and diffusion tensor imaging in visualization of crossing neural fibers in the brain. *Surgical and Radiologic Anatomy*, *41*(9), 1019–1028. https://doi.org/10.1007/s00276-019-02264-1

Licis, A., Davis, G., Eisenstein, S. A., Lugar, H. M., & Hershey, T. (2019). Sleep disturbances in Wolfram syndrome. *Orphanet Journal of Rare Diseases*, *14*(1). https://doi.org/10.1186/s13023-019-1160-z

Lucariello, A., Perna, A., Sellitto, C., Baldi, A., Iannaccone, A., Cobellis, L., … De Falco, M. (2014). Modulation of wolframin expression in human placenta during pregnancy: Comparison among physiological and pathological states. *BioMed Research International*, *2014*. https://doi.org/10.1155/2014/985478

Lugar, H. M., Koller, J. M., Rutlin, J., Eisenstein, S. A., Neyman, O., Narayanan, A., … Hershey, T. (2019). Evidence for altered neurodevelopment and neurodegeneration in Wolfram syndrome using longitudinal morphometry. *Scientific Reports*, *9*(1), 6010. https://doi.org/10.1038/s41598-019-42447-9

Lugar, H. M., Koller, J. M., Rutlin, J., Marshall, B. A., Kanekura, K., Urano, F., … Washington University Wolfram Syndrome Research Study Group. (2016). Neuroimaging evidence of deficient axon myelination in Wolfram syndrome. *Scientific Reports*, *6*, 21167. https://doi.org/10.1038/srep21167

MacKay, A. L., & Laule, C. (2016). Magnetic Resonance of Myelin Water: An in vivo Marker for Myelin. *Brain Plasticity*, *2*(1), 71–91. https://doi.org/10.3233/bpl-160033

Mackay, A., Whittall, K., Adler, J., Li, D., Paty, D., & Graeb, D. (1994). In vivo visualization of myelin water in brain by magnetic resonance. *Magnetic Resonance in Medicine*, *31*(6), 673–677. https://doi.org/10.1002/mrm.1910310614

McBain, S. C., & Morgan, N. G. (2003). Functional effects of expression of wolframin-antisense transcripts in BRIN-BD11 β-cells. *Biochemical and Biophysical Research Communications*,

307(3), 684–688. https://doi.org/10.1016/S0006-291X(03)01243-9

Monje, M. (2018). Myelin Plasticity and Nervous System Function. *Annual Review of Neuroscience*, *41*(1), 61–76. https://doi.org/10.1146/annurev-neuro-080317-061853

Mori, S., & Zhang, J. (2006, September 7). Principles of Diffusion Tensor Imaging and Its Applications to Basic Neuroscience Research. *Neuron*, Vol. 51, pp. 527–539. https://doi.org/10.1016/j.neuron.2006.08.012

Osman, A. A., Saito, M., Makepeace, C., Permutt, M. A., Schlesinger, P., & Mueckler, M. (2003). Wolframin Expression Induces Novel Ion Channel Activity in Endoplasmic Reticulum Membranes and Increases Intracellular Calcium. *Journal of Biological Chemistry*, *278*(52), 52755–52762. https://doi.org/10.1074/jbc.M310331200

Özarslan, E., & Mareci, T. H. (2003). Generalized Diffusion Tensor Imaging and Analytical Relationships Between Diffusion Tensor Imaging and High Angular Resolution Diffusion Imaging. *Magnetic Resonance in Medicine*, *50*(5), 955–965. https://doi.org/10.1002/mrm.10596

Philbrook, C., Fritz, E., & Weiher, H. (2005). Expressional and functional studies of Wolframin, the gene function deficient in Wolfram syndrome, in mice and patient cells. *Experimental Gerontology*, *40*(8–9), 671–678. https://doi.org/10.1016/j.exger.2005.06.008

Pickett, K. A., Duncan, R. P., Hoekel, J., Marshall, B., Hershey, T., & Earhart, G. M. (2012). Early presentation of gait impairment in Wolfram Syndrome. *Orphanet Journal of Rare Diseases*, *7*, 92. https://doi.org/10.1186/1750-1172-7-92

Pickett, K. A., Duncan, R. P., Paciorkowski, A. R., Permutt, M. A., Marshall, B., Hershey, T., …

Washington University Wolfram Study Group. (2012). Balance impairment in individuals with Wolfram syndrome. *Gait & Posture*, *36*(3), 619–624. https://doi.org/10.1016/j.gaitpost.2012.06.008

Sakakibara, Y., Sekiya, M., Fujisaki, N., Quan, X., & Iijima, K. M. (2018). *Knockdown of wfs1, a fly homolog of Wolfram syndrome 1, in the nervous system increases susceptibility to age- and stress-induced neuronal dysfunction and degeneration in Drosophila*. https://doi.org/10.1371/journal.pgen.1007196

Samara, A., Rahn, R., Neyman, O., Park, K. Y., Samara, A., Marshall, B., … Hershey, T. (2019, December 3). Developmental hypomyelination in Wolfram syndrome: New insights from neuroimaging and gene expression analyses. *Orphanet Journal of Rare Diseases*, Vol. 14. https://doi.org/10.1186/s13023-019-1260-9

Shannon, P., Becker, L., & Deck, J. (1999). Evidence of widespread axonal pathology in Wolfram syndrome. *Acta Neuropathologica*, *98*(3), 304–308. https://doi.org/10.1007/s004010051084

Snaidero, N., & Simons, M. (2014). Myelination at a glance. *Journal of Cell Science*, *127*(14), 2999–3004. https://doi.org/10.1242/jcs.151043

Song, S. K., Sun, S. W., Ramsbottom, M. J., Chang, C., Russell, J., & Cross, A. H. (2002). Dysmyelination revealed through MRI as increased radial (but unchanged axial) diffusion of water. *NeuroImage*, *17*(3), 1429–1436. https://doi.org/10.1006/nimg.2002.1267

Strom, T. (1998). Diabetes insipidus, diabetes mellitus, optic atrophy and deafness (DIDMOAD) caused by mutations in a novel gene (wolframin) coding for a predicted transmembrane protein. *Human Molecular Genetics*, *7*(13), 2021–2028.

https://doi.org/10.1093/hmg/7.13.2021

Swift, R. G., Perkins, D. O., Chase, C. L., Sadler, D. B., & Swift, M. (1991). Psychiatric disorders in 36 families with Wolfram syndrome. *American Journal of Psychiatry*, *148*(6), 775–779. https://doi.org/10.1176/ajp.148.6.775

Takeda, K., Inoue, H., Tanizawa, Y., Matsuzaki, Y., Oba, J., Watanabe, Y., … Oka, Y. (2001). WFS1 (Wolfram syndrome 1) gene product: predominant subcellular localization to endoplasmic reticulum in cultured cells and neuronal expression in rat brain. In *Human Molecular Genetics* (Vol. 10).

Takei, D., Ishihara, H., Yamaguchi, S., Yamada, T., Tamura, A., Katagiri, H., … Oka, Y. (2006). WFS1 protein modulates the free Ca2+ concentration in the endoplasmic reticulum. *FEBS Letters*, *580*(24), 5635–5640. https://doi.org/10.1016/j.febslet.2006.09.007

Torkildsen, Brunborg, L. A., Myhr, K. M., & Bø, L. (2008, May). The cuprizone model for demyelination. *Acta Neurologica Scandinavica*, Vol. 117, pp. 72–76. https://doi.org/10.1111/j.1600-0404.2008.01036.x

Tuch, D. S. (2004). Q-ball imaging. *Magnetic Resonance in Medicine*, *52*(6), 1358–1372. https://doi.org/10.1002/mrm.20279

Urano, F. (2016, January 1). Wolfram Syndrome: Diagnosis, Management, and Treatment. *Current Diabetes Reports*, Vol. 16, pp. 1–8. https://doi.org/10.1007/s11892-015-0702-6

Wang, X., Cusick, M. F., Wang, Y., Sun, P., Libbey, J. E., Trinkaus, K., … Song, S.-K. (2014). Diffusion basis spectrum imaging detects and distinguishes coexisting subclinical inflammation, demyelination and axonal injury in experimental autoimmune

encephalomyelitis mice. *NMR in Biomedicine*, *27*(7), 843–852. https://doi.org/10.1002/nbm.3129

Wang, Y., Sun, P., Wang, Q., Trinkaus, K., Schmidt, R. E., Naismith, R. T., … Song, S.-K. (2015). Differentiation and quantification of inflammation, demyelination and axon injury or loss in multiple sclerosis. *Brain : A Journal of Neurology*, *138*(Pt 5), 1223–1238. https://doi.org/10.1093/brain/awv046

Wang, Y., Wang, Q., Haldar, J. P., Yeh, F.-C., Xie, M., Sun, P., … Song, S.-K. (2011). Quantification of increased cellularity during inflammatory demyelination. *Brain*, *134*(12), 3590–3601. https://doi.org/10.1093/brain/awr307

West, R. K., Ravona-Springer, R., Schmeidler, J., Leroith, D., Koifman, K., Guerrero-Berroa, E., … Schnaider-Beeri, M. (2014). The Association of Duration of Type 2 Diabetes with Cognitive Performance is Modulated by Long-Term Glycemic Control. *The American Journal of Geriatric Psychiatry*, *22*(10), 1055–1059. https://doi.org/10.1016/j.jagp.2014.01.010

Yu, G., Yu, M. L., Wang, J. F., Gao, C. R., & Chen, Z. J. (2010). WS1 gene mutation analysis of wolfram syndrome in a Chinese patient and a systematic review of literatures. *Endocrine*, *38*(2), 147–152. https://doi.org/10.1007/s12020-010-9350-4

Yurimoto, S., Hatano, N., Tsuchiya, M., Kato, K., Fujimoto, T., Masaki, T., … Tokumitsu, H. (2009). Identification and characterization of wolframin, the product of the Wolfram syndrome gene (WFS1), as a novel calmodulin-binding protein. *Biochemistry*, *48*(18), 3946–3955. https://doi.org/10.1021/bi900260y

Zhang, J., Jones, M. V., McMahon, M. T., Mori, S., & Calabresi, P. A. (2012). In vivo and ex

vivo diffusion tensor imaging of cuprizone-induced demyelination in the mouse corpus callosum. *Magnetic Resonance in Medicine*, *67*(3), 750–759. https://doi.org/10.1002/mrm.23032

Chapter 2: Development of Myelin in White Matter

2.1 Abstract

Wolfram syndrome (WS) is characterized by juvenile-onset insulin-dependent diabetes, optic atrophy, deafness, and neurodegeneration. It is known that white matter is compromised, but the trajectory of deficits has never been characterized. We followed a longitudinal cohort of children and young adults with WS and healthy and type 1 diabetes control groups, using two approaches to assess myelin: diffusion basis spectrum imaging (DBSI) and myelin mapping. The WS group had decreased rate of myelination compared to controls throughout most of the brain, with a divergence in myelin integrity in early adulthood. However, tracts associated with visual processing were hypomyelinated in early childhood followed by a normal rate of myelination. Gray matter myelin was largely equivalent across all groups. This study confirms the strong involvement of white matter integrity in the pathology of the disease and suggests a regionally specific pattern of vulnerability in the timing and rate of myelin development.

2.2 Introduction

Wolfram syndrome (OMIM #222300) is a rare autosomal recessive genetic disorder. It was originally denominated as DIDMOAD for its characteristic symptoms- diabetes insipidus (DI), juvenile onset diabetes mellitus (DM), optic atrophy (OA), and sensorineural hearing loss (D)(Barrett, Bundey, & Macleod, 1995). However, the discovery of the causative genes (Inoue et al., 1998) and studies of patients with the genetic mutation have proven the disease to be significantly more complex. Many patients experience a larger myriad of psychiatric and neurologic symptoms, such as balance and gait abnormalities, urinary and bowel dysfunction, temperature dysregulation, and poor sleep (Barrett & Bundey, 1997; Chaussenot et al., 2011; Licis, Davis, Eisenstein, Lugar, & Hershey, 2019; Pickett, Duncan, Hoekel, et al., 2012). Disease presentation and progression is heterogenous, with many patients developing only a subset of symptoms and showing large variability in severity of affliction (Eljamel et al., 2019).

The vast majority of Wolfram cases are caused by mutations in the *WFS1* gene which codes for the protein wolframin (Inoue et al., 1998). The protein operates in the endoplasmic reticulum (Takeda, 2001) and contributes to the regulation of ER stress (Fonseca et al., 2010) and calcium homeostasiss (Takei et al., 2006; Yurimoto et al., 2009). In the pancreatic β cells, this causes ER stress-mediated apoptosis (Fonseca et al., 2005; Ueda et al., 2005; Yamada et al., 2006) and impaired insulin secretion (Hatanaka et al., 2011). The mechanism behind the neurological abnormalities is poorly understood, though ER stress caused by disturbances in Ca^{2+} homeostasis, leading toward the dysregulation of mitochondrial dynamics (Angebault et al., 2018) and, in turn, inhibited neural development, has been suggested (Cagalinec et al., 2016). A handful of neuropathological studies of brains afflicted with Wolfram syndrome show a loss of neurons, myelin, and myelinated axons, though the timing of these changes is unknown (Carson, Slager, & Steinberg, 1977; Genís, Dávalos, Molins, & Ferrer, 1997; Hilson, Merchant, Adams, &

Joseph, 2009; Padmanabhan, Parihar, C Vartak, & Gadgil, 2019; Shannon, Becker, & Deck, 1999). The particular susceptibility of disturbances in myelin may be explained by the high metabolic requirements of oligodendrocytes – the myelinating cells of the brain, which makes them particularly vulnerable to ER stress (Lugar et al., 2019; Roth & Núñez, 2016; Samara et al., 2019; Volpi, Touvier, & D'Antonio, 2017).

Neuroimaging studies provide the best opportunity for following the trajectory of the impact of the disease on the brain. We have studied a cohort of Wolfram patients and controls on an annual basis for up to five years in order to collect the largest longitudinal cohort of Wolfram patients to date. Previous findings suggest that the brains of Wolfram patients are smaller than normal, with particularly decreased volume in the pons, thalamus, cerebellum, and visual cortex when controlled for whole brain volume (Hershey et al., 2012; Hilson et al., 2009; Lugar et al., 2016). Longitudinal analyses of volumes found an active decrease in volume over time in the brainstem, ventral pons, cerebellar gray, and thalamus, while these same regions either increased or maintained their volume in control subjects. Cerebellar white matter volume did not change with time in Wolfram, contrary to the growth seen in controls (Lugar et al., 2019). In our prior cross sectional studies we have shown that white matter integrity is compromised; specifically, subjects have significantly lower fractional anisotropy (FA) and higher radial diffusivity (RD) throughout the major white matter tracts, including in the optic radiations, middle cerebellar peduncle, inferior fronto-occipital fasciculus and acoustic radiations (Lugar et al., 2016). These neuroimaging metrics suggest prominent hypomyelination in Wolfram syndrome, but as of yet, we do not understand the evolution of these white matter microstructural abnormalities and how they are related to the progression of the disease.

In this paper, we use tractography and whole white matter mask analysis, in conjunction with cutting edge diffusion weighted imaging methods, to follow myelin integrity in white matter tracts over time. The use of both white matter mask and tract-specific analyses provided converging evidence for a thorough picture of the developmental trajectory of white matter in Wolfram syndrome. Instead of using standard diffusion tensor imaging analysis, we use diffusion basis spectrum imaging (DBSI), which gives not only the standard measurements of anisotropic diffusion: fractional anisotropy (FA), radial diffusion (RD), and axial diffusion (AD), but also gives us information on the isotropic diffusion in the form of a restricted fraction (RF – a measure of cellularity), hindered fraction (HF- a measure of edema), and fiber fraction (FF- a measure of how much of the signal is represented by anisotropic diffusion) (Cross & Song, 2017). These myelin integrity metrics are correlated with metrics of clinical presentation of the disease. We also use myelin mapping (a T1w/Tw2 ratio) in order to see whether the myelin in gray matter is also affected (Glasser, Goyal, Preuss, Raichle, & Van Essen, 2014), as could be hypothesized if there were broad oligodendrocyte involvement. We aim to gain a better understanding of how myelin in an individual with Wolfram syndrome changes with time and age, the degree to which various regions of the brain are affected, and how this relates to their symptom presentation.

2.2 Materials and Methods

Participants

This study was approved by the Human Research Protection Office at Washington University in St. Louis and all methods were conducted in accordance with relevant ethical guidelines and regulations. Children under age 18 gave informed assent and parents/guardians gave informed, written consent. Participants 18 or older gave informed, written consent.

Wolfram syndrome group

The Wolfram syndrome group consists of participants who were recruited into the Washington University Syndrome Research Clinic by self or physician referral, or from the Washington University Wolfram Syndrome Registry. In order to enroll, individuals had to have a confirmed *WFS1* mutation, be aware of their diagnosis, be under the age of 30 and able to travel to St. Louis for annual research clinics. During the clinic, participants underwent a battery of tests and answered questionnaires to evaluate disease symptoms and progression. Metrics on cognitive function, sensory acuities, and endocrine function were included and results on many of these have been reported elsewhere (Bischoff et al., 2015; Hoekel et al., 2018; Marshall et al., 2013; Nguyen et al., 2012; Pickett, Duncan, Hoekel, et al., 2012; Pickett, Duncan, Paciorkowski, et al., 2012). The subset of participants without any contraindications for magnetic resonance imaging (MRI) were also scanned at each visit for up to 5 years. Some of these data have also been reported (Hershey et al., 2012; Lugar et al., 2019, 2016) .

Control group

The control group consists of healthy individuals and individuals with type 1 diabetes mellitus (T1D) who were otherwise healthy. Individuals with T1D were recruited from the Pediatric Diabetes Clinic at St. Louis Children's Hospital and Washington University School of Medicine in St. Louis. Exclusion criteria included psychiatric illness, significant neurological history not due to diabetes, known premature birth (<36 weeks gestation) with complications, psychoactive medications, or physical limitations that would interfere with testing. Individuals in the T1D group did not have neuropathy, retinopathy, or nephropathy. Healthy siblings of T1D

participants or members from the community made up the non-diabetic control group. MRI scans and cognitive testing were collected for up to three consecutive years.

Neuroimaging

Participants with diabetes had their blood glucose levels tested before and after scanning for safety. Insulin doses were adjusted if blood glucose was above 300 mg/dl, and food or juice was provided if levels were below 70 mg/dl. A Siemens 3T Tim Trio was used to acquire the following sequences: T1-weighted Magnetization-Prepared Rapid Gradient-Echo (MPRAGE): sagittal acquisition, repetition time (TR) = 2400 ms, echo time (TE) = 3.16 ms, inversion time (TI) = 1000 ms, voxel resolution = 1 x 1 x 1 mm, time = 8:09 minutes. T2-weighted: sagittal acquisition, TR = 3200 ms, TE = 455 ms, voxel resolution = 1 x 1 x 1 mm, time = 4:43 minutes. Diffusion-weighted images: Echo planar, 27 directions, b-values ranging from 0 to 1400 s/mm, transverse acquisition, TR = 12300 ms, TE = 108 ms, voxel resolution = 1.98 x 1.98 x 2 mm, time = 5:44 minutes, Field map: transverse acquisition, TR = 400 ms, TE1 = 4.92 ms, TE2 = 7.38 ms, voxel resolution = 4 x 4 x 4 mm, time = 0:54 minutes. Resting BOLD scans were attempted in some participants, but results are not provided here.

Two complimentary analyses – white matter mask and tract-specific – were conducted in order to provide converging evidence and a thorough picture of the developmental trajectory of white matter in Wolfram syndrome. A third analysis using a ratio of T1w to T2w, known as myelin mapping (Glasser et al., 2013), – was used to explore the involvement of myelin in gray matter.

Diffusion Basis Spectrum Imaging (DBSI) Methodology

For all reported neuroimaging analyses, DWI images were skull-stripped and corrected for motion and eddy-current distortion using FMRIB Software Library (FSL). General image quality was manually assessed. Quantitative metrics of motion using the average volume to volume translation and rotation were calculated to provide an objective metric for data quality. A movement metric (RMS) was calculated by averaging the squares of the displacement of each voxel relative to the first volume. Data surpassing a standard motion threshold was excluded. Motion parameters were not significantly different between groups (Wolfram group RMS = 1.65 ± 0.54, Control group RMS = 1.60 ± 0.56).

Maps of diffusion metrics were calculated using the diffusion basis spectrum imaging (DBSI) pipeline described by Song et al (Cross & Song, 2017). The diffusion-weighted signal is modeled by a linear combination of multiple discrete anisotropic tensors and a spectrum of isotropic tensors. The anisotropic tensors characterized by fractional anisotropy (FA), radial diffusivity (RD), and axial diffusivity (AD) reflect fiber integrity within each image voxel. As commonly accepted notion for the traditional diffusion tensor imaging, decreased DBSI-derived FA is suggestive of white matter tract axonal injury (decreased AD) or myelin injury (increased RD). It is worthwhile to note that these anisotropic diffusion metrics are more sensitive and specific to white matter injury since the confounding extra-axonal pathologies have been modeled by isotropic tensors in DBSI. Isotropic diffusion is further subdivided into restricted and non-restricted components, with restricted diffusion being defined as apparent diffusivity under 0.3 μm^2/ms, reflecting resident and infiltrating cellularity. The non-restricted component has been interpreted as extracellular space excluding cellularity (Cross & Song, 2017). Fiber fraction represents the anisotropic diffusion tensor signal fraction, the apparent axon/fiber density. The

extra-axonal space is composed of the summation of the isotropic component, which includes the restricted and hindered fractions.

We chose to investigate 6 diffusion metrics (FA, RD, AD, restricted, non-restricted and fiber fraction) using two statistically independent, yet complimentary analyses (whole white matter mask and tract-specific) to look for converging evidence and provide a thorough picture of the developmental trajectory of white matter in Wolfram syndrome.

In order to maximize the use of our longitudinal data, we chose statistical models that could handle data with varying number of time points across individuals. To simplify the models and maximize power, the two control groups (healthy and T1D) were collapsed for all reported analyses, given that previous analyses have not revealed significant differences between healthy and diabetic groups when analyzed separately or with diabetes as a covariate (Lugar et al., 2019, 2016).

White Matter Mask Analysis

For each participant, the T1 and T2 images for each time point were processed using SPM 12's serial longitudinal registration toolbox on default settings, generating an all-time-point average. The all-time-point average T1 and T2 images were segmented with SPM segment in order to generate a white matter tissue probability map. A study-specific white matter mask was made from the tissue probability maps using SPM DARTEL (Ashburner, 2007). The MNI152 VI template was also segmented and a tissue probability map was generated to compute the warp between the MNI and study-specific template. Diffusion images with a b value of 0 were then used to coregister the DBSI metric maps to the T2, and the previously calculated warps were

used to align each DBSI metric (FA, RD, AD, fiber fraction (FF), restricted fraction (RF), and hindered fraction (HF) maps) – now in T2 space – to white matter mask in MNI space.

In order to maximize the use of our data, it was important to use a statistical model that could handle longitudinal data with missing timepoints. The sandwich estimator toolbox (Version 2.1.1) was then used to analyze the DBSI metric maps longitudinally, given that it is suited for small, unbalanced neuroimaging datasets with missing data. The toolbox combines an ordinary least squares model with the sandwich variance estimator for standard error (Guillaume, Hua, Thompson, Waldorp, & Nichols, 2014). The main effect of group (Wolfram vs control), midpoint age, and time, and the interactions of each effect on each DBSI metric were tested. Wild bootstrapping with 999 permutations was used to make non-parametric inferences about cluster level data using family-wise error correction, while avoiding random field theory assumptions. The threshold for cluster-forming was $p=0.001$ and cluster p-values were considered significant at $p\ 0<0.05$ (Lugar et al., 2019).

Tract-specific Analysis

Tracts were chosen for having strong group effects in the white matter mask analysis, along with several that had no effect for comparison. The following tracts were included for tractography: the optic radiations, acoustic radiations, inferior fronto-occipital fasciculus, inferior longitudinal fasciculus, corpus callosum, corticospinal tract, and middle cerebellar peduncle.

Using FMRIB Software Library (FSL)(Jenkinson, Beckmann, Behrens, Woolrich, & Smith, 2012), seed masks were generated in MNI space and probtrackx was used to generate probabilistic connectivity masks for each tract (Woolrich et al., 2009). Each tract was uniformly thresholded and average values for each tract were extracted from the DBSI metric maps.

Statistical analysis was conducted in MATLAB using built-in mixed linear model functionality. The model tested is shown below:

DBSI Metric = Group + Age + Time + Group X Age + Group X Time + Group X Age X Time

The DBSI metrics tested included FA, RD, AD, FF, HF, and RF. P values of < 0.05 were considered significant.

Myelin Mapping Analysis

Myelin mapping uses the T1w/T2w ratio (myelin index) as a surrogate marker for myelin (Glasser et al., 2013; Glasser & Van Essen, 2011). Myelin mapping was performed using the Minimal Processing Pipeline from the Human Connectome Project (Glasser et al., 2013) with changes to allow for comparison between subjects. Briefly, T1w and T2w images were motion and eddy current corrected. The myelin index was then calculated across the brain. In order to be able to compare the myelin index between subjects and sessions, images needed to be normalized using regions expected to be consistent across subjects (Ganzetti, Wenderoth, & Mantini, 2014; Lee et al., 2015). Masks of the face, outside of the brain and including the eyeballs, were made in MNI space and registered to native T1w and T2w images. Using the distribution of the myelin index in the face ROI and peaks in a kernel regression, a minimum mode and whole region mode were found. These modes, along with standardized values were used for linear rescaling for the original T1w/T2w image. Regions for analysis were taken from a midthickness strip of gray matter using Freesurfer-generated parcellations, along with select parcels such as the brainstem and cerebellar gray matter. The same mixed linear model from the tract specific analysis was used to ascertain significance.

Clinical Correlations

The disease presentation of the Wolfram subjects was assessed with a small number of metrics known to be reliable in capturing disease severity – WURS (Wolfram United Rating Scale) Total, WURS Physical, PANESS (Physical and Neurological Examination for Soft Signs), visual acuity (LOGMAR), average RNFL (retinal nerve fiber layer) thickness, pure tone auditory acuity, and high frequency auditory acuity - were chosen to explore the relationship between myelin integrity and disease presentation. Metrics were collected annually, except for auditory data, which was no longer collected after stability of hearing was established. The relationship was explored using a mixed linear model:

Symptom = DBSI Metric + Age + Time + DBSI Metric X Age + DBSI Metric X Time + DBSI Metric X Age X Time + (Time | Subjects)

The DBSI metrics tested included FA, RD, AD, FF, HF, and RF. P values of < 0.05 were considered significant.

Data Availability

The raw data used in the analyses described in this manuscript cannot be made available in the manuscript, supplemental files, or a public repository because the sample size of our Wolfram syndrome patient group is so small, and the disease so rare, that human participant characteristics such as sex, age, and number of visits could be used to identify individuals even after de-identification of the data. The corresponding author, Dr. Hershey, may be contacted to request data. As per the Human Research Protection Office (HRPO) at Washington University in

St. Louis, a preface to data sharing agreement and a data sharing agreement reviewed by the research office will be employed prior to data sharing. HRPO regulations permit access to potentially identifiable data only to research personnel on our study protocol and approved through the University.

2.3 Results

Demographic and clinical characteristics of participants

Adequate T1, T2, and DWI images were acquired on 28 patients with Wolfram syndrome seen annually between 1 and 5 times (mean follow-up = 2.58 years) (Table 1).

Variable		Wolfram (n=28)	Controls (n=47)	Control Subsets	
				Non-diabetic controls (n=26)	Diabetic controls (n=21)
Sex	M/F	15/13	25/22	12/14	13/8
Age (years)	Mean ± SD	14.8 ± 5.5	14.1 ± 5.2	14.1 ± 5.5	14.1 ± 4.9
	Range	6.0-26.8	6.0-26.2	6.0-26.1	7.6-26.2
***Follow-up period (years)**	Mean ± SD	2.6 ± 1.2	1.9 ± 0.4	1.9 ± 0.4	1.9 ± 0.4
	Range	1.0-4.0	1.0-2.3	1.0-2.3	1.0-2.3

Diabetes duration (years)	Mean ± SD	8.8 ± 5.0	--	--	8.0 ± 5.1
	Range	1.8-18.6	--	--	0.1-16.7
Diabetes mellitus	Prevalence	28/28	--	--	--
Age at dx (years)	Mean ± SD	5.9 ± 3.1	--	--	--
	Range	2.7-13.9	--	--	--
Diabetes insipidus	Prevalence	18/28	--	--	--
Age at dx (years)	Mean ± SD	11.5 ± 3.8	--	--	--
	Range	5.5-17.0	--	--	--
Hearing loss	Prevalence	20/28	--	--	--
Age at dx (years)	Mean ± SD	11.0 ± 4.8	--	--	--
	Range	6.0-25.8	--	--	--
Optic nerve atrophy	Prevalence	27/28	--	--	--
Age at dx (years)	Mean ± SD	9.8 ± 3.7	--	--	--
	Range	3.8-18.0	--	--	--

*Table 2.1:Mean and standard deviation (SD) of demographic and clinical variables across Wolfram and control groups at session 1. There were no differences between the Wolfram and control groups for age (p=0.60) or sex (p=0.98), and there were no differences between Wolfram and the diabetic control groups for duration of diabetes (p=0.56) at session 1. *Excludes participants with a single time point (Wolfram, n=4; Non-diabetic control=4; diabetic control=4). Abbreviations: M, male; F, female; dx, diagnosis.*

Control group

Adequate T1, T2, and DWI images were also acquired on 21 T1D and 26 non-diabetic participants, annually between 1 and 3 times (mean follow-up = 1.88 years). The T1D group had marginal to higher HbA1c than the Wolfram group (sessions 1-2, $p < 0.022$; session 3, $p = 0.080$), as well as higher pre-MRI blood glucose levels in session 3 ($p = 0.022$). However, these groups did not differ in diabetes duration ($t(47) = -0.58$, $p = 0.56$) or blood glucose levels before or after scans in any other sessions ($p > 0.17$). Wolfram and control groups did not differ in age at their first visit (baseline age range 6-27 and 6-26, respectively; $t(73) = -0.52$, $p = 0.60$) or in sex distribution (χ^2 (1, 75) = 0, $p = 0.98$). See Table 1 for demographics for a plot of all participant ages and number of sessions.

Inferior posterior white matter is most prominently affected in Wolfram syndrome

White matter masks were generated for each subject at each timepoint. A sandwich estimator analysis was used to calculate significant group, group X age, and group X age X time effects to look for differences between the Wolfram and control groups in each of the anisotropic (FA, RD, AD) and isotropic (FF, RF, HF) DBSI metrics on a voxelwise level.

The significant main effects of group for each anisotropic diffusivity metric are shown in Fig 1. The posterior inferior areas of the brain are most affected. Consistent with past cross-sectional analyses, the optic radiations stand out as an affected region, with both a significant increase in RD and decrease in FA in Wolfram subjects as compared to controls. The affected area also includes white matter of the occipital lobe and the inferior longitudinal fasciculus. The diffusion pattern is consistent with lower levels of myelination. Smaller areas within these regions also show decreased AD in Wolfram, reflecting axonal damage. The brainstem is also affected, with evidence of decreased FA and increased RD in Wolfram as compared to controls.

Compared to the rest of the brain, the area of decreased AD in Wolfram is particularly prominent here, suggesting axonal damage is most pronounced in the brainstem.

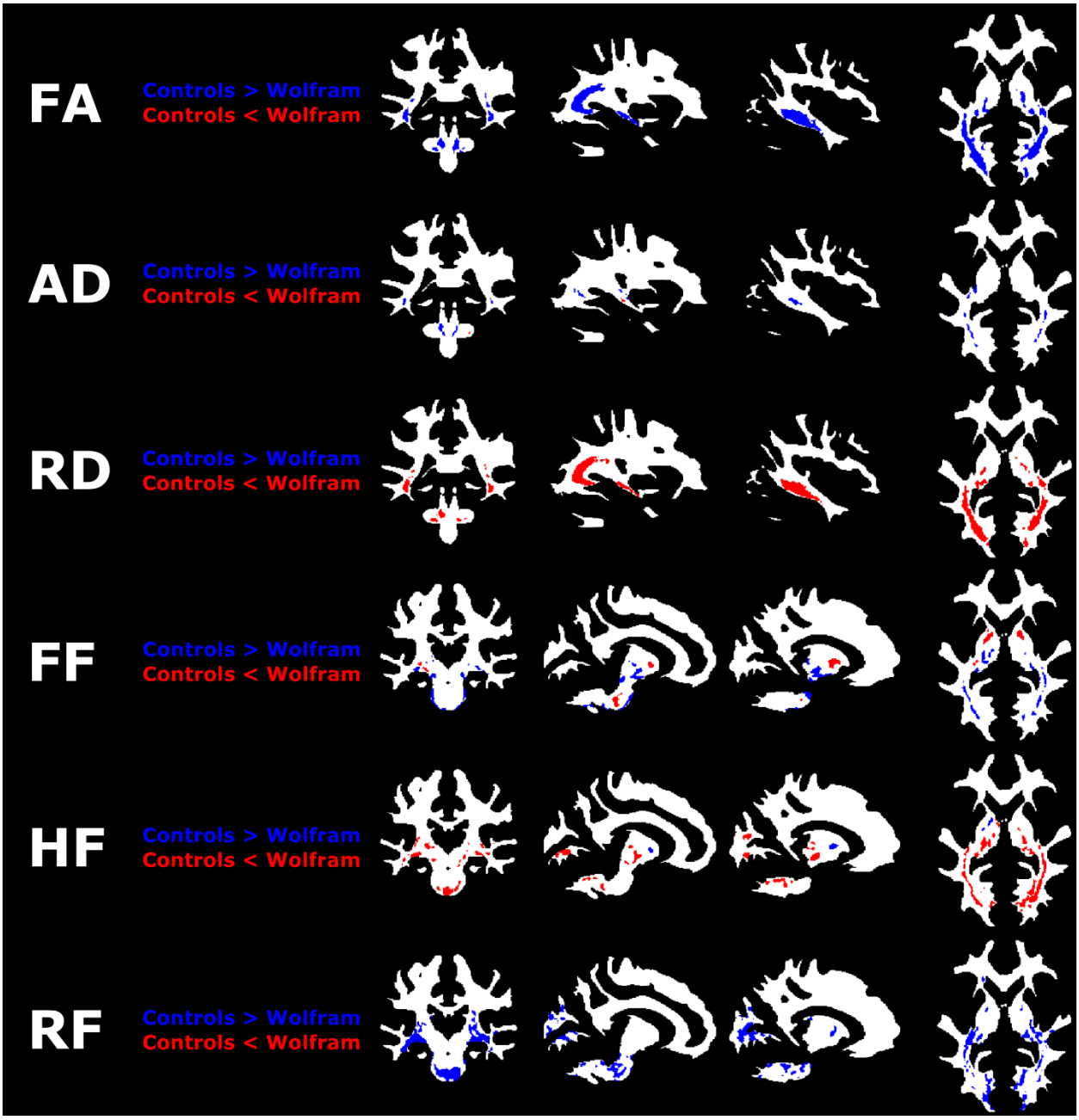

Figure 2.1: Significant group effects of the anisotropic metrics (FA, RD, and AD) and isotropic metrics (FF, HF, RF) within the white matter skeleton ($p<0.05$). Effects are particularly prominent in the optic radiations and brainstem. FA: fractional anisotropy, RD: radial diffusion, AD: axial diffusion, FF: fiber fraction, HF: hindered fraction, and RF: restricted fraction

The bottom half of Fig 1 demonstrates the statistically significant group effects of the isotropic metrics. The main group effects of FF and HF mostly oppose each other. This is not unexpected as fractional components need to sum to 1. The control group has a larger FF and smaller HF within the optic radiations, inferior longitudinal fasciculus, globus pallidus and cerebellum. FF is the portion of the diffusion signal explained by anisotropic diffusion and thus the proportion of the voxel consisting of axons versus extra-axonal space, which is, in turn, explained by the HF. The mirrored topography of these fractions suggests a smaller apparent axonal density with Wolfram syndrome. The group effect for RF covered the largest area, with diffuse involvement in the posterior and inferior portions of the brain. Despite this, regions with the greatest differences in anisotropic diffusivity measures – such as the optic radiations – have relatively little difference in restricted fraction.

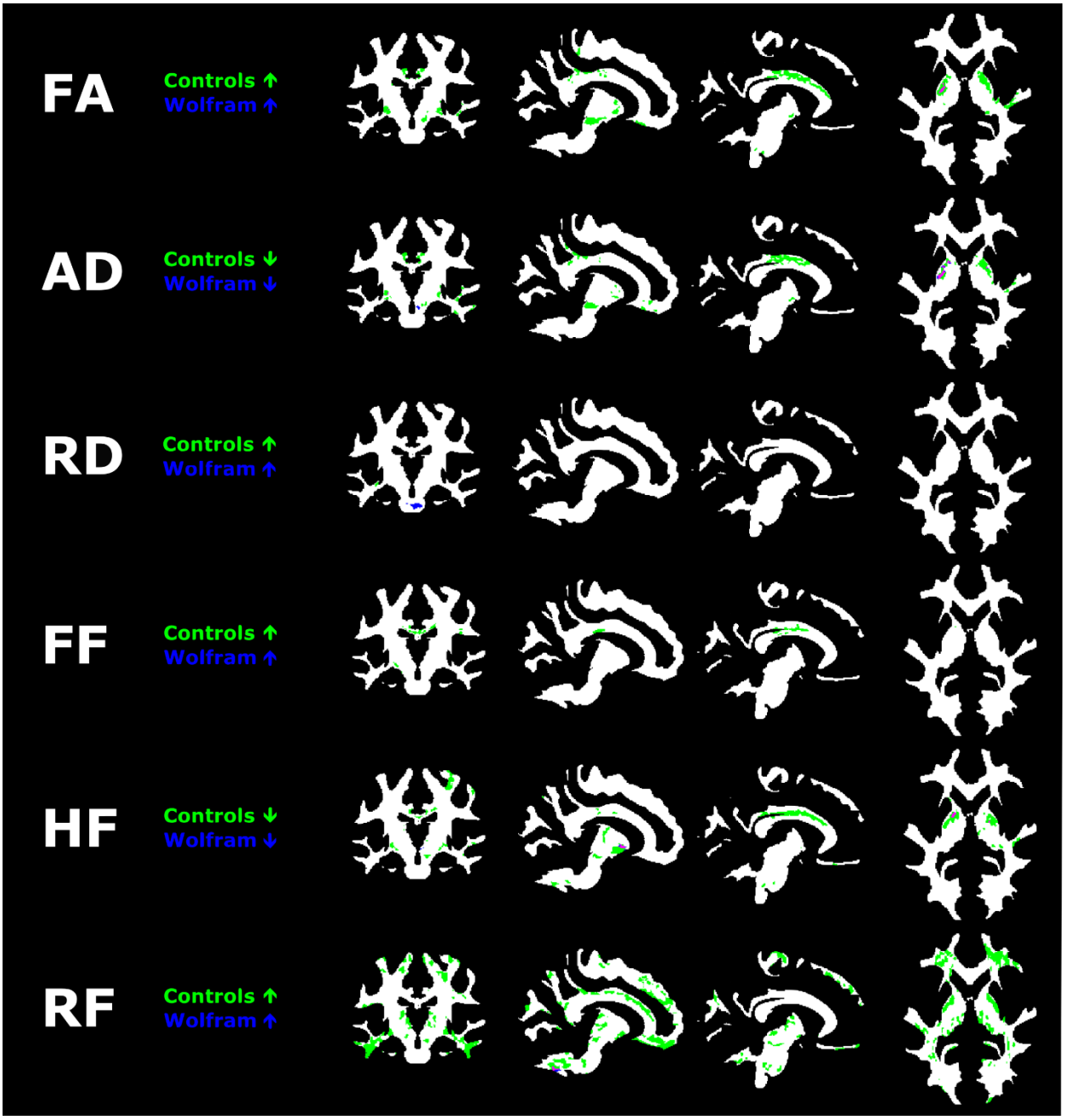

Figure 2.2: Significant age effects of the anisotropic and isotropic metrics within each of the two groups in the white matter skeleton ($p<0.05$). The Wolfram group (blue) and control group (green) were analyzed separately in this analysis. Overlap of the regions is shown in pink. Controls demonstrate a more prominent age effect throughout the brain. FA: fractional anisotropy, RD: radial diffusion, AD: axial diffusion, FF: fiber fraction, HF: hindered fraction, and RF: restricted fraction

The RF was the only diffusivity metric to have a significant group X age interaction, with controls showing a higher increase in restricted fraction than the Wolfram group over the ages studied. There is no significant effect of group X age, group X time, nor group X age X time for any other diffusion metrics. In order to explore these interactions deeper, we examined the effect of age and time on each group separately (Fig 2). The control group shows some scattered increases in FA, decreases in RD, and increases in AD. The direction of these trends is consistent with normal development. However, one would expect these changes over a more diffuse area. This discrepancy is likely due to limitations with the statistical approach. The Wolfram group has a much smaller significant area of increased FA and decreased RD in the internal capsule, as well as increased AD in the brainstem, suggesting that myelination rates over age in Wolfram may be slower than normal development to a greater extent than the original statistical model depicts. While the restricted fraction stays constant with age across the brain in the Wolfram group, controls have a diffuse increase, with the majority of the white matter mask being involved. Patches tend to be closer to the edges of the white matter mask, as compared to the topography of changes seen in the HF or FF.

Examining individual tracts demonstrates different patterns of divergence from normal white matter development

Based upon results from the white matter mask approach and prior studies, we chose the following tracts for tractography: the optic radiations, acoustic radiations, inferior fronto-occipital fasciculus, inferior longitudinal fasciculus, corpus callosum, corticospinal tract, and middle cerebellar peduncle. We also included an analysis of the average of the whole white matter mask, using subject specific masks. As shown in Fig 3, over the whole white matter mask,

FA and RD show a divergence in development during adolescence and early adulthood (Fig 5: start age X group effect: $p< 0.01$). This pattern is consistent with many of the tracts we examined, including the arcuate fasciculus and corpus callosum (Fig 5: start age X group effect: $p<0.05$). Several tracts follow a different trajectory. From the earliest years studied, the optic radiations, IFOF, and ILF have decreased FA and increased RD in the Wolfram subjects (Fig 3). The magnitude of this difference generally larger than differences seen in the earlier trajectory. However, the rate of myelination – as reflected by change of RD and FA with respect to age - is similar to that of normal development. These tracts do not have a significant group X start age interaction (Fig 5). The development trajectory for fiber fraction between groups in the whole white matter mask does not show any age X group effects. This is consistent with many of other tracts such as the arcuate fasciculus and corpus callosum. However, in the visual tracts, the fiber fraction is also smaller in Wolfram in early childhood.

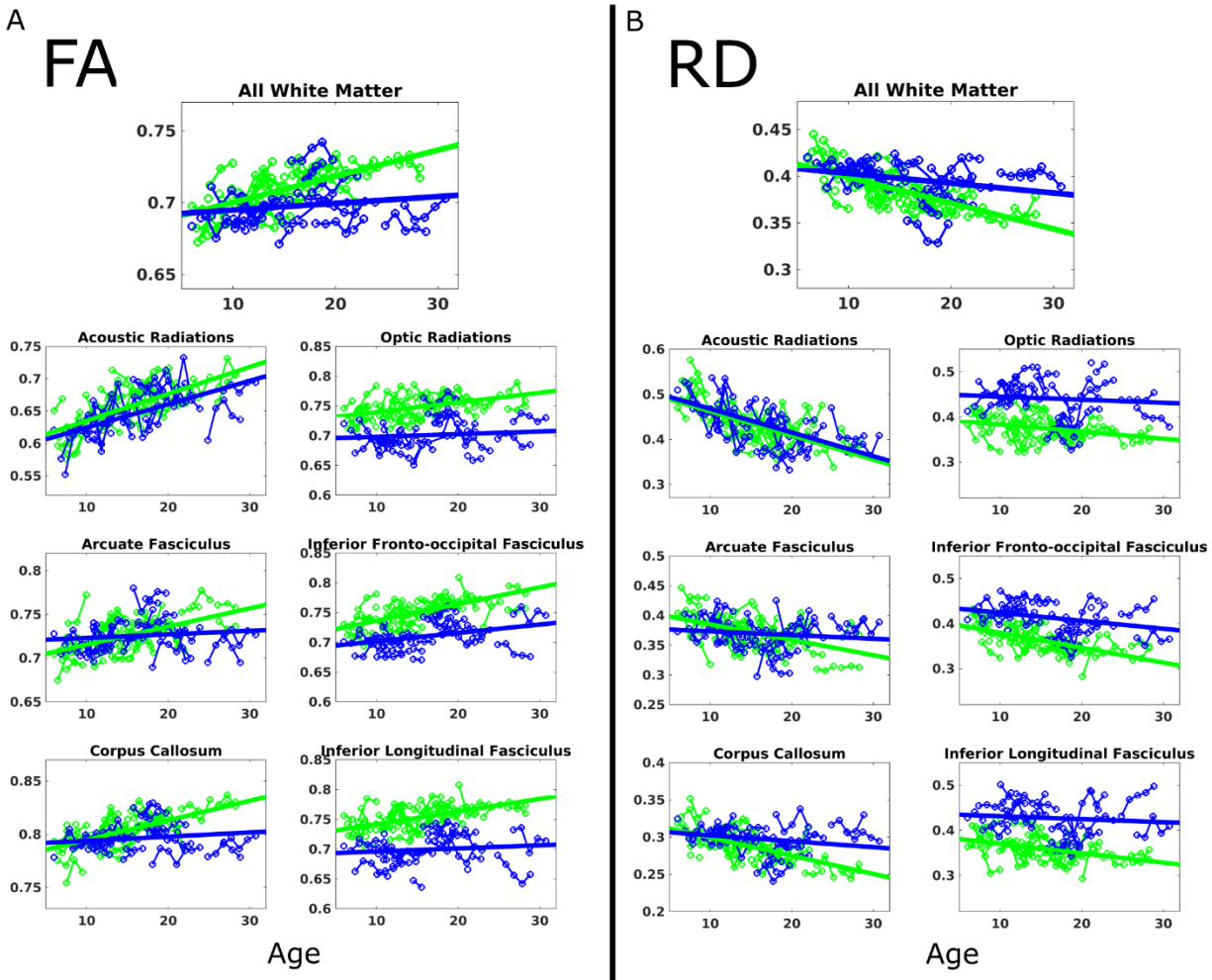

Figure 2.3: Fractional anisotropy (A) and radial diffusivity (B) averages in the whole white matter mask and selected white matter tracts. Wolfram subjects are in blue, controls are in green. Data from individuals with repeated time points are connected by a line. Tracts in the second column of each metric show group differences in early childhood. Statistical comparison of all data is shown in Fig 5.

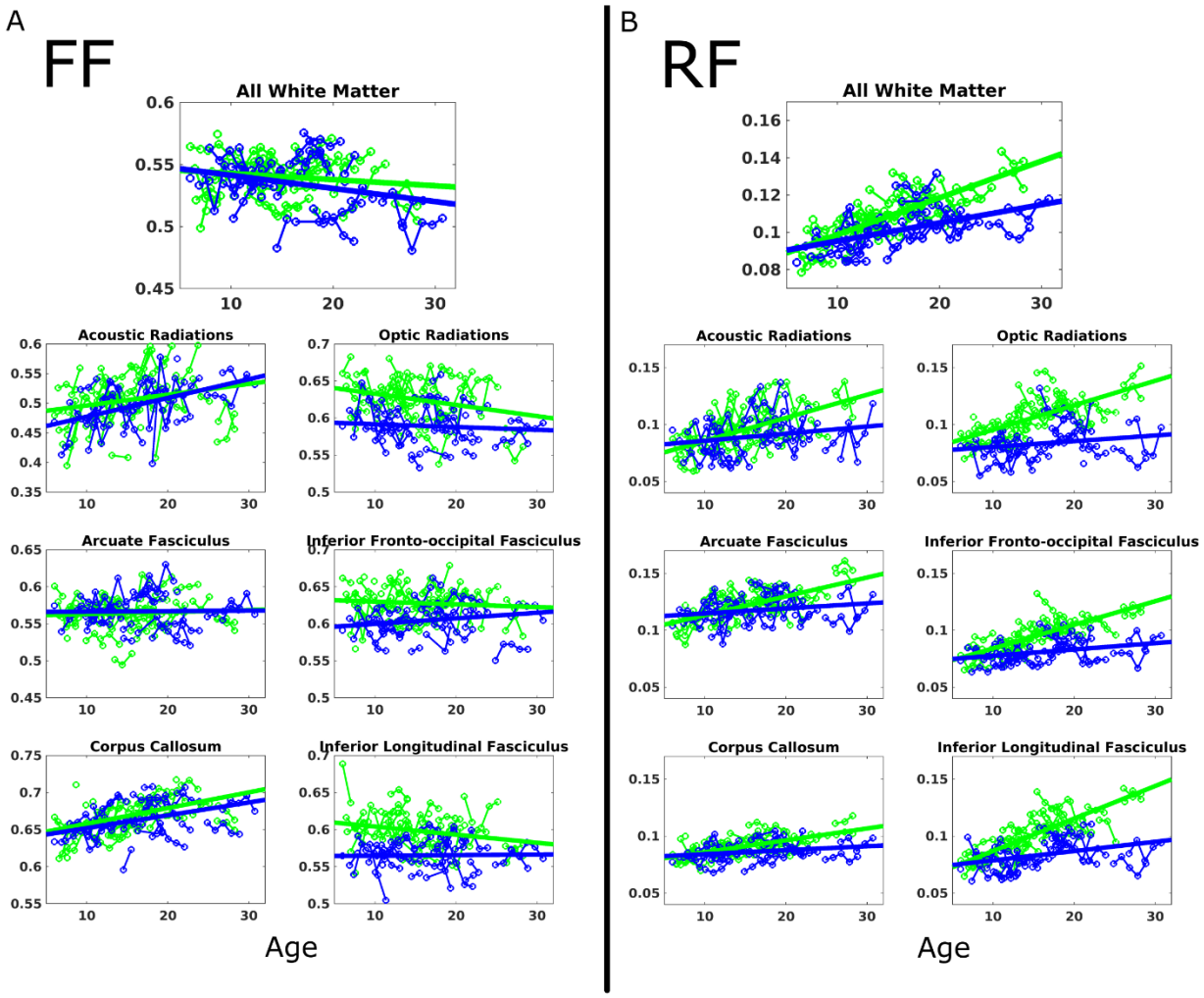

Figure 2.4: Fiber fraction (A) and restricted fraction (B) averages in the whole white matter mask and in selected white matter tracts. Wolfram subjects are in blue, controls are in green. Data from individuals with repeated time points are connected by a line. The second column of tracts in A show greater group differences that the first column. All tracts in B show a significant group x start age effect. Full statistical comparison of groups is shown in Fig 5.

The largest group X age effects are seen with respect to the restricted fraction (Fig 4). Restricted fraction increases with age significantly faster in normal development as compared to the Wolfram group. Unlike the developmental patterns described earlier, this effect is not limited to particular tracts, but rather appears to be a whole brain phenomenon. A table of all significant effects is provided in Fig 5.

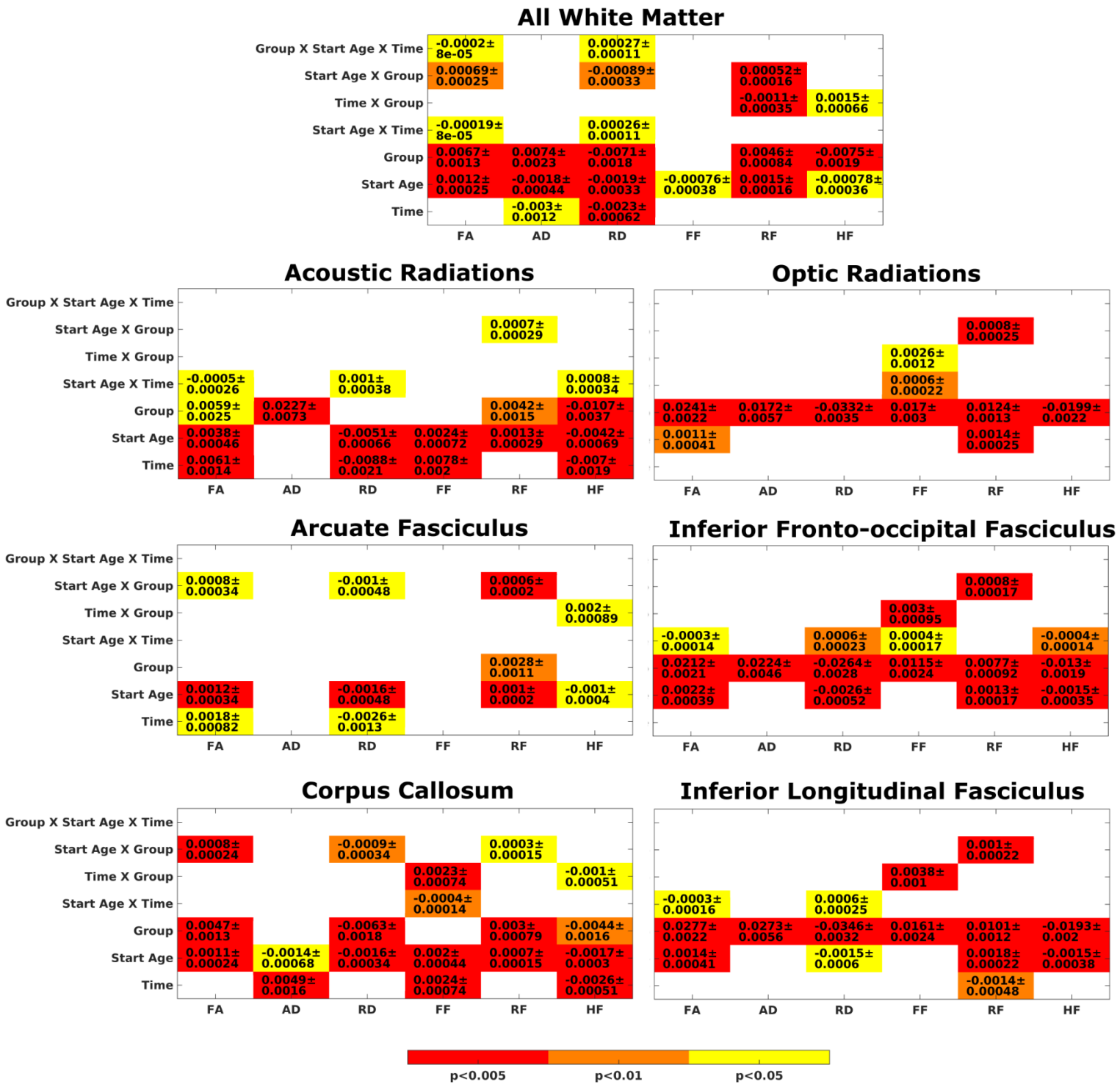

Figure 2.5: Mixed linear model results for all tractography. Significant (p<0.05) estimate coefficients with SE margins are shown for six specific tracts and the white matter mask.

Gray matter myelin in Wolfram syndrome is largely unaffected

The myelin index – a measure derived from a T1w/T2w (myelin mapping) ratio - across a representative set of parcellations is shown in Fig 6. Fourteen data points were excluded from the full dataset after being found to be outliers as defined by being more than 1.5 interquartile ranges above the upper quartile or below the lower quartile. This was caused by movement in the T2 images. Significant differences between Wolfram and controls were evaluated using linear mixed models. No group X start age X time effects were found. Significant group X time effects are present in several regions, showing a greater increase in myelination over time in controls, though the magnitude of this effect is very small. Significant start age and time effects are seen in almost all regions, with myelin index increasing with increased age. Average myelin index values were also examined in the brainstem and cerebellum. The brainstem, cerebellar cortex, and cerebellar white matter –areas known to be particularly affected in Wolfram syndrome – show significant group differences, with a higher myelin index in controls (Fig 6, Supplementary Fig 1). The brainstem stands out, with the largest magnitude of differences.

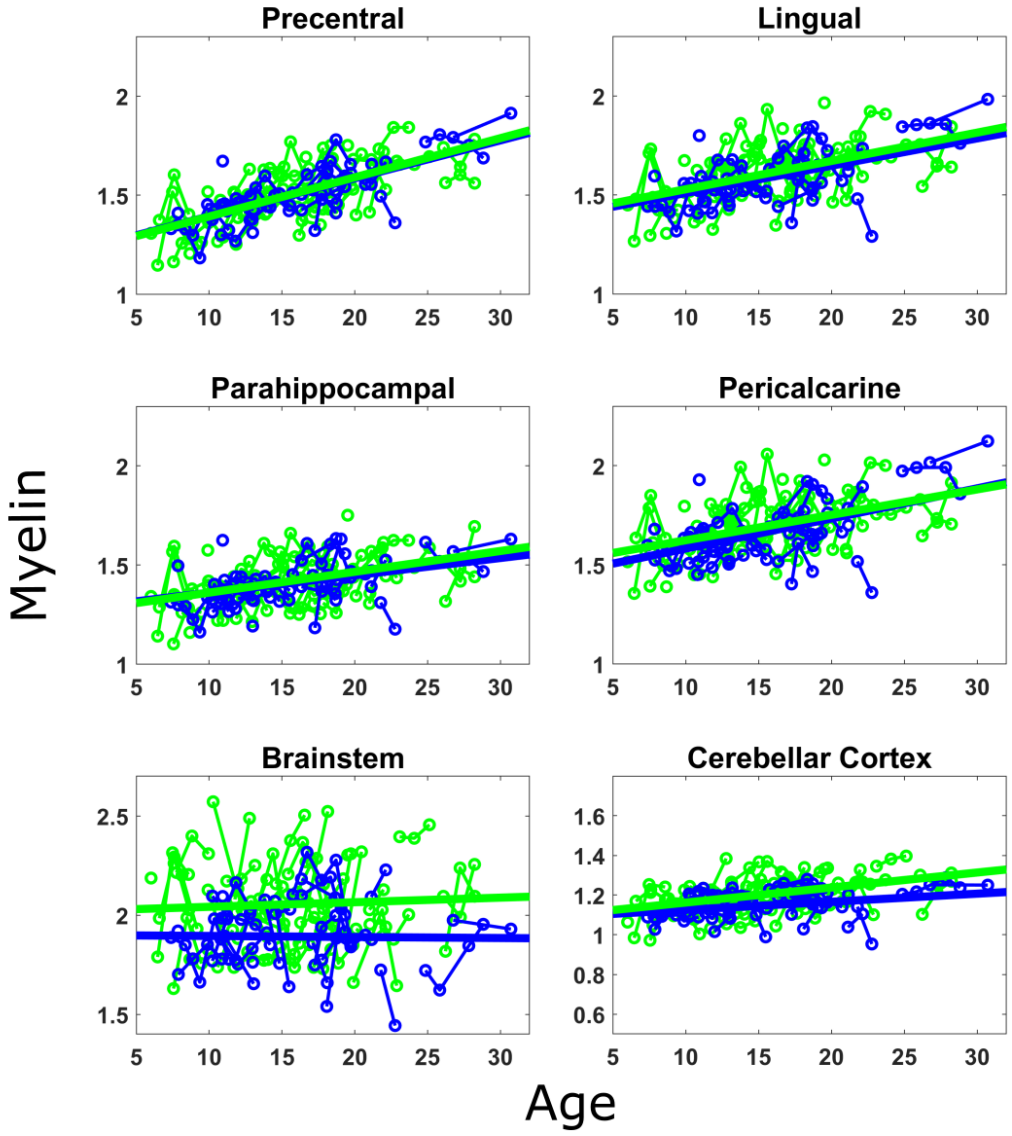

Figure 2.6: Normalized myelin index in select gray matter regions of the brain. Wolfram subjects are in blue, controls are in green. Left and right sides are averaged together when applicable. Data from individuals with repeated time points are connected by a line. The brainstem shows the largest significant group effect. Full statistical analysis is shown in Supplementary Fig 1.

Myelin integrity poorly correlates with clinical presentation

A group of metrics which capture the severity of symptoms in the Wolfram group were correlated with the imaging metrics derived from tractography. Fig 7 shows the relationship

between the whole white matter mask myelin integrity metrics and selected clinical symptoms. Greater FA and RD deficits in the whole white matter were associated with greater symptom severity (e.g. WURS, WURS physical scale, PANESS, and RNFL) (Fig 7). Relationships between symptoms and a couple example tracts - the optic and acoustic radiations - are shown in the supplement. The myelin integrity of specific tracts did not necessarily correlate with the symptom they would be most logically associated with, i.e. visual symptoms were not uniquely and most correlated with the optic radiations. In fact, visual acuity had a significant relationship with the FA of the acoustic radiations, and not with the FA of the optic radiations, demonstrating a poor association with a specific clinical presentation (Supplementary Figs 2 and 3).

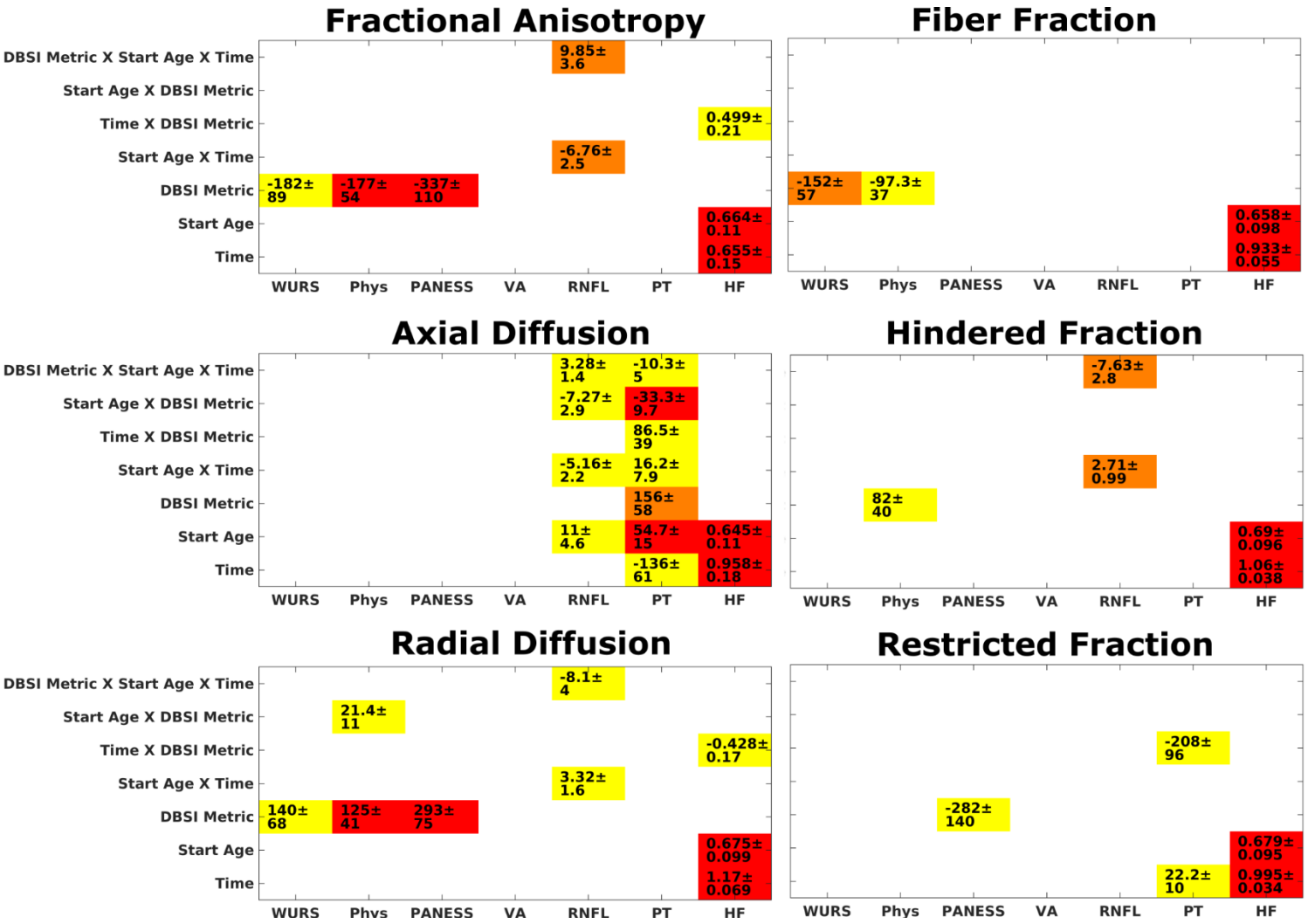

Figure 2.7: Estimate coefficients with SE margins ($p<0.05$) for a linear mixed model analysis of the relationship between myelin metrics in the whole white brain mask and symptoms. Significant relationships between DBSI metrics were particularly found with respect to vision and hearing. Clinical metrics: WURS overall score (WURS), WURS physical score (Phys), PANESS Score, Visual acuity (VA), RNFL thickness, Pure tone hearing (PT), High frequency hearing (HF).

2.4 Discussion

There has been abundant evidence that myelin is particularly affected in Wolfram syndrome. Our longitudinal study expands on this body of knowledge by providing insight into

the timing, regional distribution and magnitude of myelin deficits, and their progression in individuals. Specifically, we have shown that while white matter myelin is affected broadly in Wolfram syndrome, tracts can be differentially affected in either early childhood or early adulthood, and that myelination in many, but not all, tracts appears to stall during development. In addition, we found that myelin in gray matter is less vulnerable than myelin in white matter during development in Wolfram syndrome. Overall, white matter myelin deficiency correlated with broad measures of symptom severity, however, no selective regional structure-function relationships were observed.

White matter integrity differences in Wolfram syndrome can be found over all white matter, though the largest differences are found in the posterior inferior regions of the brain. The level and development of myelin deficits across the brain tended to follow one of two primary patterns. The first pattern is seen through most of the white matter and exemplified by tracts such as the corpus callosum (Figs 3 and 4). In these regions, myelin metrics appear normal in early childhood, but are deficient by early adulthood in Wolfram syndrome. Within the Wolfram group, there is little change in myelin metrics over age, but as expected, there is an increase in FA and reduction in RD with age in controls (Lebel, Treit, & Beaulieu, 2019). A different pattern appears in the tracts associated with the visual system (optic radiations, ILF, IFOF). Within these tracts, the Wolfram group appears to have deficient myelin (decreased FA, increased RD) compared to controls, even at the earliest age studied.

The existence of two developmental patterns of myelin suggests varied regional susceptibility to the pathological processes in Wolfram syndrome. Regional differences in normal white matter development are expected. It is known that myelin first increases sharply through the first two years of age and then continues to increase at a lower rate through thirty

years of age before decreasing through the rest of life. Myelin development and peak myelination level varies between tracts, with tracts like splenium of the corpus callosum being highly myelinated and those like the uncinate or superior fronto-occiptial tract peaking at relatively low levels. Rate of myelination also differs between tracts, with the corticospinal tract showing the highest increasing slope before the peak level is achieved (Lebel & Beaulieu, 2011). In addition, other white matter diseases demonstrate distinct regional vulnerabilities. For example, multiple sclerosis primarily affects periventricular white matter (Dobson & Giovannoni, 2019). Interestingly, Krabbe disease, a neurodevelopmental lysosomal storage disease caused by a deficiency of the lysosomal enzyme galactocerebrosidase, has a similarly topographic pattern to Wolfram syndrome, with white matter abnormalities in the corticospinal tracts, optic radiations, and posterior part of the corpus callosum (Debs et al., 2013).

The mechanism behind the regional differences of myelin deficits across development observed in Wolfram syndrome is unknown. Many of the regions that seem particularly vulnerable in Wolfram syndrome are known to myelinate very early (≤ 68 weeks after conception), including the optic radiations, middle cerebellar peduncle, and the corticospinal tract at the level of the brainstem (Kinney, Brody, Kloman, & Gilles, 1988). Areas that do not show hypomyelination in Wolfram syndrome that also fall within the visual system, like the Band of Gennari (Hilson et al., 2009), are categorized as late developing (>144 weeks post conception)(Kinney et al., 1988). A timing hypothesis is however not sufficient as several early-developing regions like the corpus callosum are not affected in early childhood in Wolfram. Furthermore, association fibers that are affected early in the disease, like the inferior longitudinal fasciculus, develop between 119-142 weeks post conception (Kinney et al., 1988).

The tracts affected early in Wolfram syndrome are largely related to the visual system, namely the optic radiations, inferior longitudinal fasciculus and inferior fronto-occipital fasciculus. This is consistent with optic atrophy being pervasive in the disease and patients experiencing potentially severe visual deficits, however, damage of the tracts appears to precede the diagnosis of visual impairment (Table 1). Retinal nerve fiber layer thickness is significantly below normal from our earliest observations and decreases with time (Hoekel et al., 2018; Zmyslowska et al., 2017). This thinning of the retinal layer is likely impacting the structural integrity of the tracts on top of any independent effects due to faulty myelination mechanisms. Reduced fractional anisotropy in the optic radiations, one of the primary deficits in Wolfram, is also found in Leber's hereditary optic neuropathy which causes a degradation in the retinal ganglion cells and their axons (Manners et al., 2015). A wider population study in the Netherlands looking for Alzheimer's biomarkers showed an association between a thinner retinal ganglion cell layer and lower fractional anisotropy in the optic radiations, inferior longitudinal fasciculus and posterior component of the inferior fronto-occipital fasciculus (Mutlu et al., 2018), consistent with what is seen in Wolfram syndrome. Similar changes have also been seen in congenitally blind and late blind patients, with late blind patients showing more extensive white matter damage (Hofstetter et al., 2019; D. Wang et al., 2013). It can thus be hypothesized that the tracts associated with the visual system are so severely affected because of the particular vulnerability of the retinal ganglion cells.

Myelin mapping was undertaken to examine if the differences in myelination seen in Wolfram syndrome also included gray matter myelin. The strongest difference detected in Wolfram syndrome was a group difference within the brainstem, which is consistent with known pathology in Wolfram. Slight time x group effects were found in a handful of cortical regions,

but the effect appears to be carried by a couple subjects. It is possible that the metric is not sensitive to detect more subtle differences in the gray matter myelin content, but also plausible that differences are minimal or may not appear until a more severe phase of the disease. A histopathological study of a single Wolfram patient did not show differences in myelin in the band of Gennari, but this was limited to visual inspection (Hilson et al., 2009). In addition, myelin mapping has been able to detect the development of gray matter myelin in normal infants (Lee et al., 2015) and has been show to correlate to diffusion imaging in adults. Thus, our tentative conclusion is that gray matter myelin is largely protected from the pathological process that affects white matter myelination in Wolfram syndrome.

Correlations between myelin integrity metrics and disease symptoms were present, but not strong or regionally specific. FA and RD, when averaged over the entirely of the white matter, appear to be the strongest indicators of the severity of symptoms. The increased noise within the tracts as compared to an average over a large region facilitates stronger results as compared to the individual tracts. Overall, there is poor correlation between symptoms and the logically corresponding tract ie. the optic radiations and visual acuity. This phenomenon is common in neuroimaging research and is also seen in other diseases such as multiple sclerosis (Mollison et al., 2017). Neuroimaging myelin integrity metrics can thus be used as biomarkers to estimate how severely a patient is affected by Wolfram syndrome, but they are not sufficient to actively follow an individual patient's progression or as a primary biomarker to test the effectiveness of novel treatments.

This study takes advantage of a novel method of diffusion weighted imaging analysis: diffusion basis spectrum imaging (DBSI). The primary advantages of this modality are estimates for isometric diffusion components (Y. Wang et al., 2015, 2011). The lower fiber fraction and

corresponding increase in hindered fraction seen in some regions is consistent with axonal damage and lower levels of myelin and is supported by the handful of available neuropathological studies of individuals with Wolfram syndrome (Hilson et al., 2009; Jackson et al., 1994). This interpretation also provides an explanation for the lack of increased volume of these areas during development seen in Wolfram syndrome (Lugar et al., 2019). The restricted fraction estimates have originally been interpreted to reflect an increase in cellularity, specifically inflammatory cells. The results of this study bring this interpretation into question, as controls show increased restricted fraction across age, which is unlikely to be explained by increased inflammation. Interestingly, whatever mechanism is driving this pattern in controls is not present in Wolfram syndrome. A difference in oligodendrocyte populations is a tempting interpretation, but in healthy development, the cell population should reach nearly its maximal size in early childhood and does not increase at a rate mirroring the increase in the restricted fraction seen in our controls (Yeung et al., 2014).

The primary limitations of this study relate to within-subject noise in the imaging data and the small sample size, issues that will plague any study of a rare disease. The longitudinal nature of the study has required the consistent use of older sequences. While we have made an effort to limit the effect of movement on our data, it nevertheless will decrease the quality of the data. Newer sequences and following subjects over a longer time frame will hopefully allow for a more detailed analysis of regional and within-person changes. Nevertheless, this study shows that despite large white matter integrity deficits, changes over time are minor at best, making neuroimaging metrics a good marker for overall patient status but a poor one for monitoring individual patient progression or testing novel forms of treatment.

Overall, the results of this study are important for understanding the progression of Wolfram syndrome. We have learned that white matter deficits are seen across the brain, but that the development of these deficits does not follow a homogenous trajectory. By early adulthood, myelin integrity is compromised throughout the brain, but particular tracts – those associated with vision – are affected more severely and as soon as early childhood, even before substantial visual acuity loss. While myelin appears to have a prominent role in Wolfram, and there appears to be a relationship between symptom severity and overall myelin integrity, it is clear that regional differences are not associated with specific symptoms. Such knowledge is invaluable in the search for novel treatment directions, both with respect to target and biomarker selections and validation of animal models of Wolfram syndrome. Finally, mechanistic explanations for neuropathological changes in Wolfram syndrome will need to consider the significant regional and developmental differences observed in this work.

2.5 Supplementary Figures

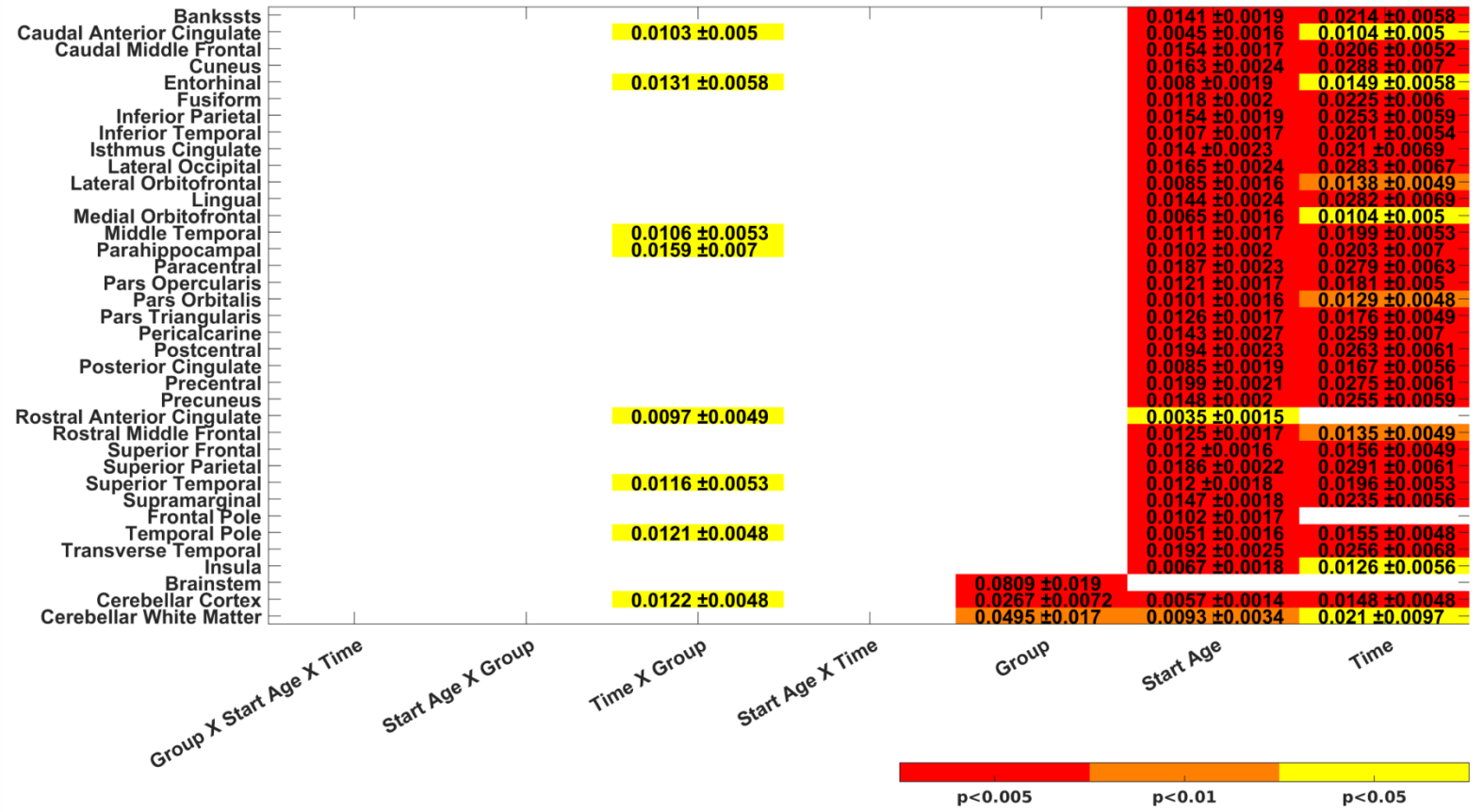

Supplementary Figure 2.1: Significant estimate coefficients with SE margins for a mixed linear model analysis of the myelin index in each gray matter region and select white matter regions ($p<0.05$). Time X group effects were found throughout the cortex. Group effects were limited to the brainstem and cerebellum. Start age effects were found in nearly all regions.

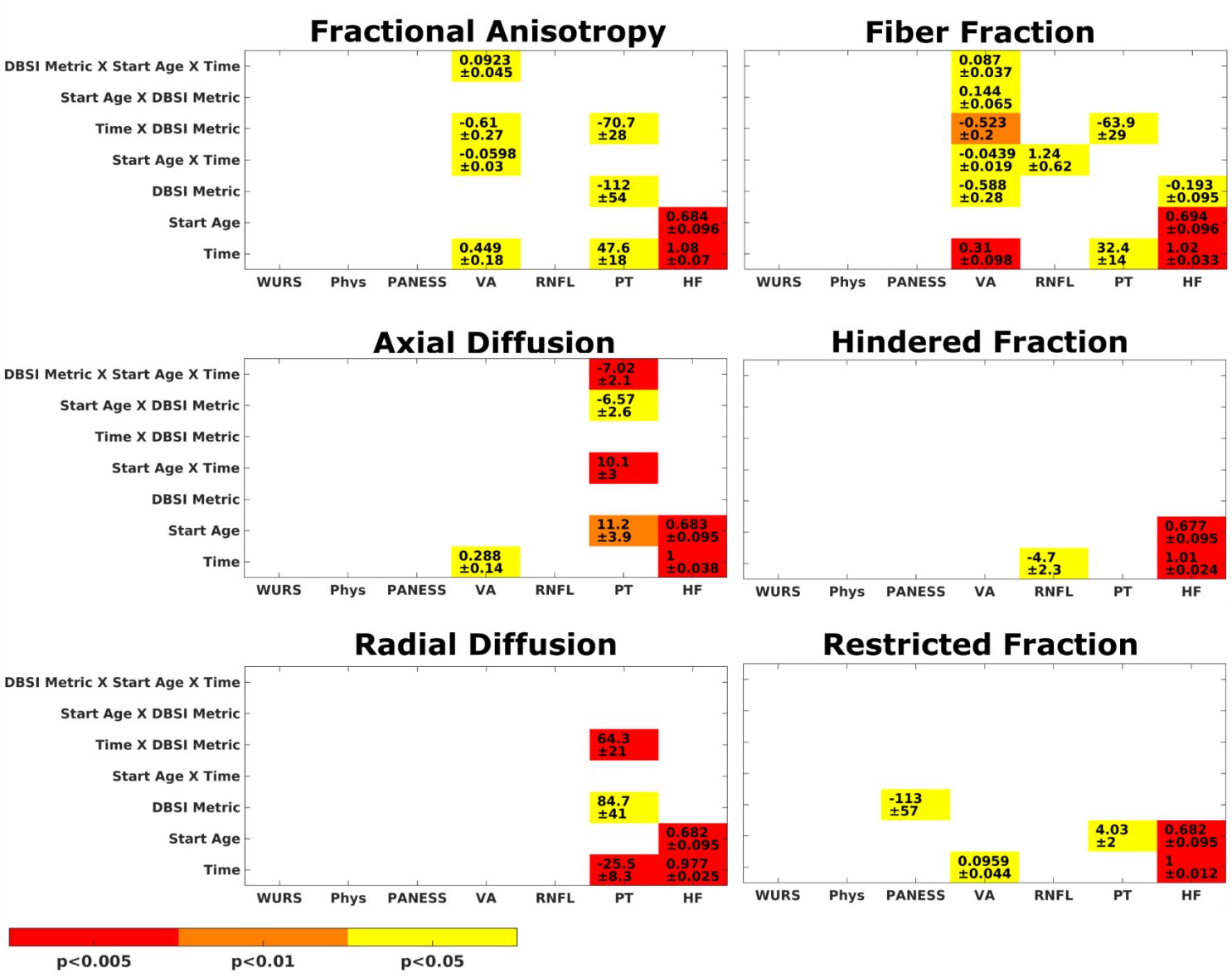

Supplementary Figure 2.2: Estimate coefficients with SE margins (p<0.05) for a linear mixed model analysis of the relationship between myelin metrics in the acoustic radiations and symptoms. Correlations with hearing are present, but so are correlations with vision. Clinical metrics: WURS overall score (WURS), WURS physical score (Phys), PANESS Score, Visual acuity (VA), RNFL thickness, Pure tone hearing (PT), High frequency hearing (HF)

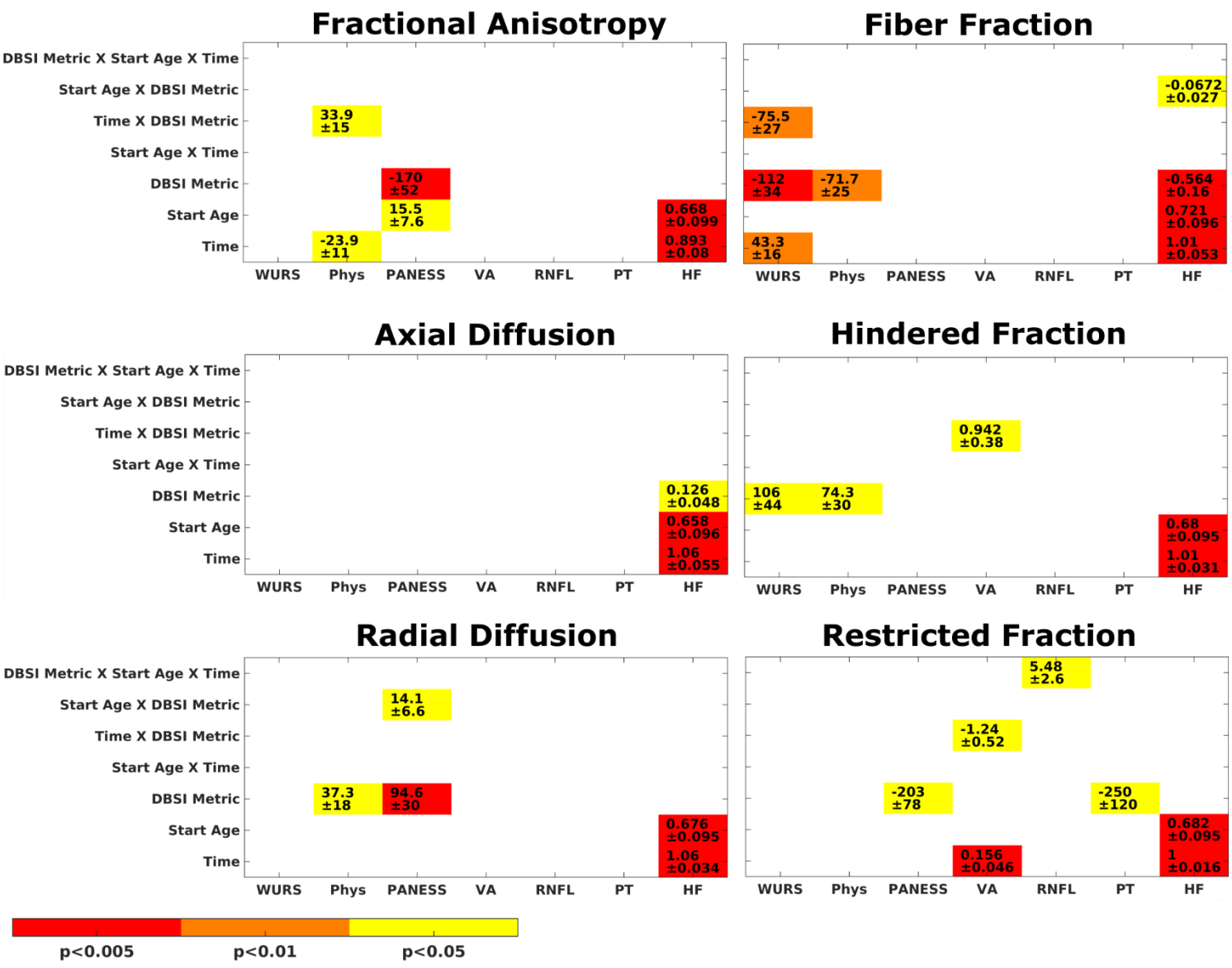

Supplementary Figure 2.3: Estimate coefficients (p<0.05) for a linear mixed model analysis of the relationship between myelin metrics in the optic radiations and symptoms. Clinical metrics: WURS overall score (WURS), WURS physical score (Phys), PANESS Score, Visual acuity (VA), RNFL thickness, Pure tone hearing (PT), High frequency hearing (HF)

2.6 Acknowledgements

We thank all of the participants and their families for their time and effort, and the study staff for their dedication. Research reported in this publication was supported by HD070855 (Hershey, PI), U54 HD087011 (Intellectual and Developmental Disabilities Research Center at Washington University), UL1 RR024992 (CTSA), DK020579 (Diabetes Research Center), The Snow Foundation, American Diabetes Association, George Decker and Julio V. Santiago Pediatric Diabetes Research Fund, Mallinckrodt Institute of Radiology and the McDonnell Center for Systems Neuroscience. We thank the former and current Washington University Wolfram Study Group Members for advice and support in the greater research program: P. Austin, MD (Surgery), B. Beato, BA (Psychiatry), E. Bihun, MA (Psychiatry), A. Bischoff, BA (Psychiatry), T. Doty, MA (Occupational Therapy), G. Earhart, PhD (Physical Therapy), S. Eisenstein, PhD (Psychiatry), T. Hershey, PhD (Psychiatry), J. Hoekel, DO (Ophthalmology), R. Karzon, PhD (Audiology & Comm. Sciences), J. Koller BSBME (Psychiatry), A. Licis, MD (Neurology), H. Lugar, MS (Psychiatry), L. Manwaring, MS (Pediatrics), B. Marshall, MD (Pediatrics), A. Narayanan, BA (Psychiatry), O. Neyman, BME (Psychiatry), A.R. Paciorkowski, MD (Neurology, URMC), T. Pearson, MD (Neurology), Y. Pepino de Gruev, PhD (University of Illinois), A. Permutt, MD (Medicine) (Deceased), K. Pickett, PhD (Physical Therapy, U Wisconsin), S. Ranck, MSW (Psychiatry), A. Reiersen, MD (Psychiatry), J. Rutlin, BS (Psychiatry), J. Shimony, MD, PhD (Radiology), L. Tychsen, MD (Ophthalmology), F. Urano MD, PhD (Medicine), A. Viehoever, MD (Neurology), J. Wasson, MS (Medicine) (Deceased), N.H. White MD, CDE (Pediatrics).

2.7 References

Angebault, C., Fauconnier, J., Patergnani, S., Rieusset, J., Danese, A., Affortit, C. A., …

Delettre, C. (2018). ER-mitochondria cross-talk is regulated by the Ca2+ sensor NCS1 and is impaired in Wolfram syndrome. *Science Signaling*, *11*(553). https://doi.org/10.1126/scisignal.aaq1380

Ashburner, J. (2007). A fast diffeomorphic image registration algorithm. *NeuroImage*, *38*(1), 95–113. https://doi.org/10.1016/j.neuroimage.2007.07.007

Barrett, T. ., Bundey, S. ., & Macleod, A. . (1995). Neurodegeneration and diabetes: UK nationwide study of Wolfram (DIDMOAD) syndrome. *The Lancet*, *346*(8988), 1458–1463. https://doi.org/10.1016/S0140-6736(95)92473-6

Barrett, T. G., & Bundey, S. E. (1997). Wolfram (DIDMOAD) syndrome. *Journal of Medical Genetics*, *34*(10), 838–841. Retrieved from http://www.ncbi.nlm.nih.gov/pubmed/9350817

Bischoff, A. N., Reiersen, A. M., Buttlaire, A., Al-lozi, A., Doty, T., Marshall, B. A., … Washington University Wolfram Syndrome Research Group. (2015). Selective cognitive and psychiatric manifestations in Wolfram Syndrome. *Orphanet Journal of Rare Diseases*, *10*(1), 66. https://doi.org/10.1186/s13023-015-0282-1

Cagalinec, M., Liiv, M., Hodurova, Z., Hickey, M. A., Vaarmann, A., Mandel, M., … Kaasik, A. (2016). Role of Mitochondrial Dynamics in Neuronal Development: Mechanism for Wolfram Syndrome. *PLoS Biology*, *14*(7). https://doi.org/10.1371/journal.pbio.1002511

Carson, M. J., Slager, U. T., & Steinberg, R. M. (1977). Simultaneous Occurrence of Diabetes Mellitus, Diabetes Insipidus, and Optic Atrophy in a Brother and Sister. *American Journal of Diseases of Children*, *131*(12), 1382–1385. https://doi.org/10.1001/archpedi.1977.02120250064010

Chaussenot, A., Bannwarth, S., Rouzier, C., Vialettes, B., Mkadem, S. A. El, Chabrol, B., … Paquis-Flucklinger, V. (2011). Neurologic features and genotype-phenotype correlation in

Wolfram syndrome. *Annals of Neurology*, *69*(3), 501–508. https://doi.org/10.1002/ana.22160

Cross, A. H., & Song, S.-K. (2017). "A new imaging modality to non-invasively assess multiple sclerosis pathology." *Journal of Neuroimmunology*, *304*, 81–85. https://doi.org/10.1016/j.jneuroim.2016.10.002

Debs, R., Froissart, R., Aubourg, P., Papeix, C., Douillard, C., Degos, B., … Sedel, F. (2013). Krabbe disease in adults: phenotypic and genotypic update from a series of 11 cases and a review. *Journal of Inherited Metabolic Disease*, *36*(5), 859–868. https://doi.org/10.1007/s10545-012-9560-4

Dobson, R., & Giovannoni, G. (2019). Multiple sclerosis - a review. *European Journal of Neurology*, *26*(1), 27–40. https://doi.org/10.1111/ene.13819

Eljamel, S., Ghosh, W., De Stone, S., Griffiths, A., Barrett, T., & Thompson, R. (2019). A cost of illness study evaluating the burden of Wolfram syndrome in the United Kingdom. *Orphanet Journal of Rare Diseases*, *14*(1), 185. https://doi.org/10.1186/s13023-019-1149-7

Fonseca, S. G., Fukuma, M., Lipson, K. L., Nguyen, L. X., Allen, J. R., Oka, Y., & Urano, F. (2005). WFS1 is a novel component of the unfolded protein response and maintains homeostasis of the endoplasmic reticulum in pacreatic β-cells. *Journal of Biological Chemistry*, *280*(47), 39609–39615. https://doi.org/10.1074/jbc.M507426200

Fonseca, S. G., Ishigaki, S., Oslowski, C. M., Lu, S., Lipson, K. L., Ghosh, R., … Urano, F. (2010). Wolfram syndrome 1 gene negatively regulates ER stress signaling in rodent and human cells. *The Journal of Clinical Investigation*, *120*(3), 744–755. https://doi.org/10.1172/JCI39678

Ganzetti, M., Wenderoth, N., & Mantini, D. (2014). Whole brain myelin mapping using T1- and

T2-weighted MR imaging data. *Frontiers in Human Neuroscience*, *8*, 671. https://doi.org/10.3389/fnhum.2014.00671

Genís, D., Dávalos, A., Molins, A., & Ferrer, I. (1997). Wolfram syndrome: A neuropathological study. *Acta Neuropathologica*, *93*(4), 426–429. https://doi.org/10.1007/s004010050635

Glasser, M. F., Goyal, M. S., Preuss, T. M., Raichle, M. E., & Van Essen, D. C. (2014). Trends and properties of human cerebral cortex: correlations with cortical myelin content. *NeuroImage*, *93 Pt 2*, 165–175. https://doi.org/10.1016/j.neuroimage.2013.03.060

Glasser, M. F., Sotiropoulos, S. N., Wilson, J. A., Coalson, T. S., Fischl, B., Andersson, J. L., … WU-Minn HCP Consortium, for the W.-M. H. (2013). The minimal preprocessing pipelines for the Human Connectome Project. *NeuroImage*, *80*, 105–124. https://doi.org/10.1016/j.neuroimage.2013.04.127

Glasser, M. F., & Van Essen, D. C. (2011). Mapping human cortical areas in vivo based on myelin content as revealed by T1- and T2-weighted MRI. *The Journal of Neuroscience : The Official Journal of the Society for Neuroscience*, *31*(32), 11597–11616. https://doi.org/10.1523/JNEUROSCI.2180-11.2011

Guillaume, B., Hua, X., Thompson, P. M., Waldorp, L., & Nichols, T. E. (2014). Fast and accurate modelling of longitudinal and repeated measures neuroimaging data. *NeuroImage*, *94*, 287–302. https://doi.org/10.1016/j.neuroimage.2014.03.029

Hatanaka, M., Tanabe, K., Yanai, A., Ohta, Y., Kondo, M., Akiyama, M., … Tanizawa, Y. (2011). Wolfram syndrome 1 gene (WFS1) product localizes to secretory granules and determines granule acidification in pancreatic β-cells. *Human Molecular Genetics*, *20*(7), 1274–1284. https://doi.org/10.1093/hmg/ddq568

Hershey, T., Lugar, H. M., Shimony, J. S., Rutlin, J., Koller, J. M., Perantie, D. C., …

Washington University Wolfram Study Group. (2012). Early brain vulnerability in Wolfram syndrome. *PloS One*, *7*(7), e40604. https://doi.org/10.1371/journal.pone.0040604

Hilson, J. B., Merchant, S. N., Adams, J. C., & Joseph, J. T. (2009). Wolfram syndrome: a clinicopathologic correlation. *Acta Neuropathologica*, *118*(3), 415–428. https://doi.org/10.1007/s00401-009-0546-8

Hoekel, J., Narayanan, A., Rutlin, J., Lugar, H., Al-Lozi, A., Hershey, T., & Tychsen, L. (2018). Visual pathway function and structure in Wolfram syndrome: Patient age, variation and progression. *BMJ Open Ophthalmology*, *3*(1). https://doi.org/10.1136/bmjophth-2017-000081

Hofstetter, S., Sabbah, N., Mohand-Saïd, S., Sahel, J. A., Habas, C., Safran, A. B., & Amedi, A. (2019). The development of white matter structural changes during the process of deterioration of the visual field. *Scientific Reports*, *9*(1). https://doi.org/10.1038/s41598-018-38430-5

Inoue, H., Tanizawa, Y., Wasson, J., Behn, P., Kalidas, K., Bernal-Mizrachi, E., … Permutt, M. A. (1998). A gene encoding a transmembrane protein is mutated in patients with diabetes mellitus and optic atrophy (Wolfram syndrome). *Nature Genetics*, *20*(2), 143–148. https://doi.org/10.1038/2441

Jackson, M. J., Bindoff, L. A., Weber, K., Wilson, J. N., Ince, P., Alberti, K. G. M. M., & Turnbull, D. M. (1994). Biochemical and Molecular Studies of Mitochondrial Function in Diabetes Insipidus, Diabetes Mellitus, Optic Atrophy, and Deafness. *Diabetes Care*, *17*(7), 728–733. https://doi.org/10.2337/diacare.17.7.728

Jenkinson, M., Beckmann, C. F., Behrens, T. E. J., Woolrich, M. W., & Smith, S. M. (2012). Review FSL. *NeuroImage*, *62*, 782–790. https://doi.org/10.1016/j.neuroimage.2011.09.015

Kinney, H. C., Brody, B. A., Kloman, A. S., & Gilles, F. H. (1988). Sequence of Central Nervous System Myelination in Human Infancy. *Journal of Neuropathology & Experimental Neurology*, *47*(3).

Lebel, C., & Beaulieu, C. (2011). Longitudinal development of human brain wiring continues from childhood into adulthood. *Journal of Neuroscience*, *31*(30), 10937–10947. https://doi.org/10.1523/JNEUROSCI.5302-10.2011

Lebel, C., Treit, S., & Beaulieu, C. (2019). A review of diffusion MRI of typical white matter development from early childhood to young adulthood. *NMR in Biomedicine*, Vol. 32. https://doi.org/10.1002/nbm.3778

Lee, K., Cherel, M., Budin, F., Gilmore, J., Zaldarriaga Consing, K., Rasmussen, J., … Styner, M. (2015). Early postnatal myelin content estimate of white matter via T1w/T2w ratio. *Medical Imaging 2015: Biomedical Applications in Molecular, Structural, and Functional Imaging*, *9417*, 94171R. https://doi.org/10.1117/12.2082198

Licis, A., Davis, G., Eisenstein, S. A., Lugar, H. M., & Hershey, T. (2019). Sleep disturbances in Wolfram syndrome. *Orphanet Journal of Rare Diseases*, *14*(1). https://doi.org/10.1186/s13023-019-1160-z

Lugar, H. M., Koller, J. M., Rutlin, J., Eisenstein, S. A., Neyman, O., Narayanan, A., … Hershey, T. (2019). Evidence for altered neurodevelopment and neurodegeneration in Wolfram syndrome using longitudinal morphometry. *Scientific Reports*, *9*(1), 6010. https://doi.org/10.1038/s41598-019-42447-9

Lugar, H. M., Koller, J. M., Rutlin, J., Marshall, B. A., Kanekura, K., Urano, F., … Washington University Wolfram Syndrome Research Study Group. (2016). Neuroimaging evidence of deficient axon myelination in Wolfram syndrome. *Scientific Reports*, *6*, 21167.

https://doi.org/10.1038/srep21167

Manners, D. N., Rizzo, G., La Morgia, C., Tonon, C., Testa, C., Barboni, P., … Lodi, R. (2015). Diffusion tensor imaging mapping of brain white matter pathology in mitochondrial optic neuropathies. *American Journal of Neuroradiology*, *36*(7), 1259–1265. https://doi.org/10.3174/ajnr.A4272

Marshall, B. A., Permutt, M. A., Paciorkowski, A. R., Hoekel, J., Karzon, R., Wasson, J., … Washington University Wolfram Study Group. (2013). Phenotypic characteristics of early Wolfram syndrome. *Orphanet Journal of Rare Diseases*, *8*, 64. https://doi.org/10.1186/1750-1172-8-64

Mollison, D., Sellar, R., Bastin, M., Mollison, D., Chandran, S., Wardlaw, J., & Connick, P. (2017). The clinico-radiological paradox of cognitive function and MRI burden of white matter lesions in people with multiple sclerosis: A systematic review and meta-analysis. *PLOS ONE*, *12*(5), e0177727. https://doi.org/10.1371/journal.pone.0177727

Mutlu, U., Ikram, M. K., Roshchupkin, G. V., Bonnemaijer, P. W. M., Colijn, J. M., Vingerling, J. R., … Vernooij, M. W. (2018). Thinner retinal layers are associated with changes in the visual pathway: A population-based study. *Human Brain Mapping*, *39*(11), 4290–4301. https://doi.org/10.1002/hbm.24246

Nguyen, C., Foster, E. R., Paciorkowski, A. R., Viehoever, A., Considine, C., Bondurant, A., … Washington University Wolfram Study Group. (2012). Reliability and validity of the Wolfram Unified Rating Scale (WURS). *Orphanet Journal of Rare Diseases*, *7*, 89. https://doi.org/10.1186/1750-1172-7-89

Padmanabhan, A., Parihar, A., C Vartak, U., & Gadgil, N. (2019). Wolfram syndrome: A rare case report. *Indian Journal of Pathology and Microbiology*, *62*(3), 477–480.

https://doi.org/10.4103/IJPM.IJPM_397_18

Pickett, K. A., Duncan, R. P., Hoekel, J., Marshall, B., Hershey, T., & Earhart, G. M. (2012). Early presentation of gait impairment in Wolfram Syndrome. *Orphanet Journal of Rare Diseases*, *7*, 92. https://doi.org/10.1186/1750-1172-7-92

Pickett, K. A., Duncan, R. P., Paciorkowski, A. R., Permutt, M. A., Marshall, B., Hershey, T., … Washington University Wolfram Study Group. (2012). Balance impairment in individuals with Wolfram syndrome. *Gait & Posture*, *36*(3), 619–624. https://doi.org/10.1016/j.gaitpost.2012.06.008

Roth, A. D., & Núñez, M. T. (2016). *Oligodendrocytes: Functioning in a Delicate Balance Between High Metabolic Requirements and Oxidative Damage*. https://doi.org/10.1007/978-3-319-40764-7_8

Samara, A., Rahn, R., Neyman, O., Park, K. Y., Samara, A., Marshall, B., … Hershey, T. (2019, December 3). Developmental hypomyelination in Wolfram syndrome: New insights from neuroimaging and gene expression analyses. *Orphanet Journal of Rare Diseases*, Vol. 14. https://doi.org/10.1186/s13023-019-1260-9

Shannon, P., Becker, L., & Deck, J. (1999). Evidence of widespread axonal pathology in Wolfram syndrome. *Acta Neuropathologica*, *98*(3), 304–308. Retrieved from http://www.ncbi.nlm.nih.gov/pubmed/10483789

Takeda, K. (2001). WFS1 (Wolfram syndrome 1) gene product: predominant subcellular localization to endoplasmic reticulum in cultured cells and neuronal expression in rat brain. *Human Molecular Genetics*, *10*(5), 477–484. https://doi.org/10.1093/hmg/10.5.477

Takei, D., Ishihara, H., Yamaguchi, S., Yamada, T., Tamura, A., Katagiri, H., … Oka, Y. (2006). WFS1 protein modulates the free Ca2+ concentration in the endoplasmic reticulum. *FEBS*

Letters, *580*(24), 5635–5640. https://doi.org/10.1016/j.febslet.2006.09.007

Ueda, K., Kawano, J., Takeda, K., Yujiri, T., Tanabe, K., Anno, T., … Tanizawa, Y. (2005). Endoplasmic reticulum stress induces Wfs1 gene expression in pancreatic β-cells via transcriptional activation. *European Journal of Endocrinology*, *153*(1), 167–176. https://doi.org/10.1530/eje.1.01945

Volpi, V. G., Touvier, T., & D'Antonio, M. (2017). Endoplasmic Reticulum Protein Quality Control Failure in Myelin Disorders. *Frontiers in Molecular Neuroscience*, *9*, 162. https://doi.org/10.3389/fnmol.2016.00162

Wang, D., Qin, W., Liu, Y., Zhang, Y., Jiang, T., & Yu, C. (2013). Altered white matter integrity in the congenital and late blind people. *Neural Plasticity*, *2013*. https://doi.org/10.1155/2013/128236

Wang, Y., Sun, P., Wang, Q., Trinkaus, K., Schmidt, R. E., Naismith, R. T., … Song, S.-K. (2015). Differentiation and quantification of inflammation, demyelination and axon injury or loss in multiple sclerosis. *Brain : A Journal of Neurology*, *138*(Pt 5), 1223–1238. https://doi.org/10.1093/brain/awv046

Wang, Y., Wang, Q., Haldar, J. P., Yeh, F.-C., Xie, M., Sun, P., … Song, S.-K. (2011). Quantification of increased cellularity during inflammatory demyelination. *Brain*, *134*(12), 3590–3601. https://doi.org/10.1093/brain/awr307

Woolrich, M. W., Jbabdi, S., Patenaude, B., Chappell, M., Makni, S., Behrens, T., … Smith, S. M. (2009). Bayesian analysis of neuroimaging data in FSL. *NeuroImage*, *45*(1 Suppl). https://doi.org/10.1016/j.neuroimage.2008.10.055

Yamada, T., Ishihara, H., Tamura, A., Takahashi, R., Yamaguchi, S., Takei, D., … Oka, Y. (2006). WFS1-deficiency increases endoplasmic reticulum stress, impairs cell cycle

progression and triggers the apoptotic pathway specifically in pancreatic β-cells. *Human Molecular Genetics*, *15*(10), 1600–1609. https://doi.org/10.1093/hmg/ddl081

Yeung, M. S. Y., Zdunek, S., Bergmann, O., Bernard, S., Salehpour, M., Alkass, K., … Frisé, J. (2014). Dynamics of Oligodendrocyte Generation and Myelination in the Human Brain. *Cell*, *159*, 766–774. https://doi.org/10.1016/j.cell.2014.10.011

Yurimoto, S., Hatano, N., Tsuchiya, M., Kato, K., Fujimoto, T., Masaki, T., … Tokumitsu, H. (2009). Identification and characterization of wolframin, the product of the Wolfram syndrome gene (WFS1), as a novel calmodulin-binding protein. *Biochemistry*, *48*(18), 3946–3955. https://doi.org/10.1021/bi900260y

Zmyslowska, A., Fendler, W., Waszczykowska, A., Niwald, A., Borowiec, M., Jurowski, P., & Mlynarski, W. (2017). Retinal thickness as a marker of disease progression in longitudinal observation of patients with Wolfram syndrome. *Acta Diabetologica*, *54*(11), 1019–1024. https://doi.org/10.1007/s00592-017-1042-6

Chapter 3: Development of Myelin in Gray Matter

3.1 Introduction

To date, the study of myelin involvement in Wolfram syndrome has been mostly limited to the white matter of the brain, which is known to be seriously compromised (Lugar et al., 2019, 2016), possibly due to the susceptibility of oligodendrocytes to ER stress (Rosko, Smith, Yamazaki, & Huang, 2019). However, myelin is also present in gray matter, albeit in significantly smaller amounts (Timmler & Simons, 2019). It could thus be hypothesized that the myelin in gray matter is also vulnerable in Wolfram syndrome.

The assessment of myelin in such regions is predominantly done using magnetization transfer or the simultaneous tissue relaxometry of R_1 and R_2 relaxation rates and proton density, both of which has been found to correlate well with histology (Heath, Hurley, Johansen-Berg, & Sampaio-Baptista, 2018). While these are the gold standard, they are not typically available in a standard set of sequences that may be collected during a study. An alternative approach is to use myelin mapping.

Myelin mapping uses the T1w/T2w ratio as a surrogate marker for myelin (referred to as myelin index in this chapter). It was originally developed by Glasser et al. as a method of increasing the signal to noise ratio, enhancing the contrast correlated with myelin (Glasser et al., 2013; Glasser & Van Essen, 2011). The original application took advantage of myelin gradients to generate brain parcellations, but has since been used in several studies as a quantifiable myelin metric (Ganzetti, Wenderoth, & Mantini, 2014; Lee et al., 2015).

In this chapter, we thus aim to assess whether myelin outside of the heavily myelinated white matter tracts is also affected in Wolfram syndrome and explore how robust any findings may be by examining the myelin index in better understood regions of the brain. We also explore two different approaches of calculating the myelin index within the gray matter: a ribbon method

which aims to take a core sample from the middle of the cortical layers and a whole area method which should be impacted less by cortical thinning.

3.2 Methodology

A myelin index was calculated using a T1w/T2w ratio. Myelin mapping was performed using the Minimal Processing Pipeline from the Human Connectome Project, with modifications that would allow for a quantifiable comparison of subjects (Glasser et al., 2013). Per the pipeline, T1w and T2w images were motion and eddy current corrected. Freesurfer surfaces were generated to be used for parcellations and graphical representation. A custom, HCP-specific version of Freesurfer was used as this version includes an update that improves surface accuracy. The myelin index was then calculated across the brain by simply finding the T1w/T2w ratio. In order to allow for meaningful comparison between subjects and sessions, images needed to be normalized. Normalization could not depend on either white or gray matter as these are the areas of interest being tested and are not expected to be consistent between groups. Instead, a mask of the face, outside of the brain and including the eyeballs, was drawn in standard MNI space and then registered to the native T1w and T2w images (Lee et al., 2015). The distribution of the myelin index within the face ROI was found for each subject in its native space. A minimum mode and whole region mode was found using the peaks of a kernel regression of the distribution. These modes, along with standardized values were used for linear rescaling for the original T1w/T2w image.

Regions for analysis were defined per FreeSurfer parcellations. To control for noise, the myelin index distributions within each parcellation were thresholded to eliminate the extreme tails of the distributions. Gray matter myelin within the cortex was examined by averaging the

myelin index over two sets of regions: whole regions and mid-thickness ribbon. The midthickness ribbon was generated by averaging the coordinates of the pial and white matter surfaces. Subcortical regions were assessed using whole region averages of FreeSurfer parcellations. Outliers were removed as defined by being more than 1.5 interquartile ranges above the upper quartile or below the lower quartile.

Statistical significance was assessed using student t tests for cross-sectional analysis and mixed linear modeling for longitudinal analysis. The model used for mixed linear modeling is as follows:

Myelin = Group + Age + Time + Group X Age + Group X Time + Group X Age X Time + (Time | Subjects)

An analysis comparing myelin mapping and conventional diffusion-weighted imaging was also completed. Normalized myelin index maps were registered through T1w images to b0 images. Myelin index values were averaged over the white matter tracts discussed in Chapter 2 and compared to FA averages of corresponding areas using Pearson coefficients.

3.3 Results

Myelin Index in the Cortical Gray Matter – Whole Region Averages

A cross-sectional group comparison was first done, comparing the myelin index within full parcellations of cortical gray matter, as shown in Figure 3.1 below. There were no

statistically significant differences between groups. Unexpectedly, in many of the parcellations, the Wolfram group was larger than the control group.

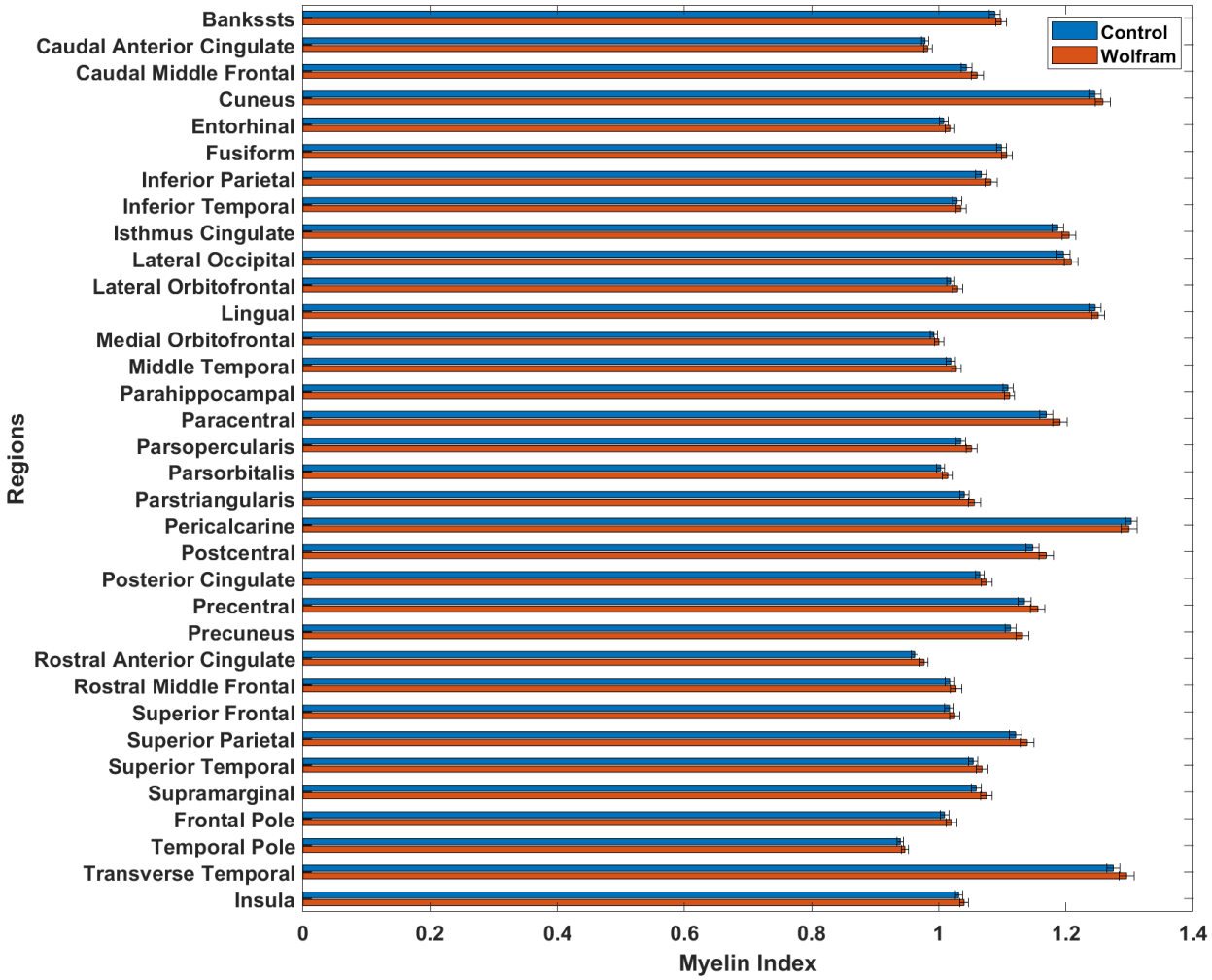

Figure 3.1 Cross-sectional differences of myelin in cortical regions

The raw data showing the average myelin index for each region is shown in Figure 2, with control subjects in green and Wolfram subjects in blue. Age is on the x-axis. Even with outliers removed, a substantial amount of noise is visible in the plots, and points in different

regions across the same subject are correlated with each. Differences between the two groups are not evident.

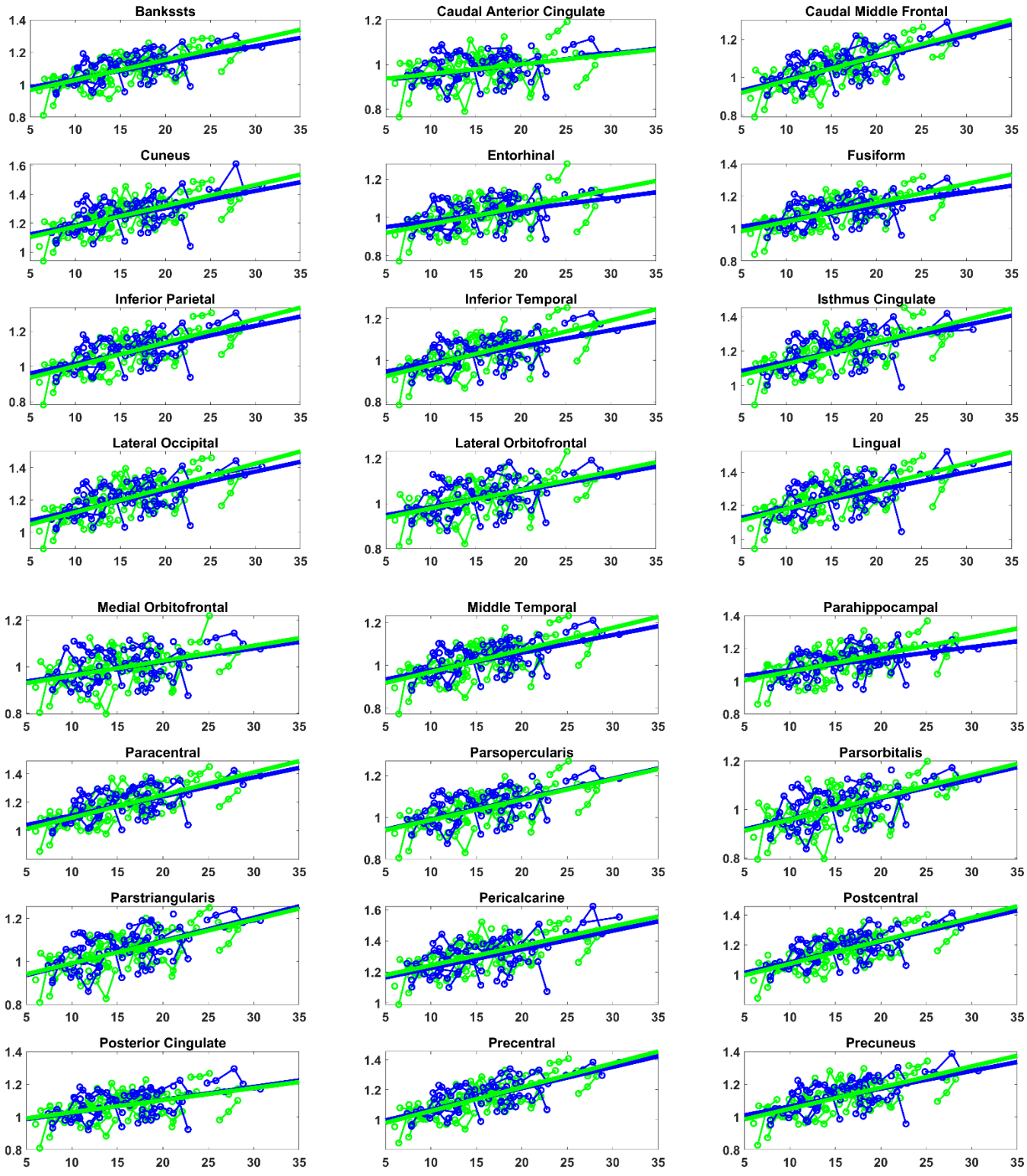
Bankssts
Caudal Anterior Cingulate
Caudal Middle Frontal
Cuneus
Entorhinal
Fusiform
Inferior Parietal
Inferior Temporal
Isthmus Cingulate
Lateral Occipital
Lateral Orbitofrontal
Lingual
Medial Orbitofrontal
Middle Temporal
Parahippocampal
Paracentral
Parsopercularis
Parsorbitalis
Parstriangularis
Pericalcarine
Postcentral
Posterior Cingulate
Precentral
Precuneus

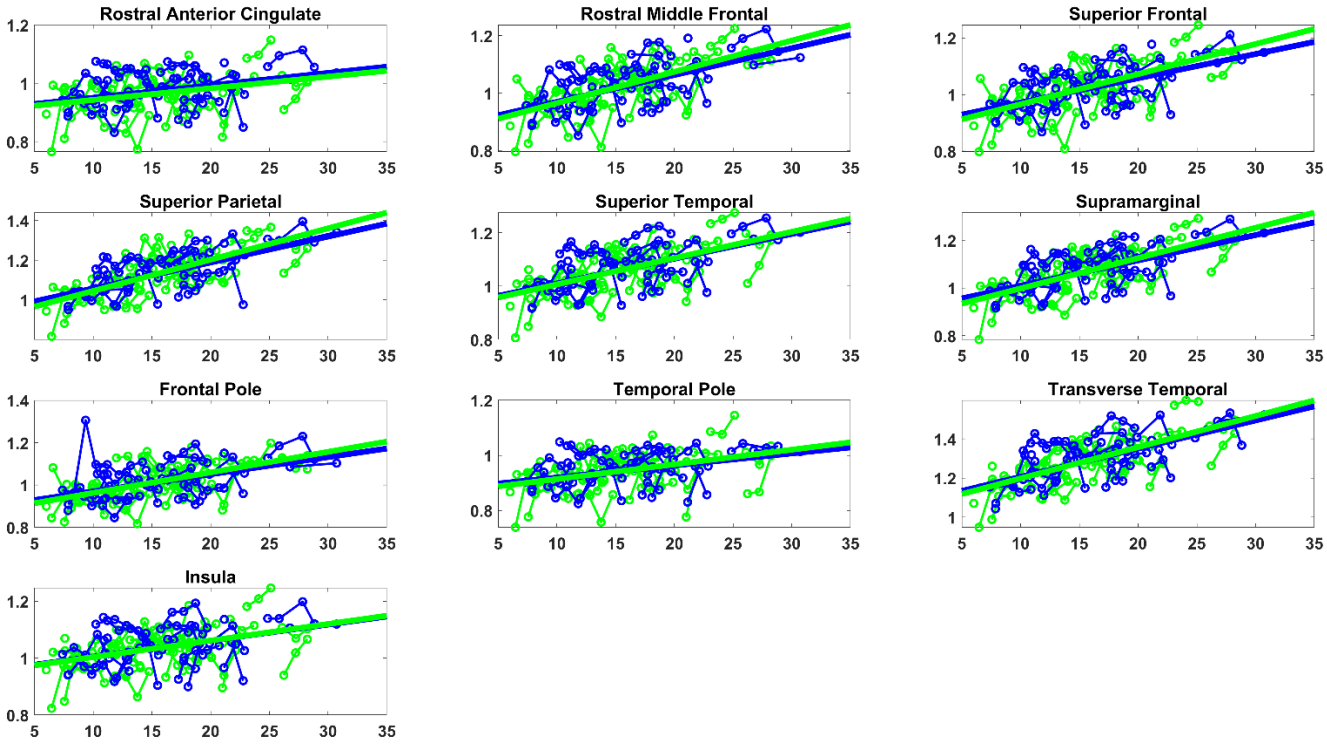

Figure 3.2 Myelin index in Wolfram (blue) and control (green) subjects in cortical areas. Age is on the x-axis

Statistical assessment of group differences within each region was done using mixed linear models. A couple regions show a significant group X time interaction: parahippocampal, temporal pole, and superior temporal regions, with controls demonstrating a slightly larger increase in myelin index over time. A significant start age and time effect were present in almost every region.

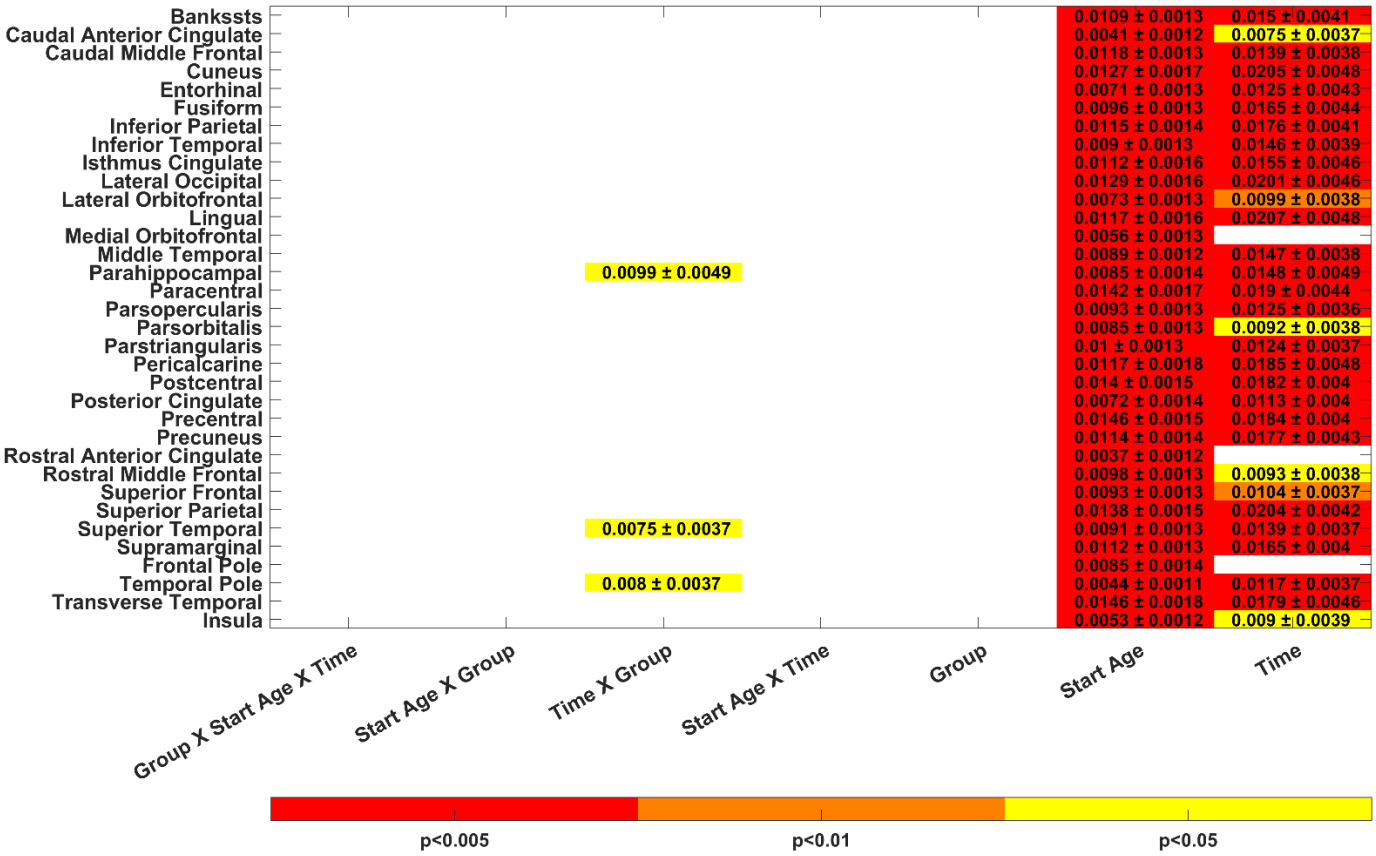

Figure 3.3 Mixed linear model results for cortical areas. Significant (p<0.05) estimate coefficients with SE margins are shown.

Myelin Index in the Cortical Gray Matter – Midthickness Ribbon Averages

Myelin index in the cortical gray matter was then examined using only the average of a midthickness ribbon between the pial and white matter surfaces. The cross-sectional comparison of groups, without taking age into account, it shown below. There are no statistically significant differences, however now the control group tends to have a larger myelin index than the Wolfram group, was would be predicted. While not significant, the largest difference is in the pericalcarine region.

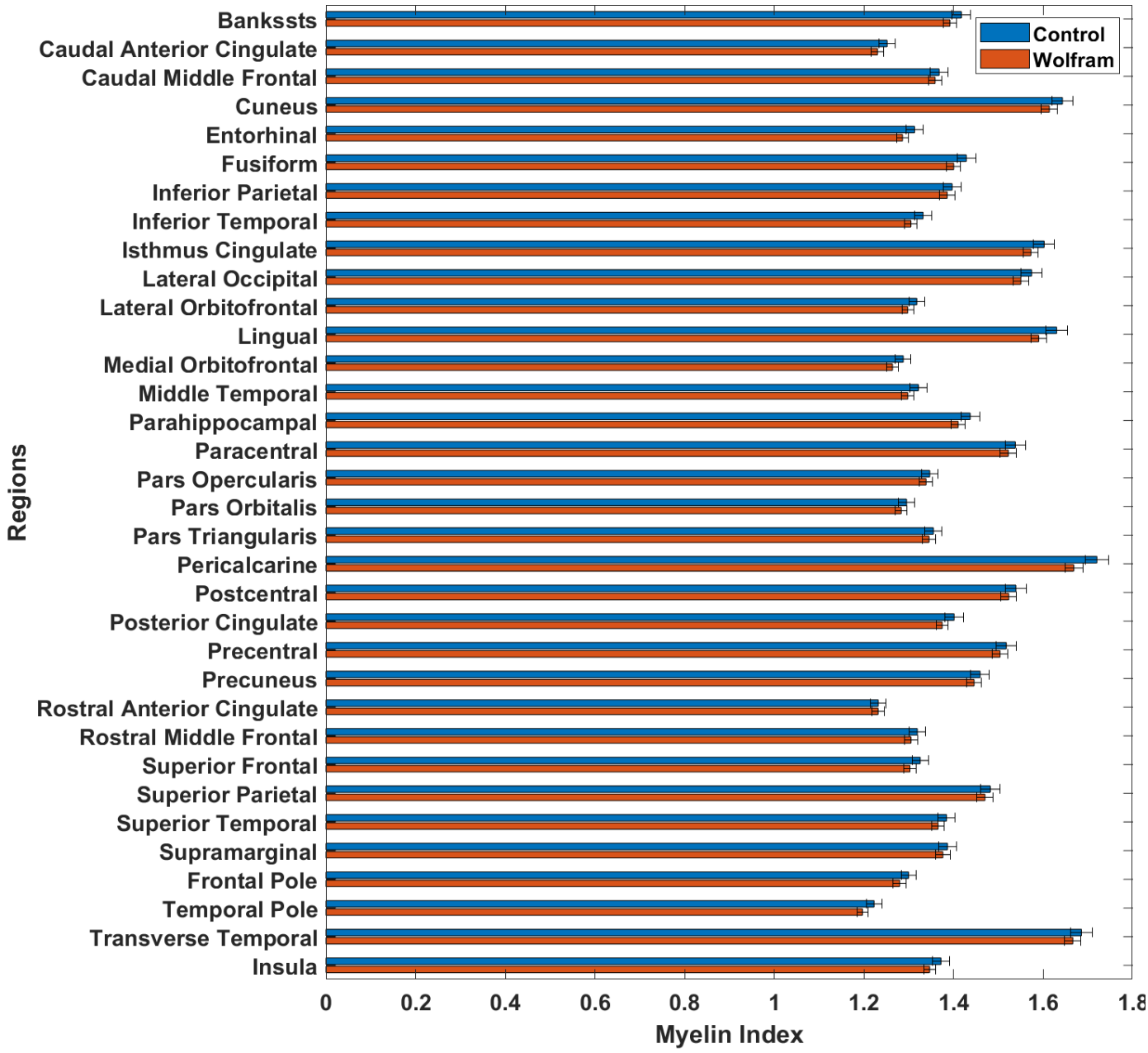

Figure 3.4 Cross-sectional differences of myelin in cortical regions using the mid-thickness approach

Average myelin index for each region, averaging over the midthickness ribbon, is shown in the figure below, with control subjects in green and Wolfram subjects in blue. Age is on the x axis. Data is noisy within subjects and no obvious group differences are present. In most cases, the control group has a slightly higher slope line with respect to age, the rostral anterior cingulate is a particular exception to this trend.

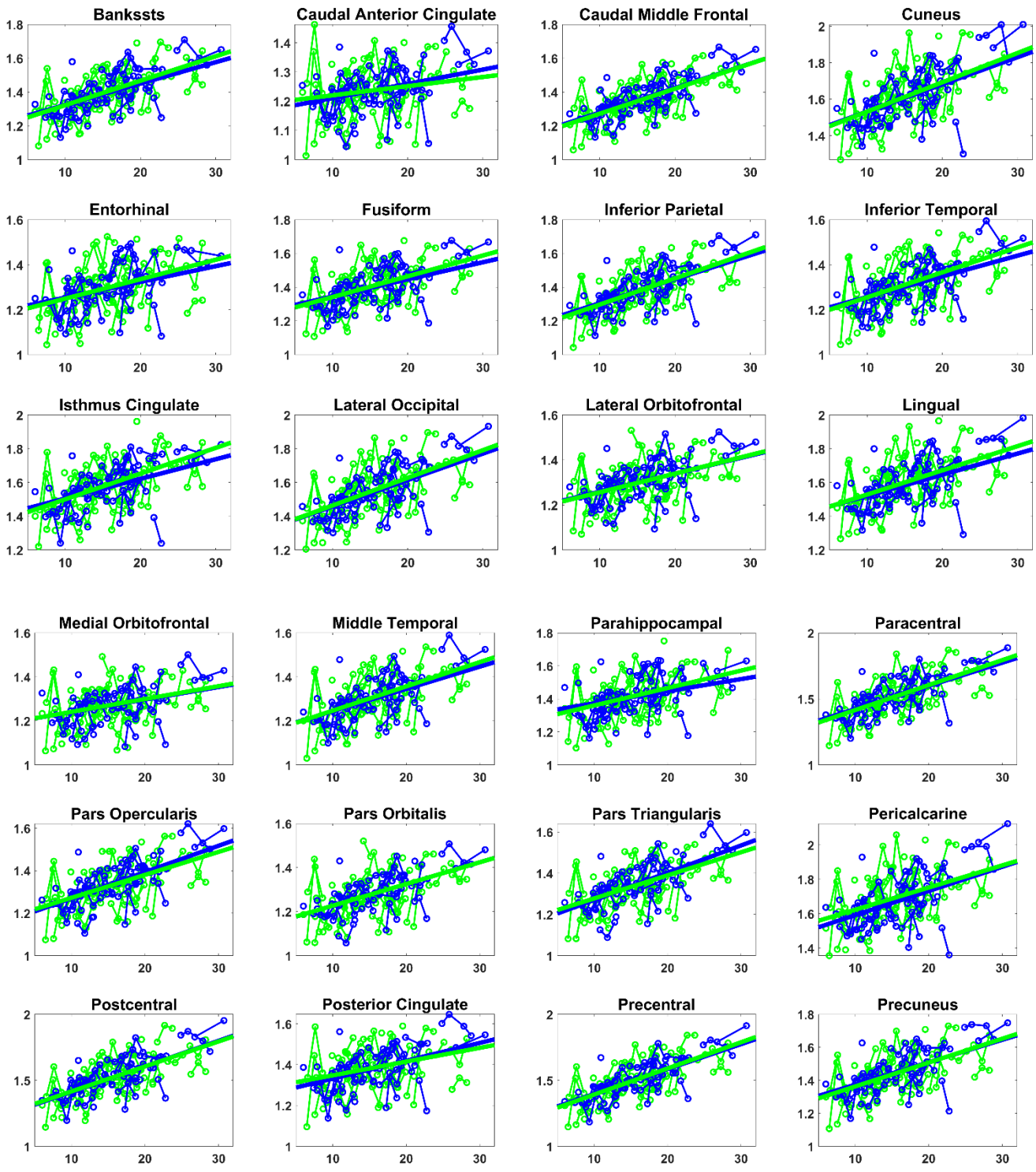
Bankssts
Caudal Anterior Cingulate
Caudal Middle Frontal
Cuneus
Entorhinal
Fusiform
Inferior Parietal
Inferior Temporal
Isthmus Cingulate
Lateral Occipital
Lateral Orbitofrontal
Lingual
Medial Orbitofrontal
Middle Temporal
Parahippocampal
Paracentral
Pars Opercularis
Pars Orbitalis
Pars Triangularis
Pericalcarine
Postcentral
Posterior Cingulate
Precentral
Precuneus

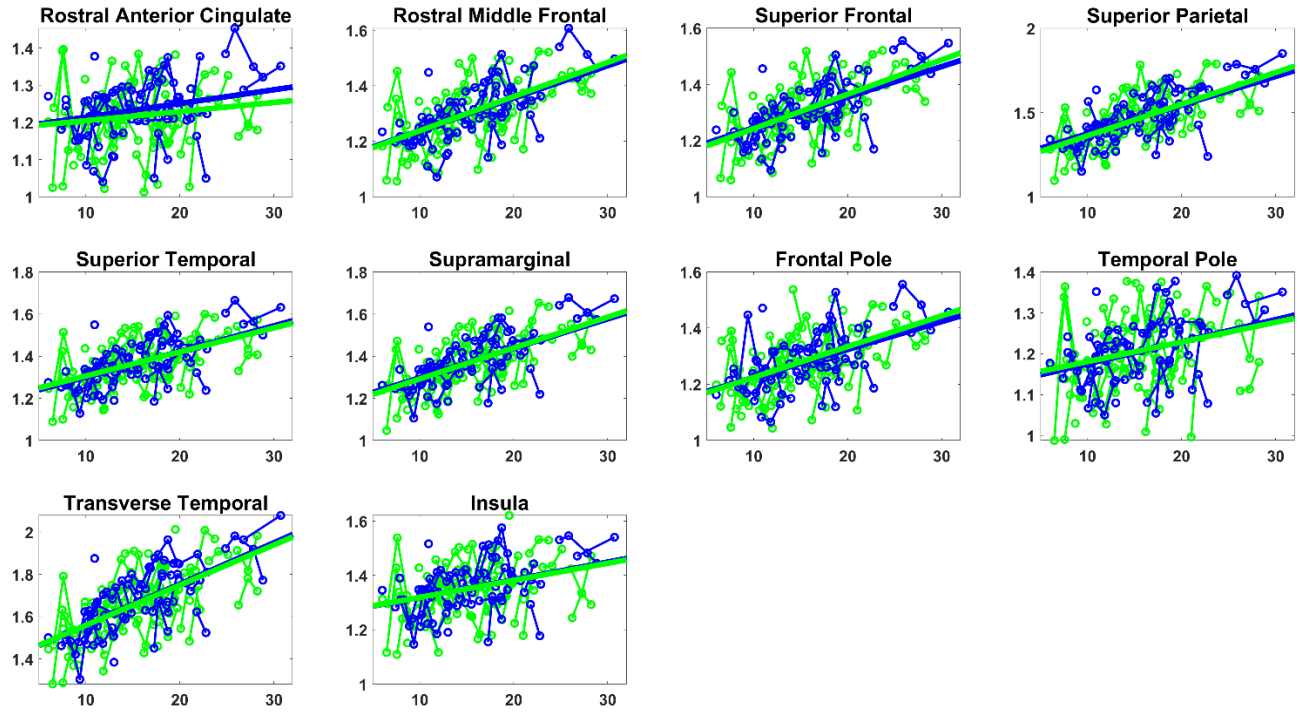

Figure 3.5 Myelin index in Wolfram (blue) and control (green) subjects in cortical areas using the mid-thickness approach. Age is on the x-axis

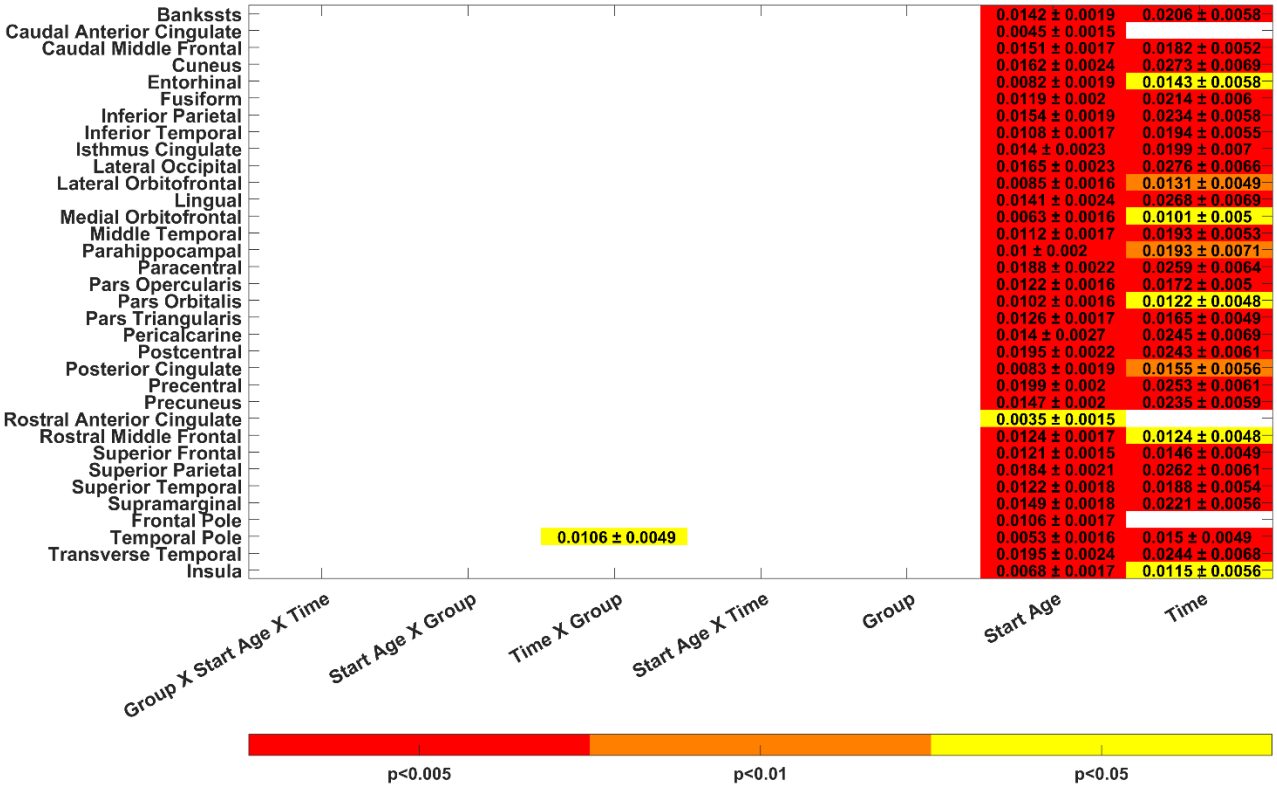

Figure 3.6 Mixed linear model results for cortical areas using the mid-thickness approach. Significant (p<0.05) estimate coefficients with SE margins are shown.

Mixed linear analysis of group differences only showed a singular time X group interaction in the temporal pole. The effect of start age and time was significant in almost every region.

Subcortical Myelin Index

Average myelin index was calculated within a series of subcortical areas. In a cross-sectional group analysis, three regions shows a statistically significant difference with a higher

myelin index in controls: cerebellar cortex (p=0.0092), cerebellar white matter (p=0.0291), and the brainstem (p=0.000042), not corrected for multiple comparisons.

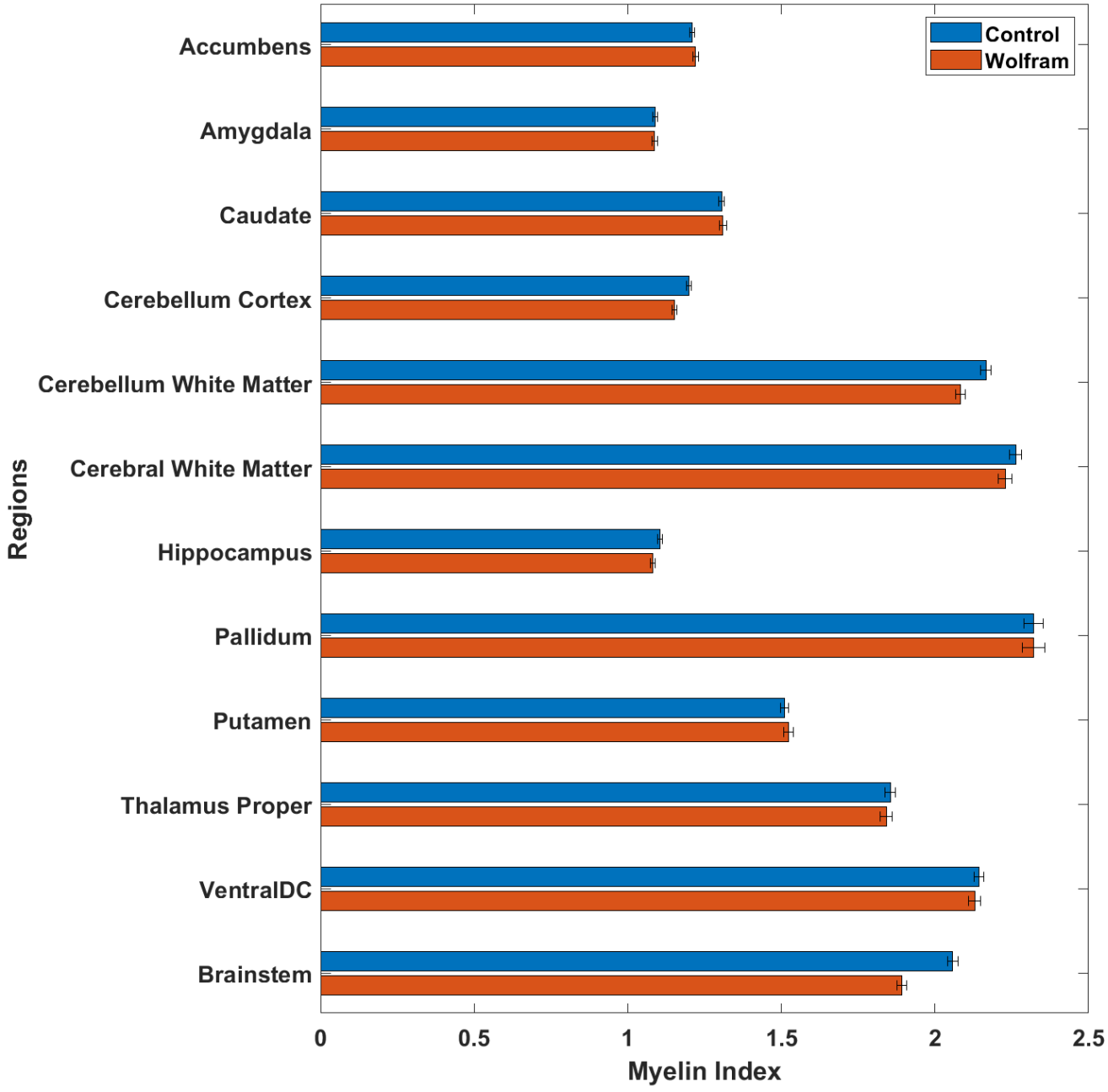

Figure 3.7 Cross-sectional differences of myelin in subcortical regions

Plots of the myelin index within the subcortical regions is shown below, with controls shown in green and Wolfram subjects shown in blue. The brainstem stands out with the largest group differences, and ones that are present from the youngest participants in the study. Trends of a diverging trajectory over age are visible in a handful of regions, including the cerebellar cortex, cerebellar white matter, and hippocampus.

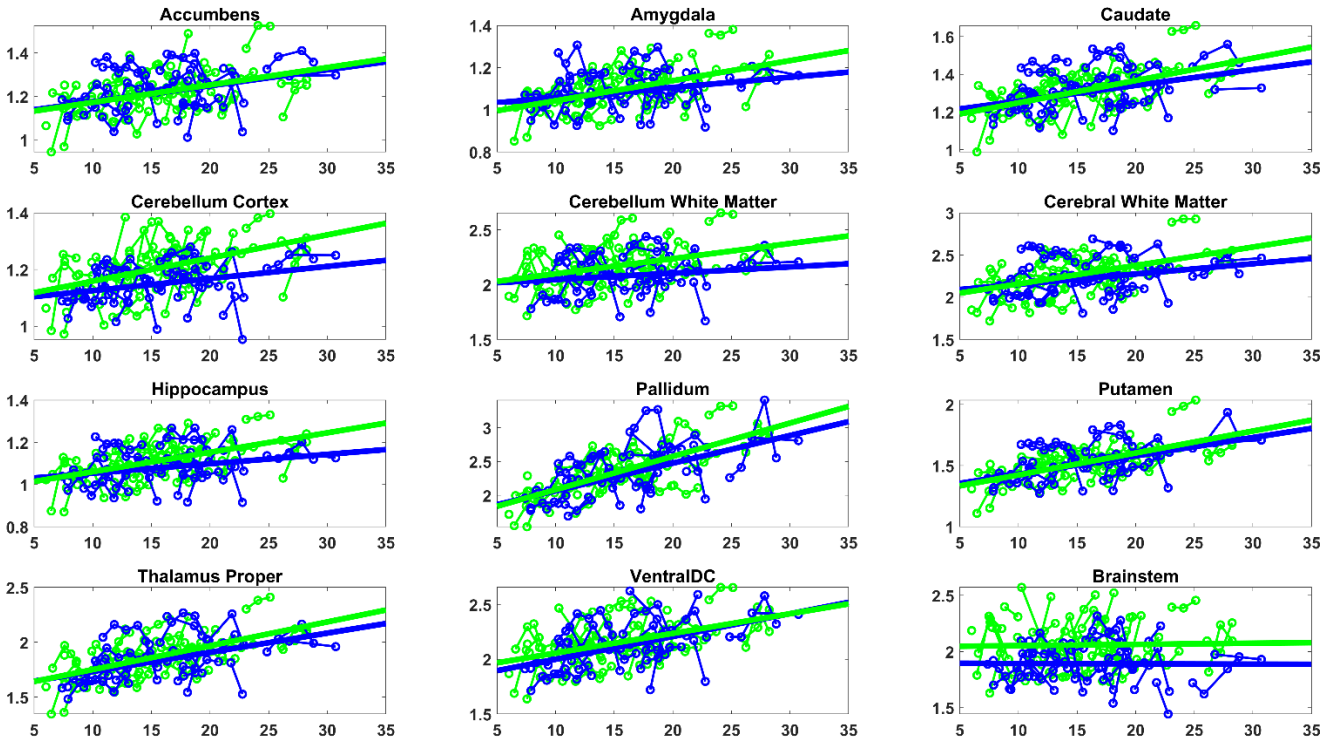

Figure 3.14 Myelin index in Wolfram (blue) and control (green) subjects in subcortical areas. Age is on the x-axis

Mixed linear model analysis showed significant group X time interactions in the amygdala, cerebellar cortex, and hippocampus. Group differences were found in the cerebellar cortex, cerebellar white matter, hippocampus, and brainstem. Age and time effects were present in almost all regions. They are notably absent from the brainstem, which shows the largest group difference.

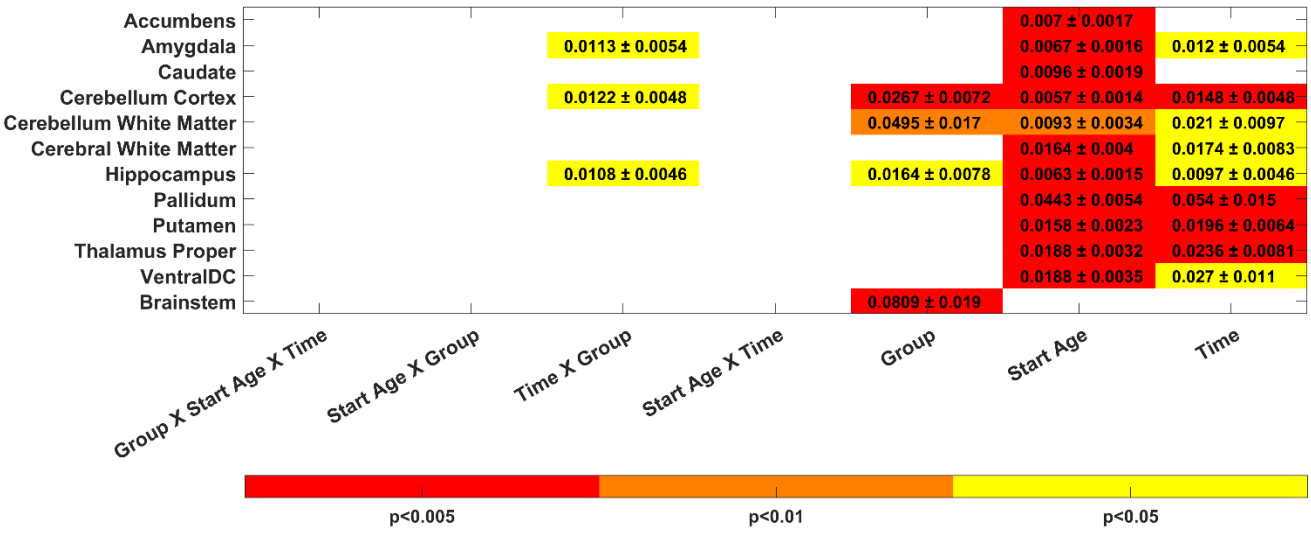

Figure 3.9 Mixed linear model results for subcortical areas. Significant (p<0.05) estimate coefficients with SE margins are shown.

Myelin Index in the White Matter

The myelin index was calculated across FreeSurfer regions of white matter, as shown below. No significant differences are found between groups, however the trend of a higher myelin index in controls is present in every region.

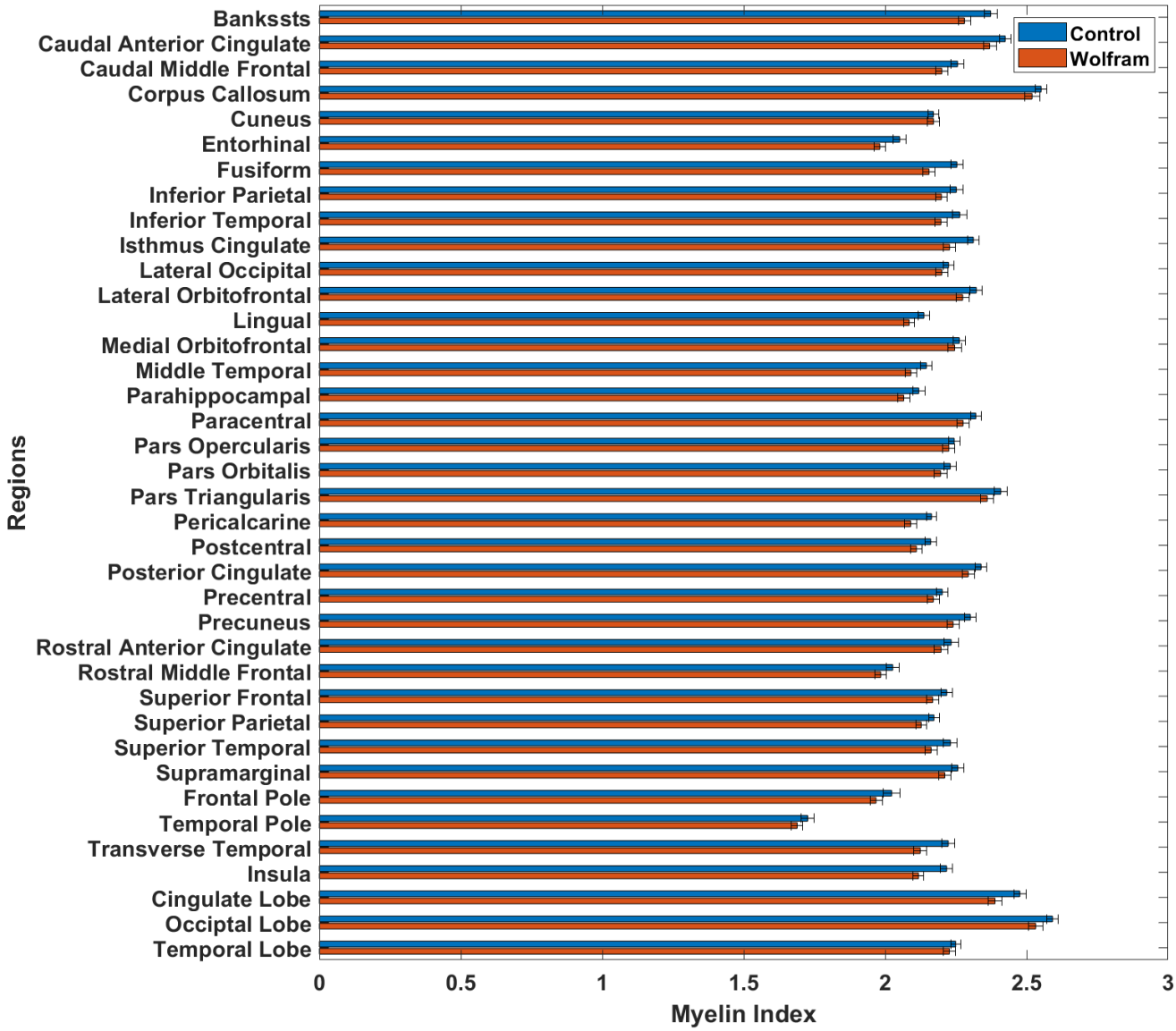

Figure 3.10 Cross-sectional differences of myelin in white matter

The myelin index in the white matter regions is shown on a subject level below, with controls in green and Wolfram subjects in blue. Noise between and within subjects is present, though all regions show a slightly higher slope with respect to age in controls.

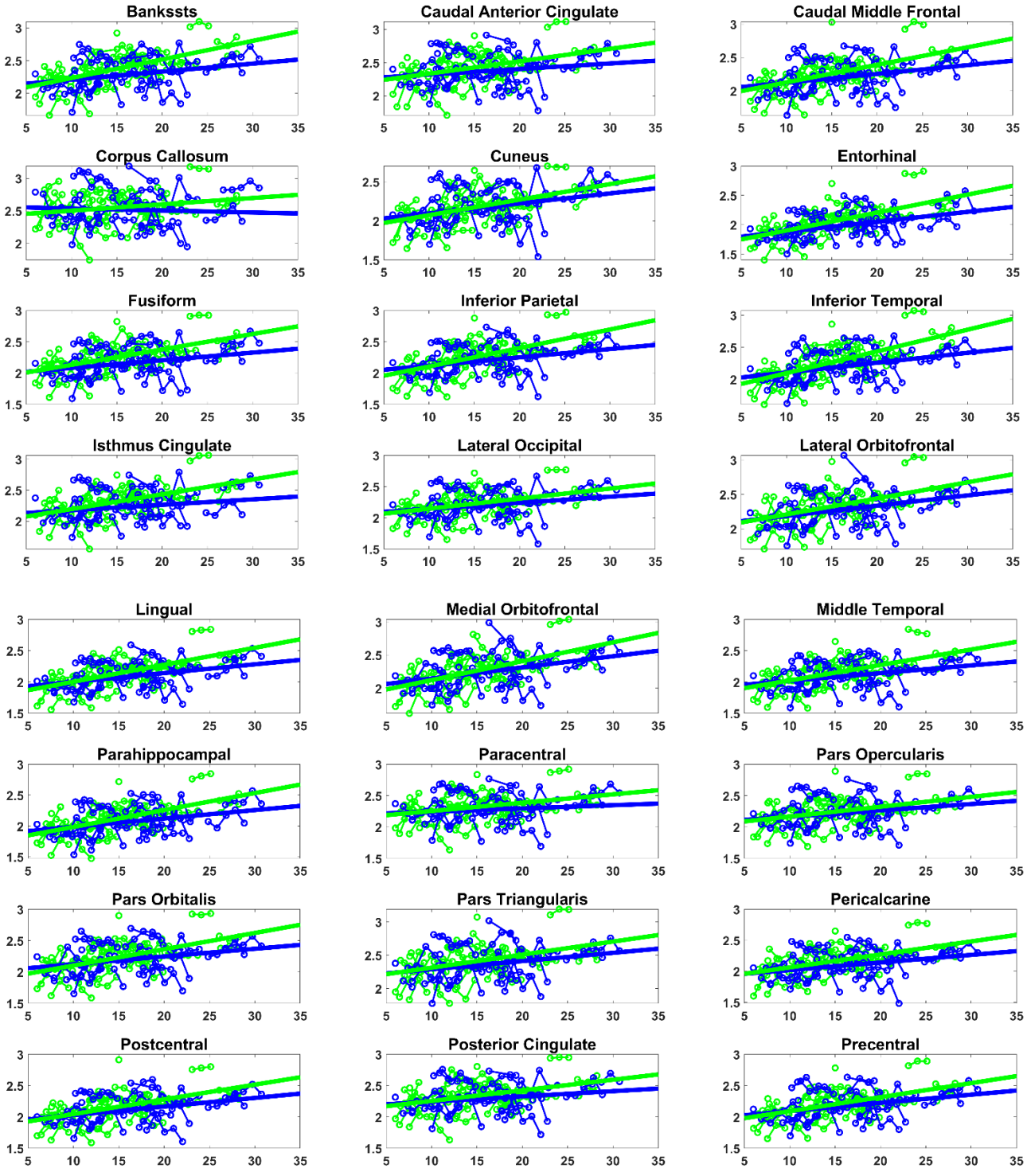
Bankssts
Caudal Anterior Cingulate
Caudal Middle Frontal
Corpus Callosum
Cuneus
Entorhinal
Fusiform
Inferior Parietal
Inferior Temporal
Isthmus Cingulate
Lateral Occipital
Lateral Orbitofrontal
Lingual
Medial Orbitofrontal
Middle Temporal
Parahippocampal
Paracentral
Pars Opercularis
Pars Orbitalis
Pars Triangularis
Pericalcarine
Postcentral
Posterior Cingulate
Precentral

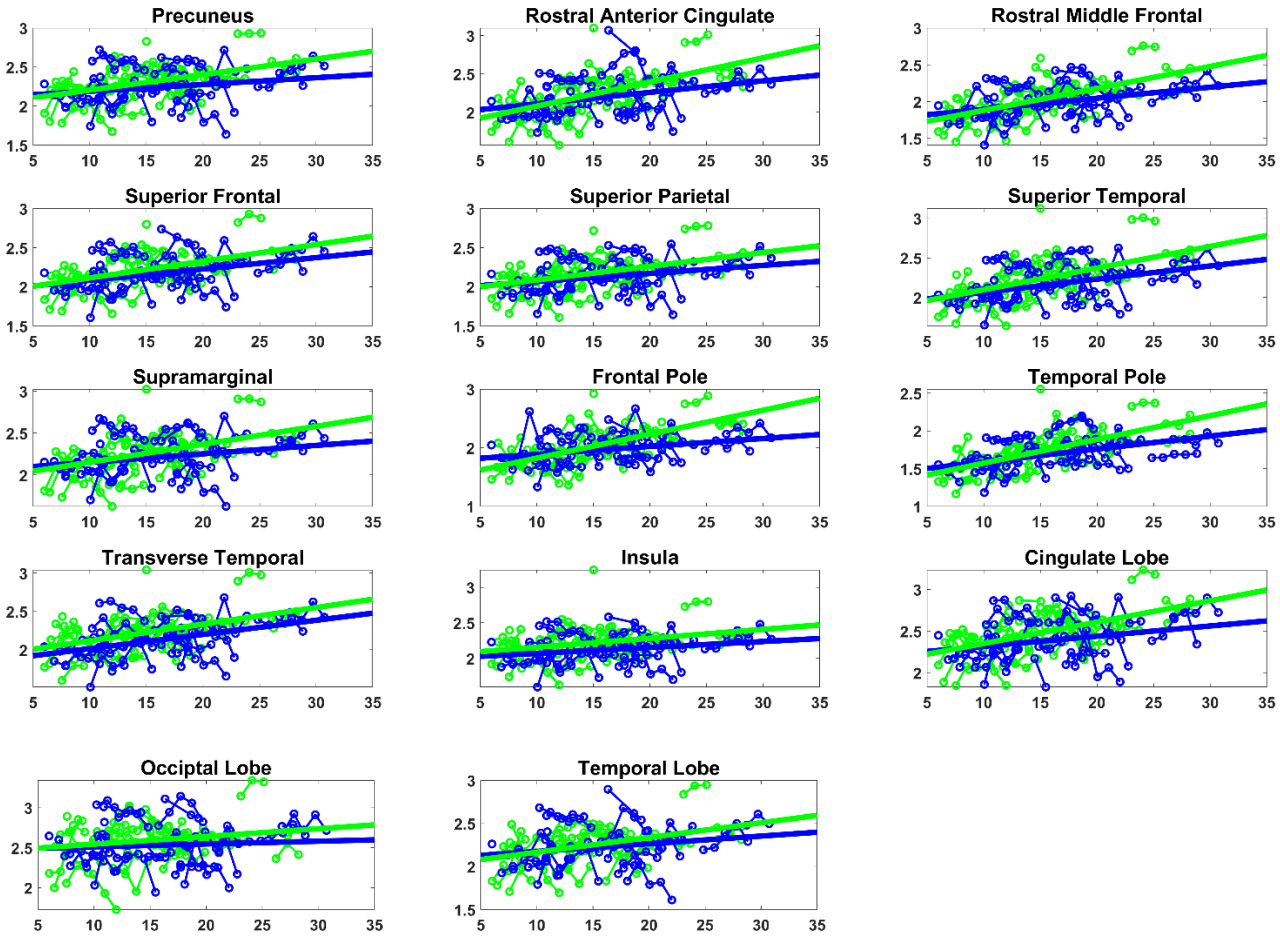

Figure 3.11 Myelin index in Wolfram (blue) and control (green) subjects in white matter. Age is on the x-axis

The mixed linear model analysis results are shown in the table below. Almost all regions show a start age effect, with several showing significant start age X group, time X group, group, and time effects. Most of these effects are in the occipital, temporal, and cingulate regions.

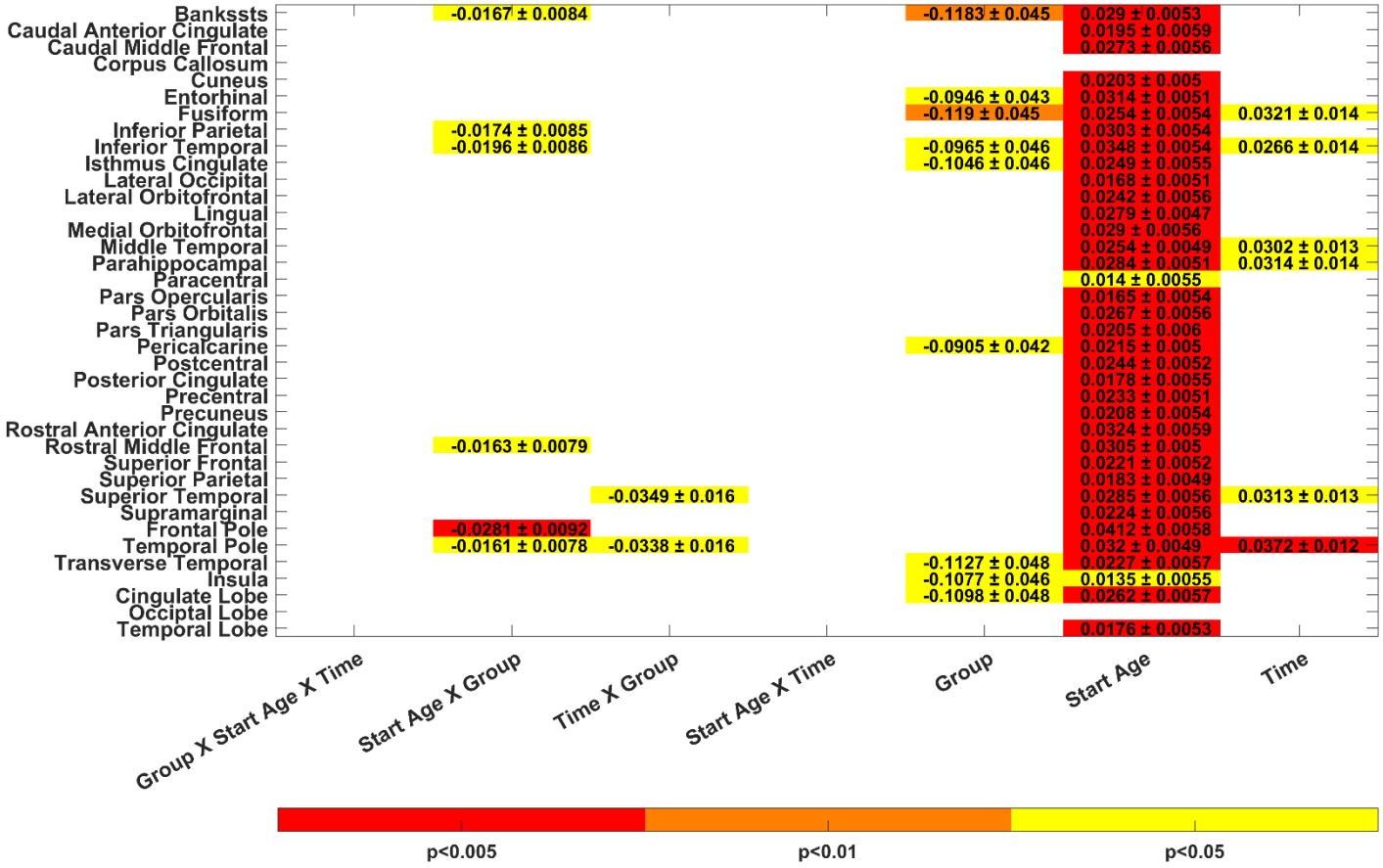

Figure 3.12 Mixed linear model results for white matter regions. Significant (p<0.05) estimate coefficients with SE margins are shown.

3.4 Discussion

Myelin mapping was undertaken to explore whether myelin is affected in the gray matter in Wolfram syndrome, as could be hypothesized from the potential vulnerability of oligodendrocytes. While a handful of studies have utilized this methodology, it has been largely underutilized in the literature. It is certainly not the gold standard for measuring myelin, but is feasible in a study with limited sequences available.

The ribbon analysis performed better than whole region averages of the gray matter. The ribbon approach allows for smaller partial volume error and centers in on the more highly myelinated regions of the cortex which lie deeper, away from the pial surface. This approach could have error if cortical thinning occurs to different degrees between groups being studied.

Overall, few group differences of the myelin index were found in the gray matter. The cortex appears to be largely unaffected, which would be consistent with the limited commentary on the matter when looking at the occipital lobe in a histology study. The significant increase found with age and time is reassuring, as one would expect myelin to increase with age. The significant effect of time suggests that contrary to the tractography analysis within Chapter 2, intrasubject comparisons are robust. A good deal of noise between subjects is still present, suggesting some error may be coming from an imperfect calibration.

The subcortical analysis of regions is also reassuring for the method validity. The brainstem, which had the largest group difference in myelin index, is known to be particularly vulnerable in Wolfram syndrome, showing some of the largest volume differences in the disease. Similarly, it is already known that the cerebellar cortex and cerebellar white matter also show large volumetric group differences. The significant difference in the hippocampus is intriguing with severe cognitive deficits seen in late stages of the disease. It should also be noted that the brainstem differences found here do not correlate with the decreasing volume found in the brainstem during this time, but instead are more reminiscent of the developmental pattern seen in the visual tracts in tractography.

Myelin index was examined in the white matter, which is known to be affected in Wolfram syndrome. As would be consistent with FA in tractography, several significant age X group effects were found, and a general trend of controls showing an increased slope with

respect to age is present. Group differences – without a significant age interaction – were found in the occipital lobe and pericalcarine region, which is also consistent with the lack of age effect in traditional tractography in the visually-associated tracts. However, looking at the raw data does not present the same clear separation in early childhood between groups that is characteristic of the aforementioned pattern. The overall magnitude of differences between the groups, even when not significant, is greater in the white matter than the gray, so that even with the limitations of the metric, myelin in gray matter is likely less compromised than myelin in white matter in Wolfram syndrome.

As with all imaging techniques, noise is a concern. The data was of overall poorer quality and required greater removal of outliers than the tractography data. Fewer clean T2w scans were collected and the sequence was rarely redo, due to its lower priority outside these analyses. However, many subjects displayed low intrasubject noise between time points, allowing for more significant effects with respect to time to be found as compared to traditional tractography, proving its ability to be robust.

While myelin in white matter is substantially and globally affected in Wolfram syndrome, gray matter appears to be spared, at least during childhood and early adulthood when cognitive impairments have rarely begun to be symptomatic. With supportive evidence from the subcortical and cortical white matter regions, it has been shown the myelin mapping can be used to broadly assess the integrity of myelin across the brain and can detect pathological states when more quantitative scanning sequences are not available.

3.5 References

Ganzetti, M., Wenderoth, N., & Mantini, D. (2014). Whole brain myelin mapping using T1- and

T2-weighted MR imaging data. *Frontiers in Human Neuroscience, 8*, 671. https://doi.org/10.3389/fnhum.2014.00671

Glasser, M. F., Sotiropoulos, S. N., Wilson, J. A., Coalson, T. S., Fischl, B., Andersson, J. L., … WU-Minn HCP Consortium, for the W.-M. H. (2013). The minimal preprocessing pipelines for the Human Connectome Project. *NeuroImage, 80*, 105–124. https://doi.org/10.1016/j.neuroimage.2013.04.127

Glasser, M. F., & Van Essen, D. C. (2011). Mapping human cortical areas in vivo based on myelin content as revealed by T1- and T2-weighted MRI. *The Journal of Neuroscience : The Official Journal of the Society for Neuroscience, 31*(32), 11597–11616. https://doi.org/10.1523/JNEUROSCI.2180-11.2011

Heath, F., Hurley, S. A., Johansen-Berg, H., & Sampaio-Baptista, C. (2018, February 1). Advances in noninvasive myelin imaging. *Developmental Neurobiology*, Vol. 78, pp. 136–151. https://doi.org/10.1002/dneu.22552

Lee, K., Cherel, M., Budin, F., Gilmore, J., Zaldarriaga Consing, K., Rasmussen, J., … Styner, M. (2015). Early postnatal myelin content estimate of white matter via T1w/T2w ratio. *Medical Imaging 2015: Biomedical Applications in Molecular, Structural, and Functional Imaging*, *9417*, 94171R. https://doi.org/10.1117/12.2082198

Lugar, H. M., Koller, J. M., Rutlin, J., Eisenstein, S. A., Neyman, O., Narayanan, A., … Hershey, T. (2019). Evidence for altered neurodevelopment and neurodegeneration in Wolfram syndrome using longitudinal morphometry. *Scientific Reports*, *9*(1), 6010. https://doi.org/10.1038/s41598-019-42447-9

Lugar, H. M., Koller, J. M., Rutlin, J., Marshall, B. A., Kanekura, K., Urano, F., … Washington

University Wolfram Syndrome Research Study Group. (2016). Neuroimaging evidence of deficient axon myelination in Wolfram syndrome. *Scientific Reports*, *6*, 21167. https://doi.org/10.1038/srep21167

Rosko, L., Smith, V. N., Yamazaki, R., & Huang, J. K. (2019). Oligodendrocyte Bioenergetics in Health and Disease. *The Neuroscientist*, *25*(4), 334–343. https://doi.org/10.1177/1073858418793077

Timmler, S., & Simons, M. (2019). Grey matter myelination. *GLIA*, *67*(11), 2063–2070. https://doi.org/10.1002/glia.23614

Chapter 4: A Wolfram Mouse Model

4.1 Introduction

Animal models of diseases open doors to experimentation that is impossible to conduct on humans, and allow us to make great strides in the understanding of mechanisms and efficacy of potential treatments. A good animal model for Wolfram syndrome has largely eluded us, though the development of an exon 5 deletion mouse model showed particular promise. We aimed to answer whether the mouse model was an accurate representation of the human neuronal imaging phenotype, to help bridge the knowledge gaps between genetic mutation and clinical presentation.

The mouse was previously shown to develop exhibit reduced volume of the optic nerve, brain stem, and cortex (Cagalinec et al., 2016). The mice showed evidence of ER stress (Cagalinec et al., 2016), a leading hypothesis behind the etiology of the disease presentation of Wolfram syndrome. However, nothing was known about the myelin integrity within the mice brains, and model had not been vetted by the Wolfram research community. Mice with this mutation were known to be small and present with a squinty eyed phenotype which hinted at visual acuity deficits that might be consistent with the human presentation, though other studies did not seen differences in the optic nerve (Delettre et al., 2014).

We began our study with a whole a brain structural and diffusion investigation. Due to the reported optic atrophy in the mouse model and the robustness of the variable in humans with Wolfram syndrome, we then focused on a high-resolution diffusion study of the optic nerve. Further study revealed that the reported squinty eyed phenotype was due to ocular enucleation. This is not a part of the human phenotype and thus presented a significant confound. To minimize the effect of this confound, we proceeded to examine white matter integrity in the rest of the brain prior to the development of enucleation in the mice.

4.2 Methodology

Scanning was conducted in three phases: an initial whole brain phase, optic nerve phase, and a second whole brain phase. The initial two batches consisted of 4 *Wfs1*$^{-/-}$ mice and 5 control mice (*Wfs1*$^{+/-}$ and *Wfs1*$^{+/+}$). Half of the Wolfram mice presented with a squinty eyed phenotype. The second phase consisted of 7 *Wfs1*$^{-/-}$ mice and 6 control mice (*Wfs1*$^{+/-}$ and *Wfs1*$^{+/+}$), scanned at 6 months of age, with eyeballs intact.

All scans were conducted on a 4.7T Agilent DirectDrive (200 MHz) MRI System.

Whole Brain Scanning

Whole brain scanning was conducted using a conventional spin-echo diffusion-weighted sequence with a 25-direction diffusion-encoding scheme and one b=0 image.(Batchelor, Atkinson, Hill, Calamante, & Connelly, 2003) Sequence parameters were TR=300ms, TE=43ms, delay between pulses = 25ms, gradient pulse duration = 5 ms, maximum b-value =2200 s/mm^2, slice thickness = 1.8mm, in-plane resolution of 104 x 104 μm^2.(Lin et al., 2019)

Optic Nerve Scanning

A single high resolution slice was used for the quantification of the optic nerve. It was thus imperative to use a protocol that would ensure that the same slice of the optic nerve would be chosen in each mouse. Five 1 mm midsagittal and coronal slices were taken with a FOV 30 x 30, TR =800, TE=5, target bval =1000, and resolution of 192 x 192. Using these images as

guides, a sagittal field of view was aligned as closely as possible to the true midsagittal plane. The field of view was then rotated 90 degrees to be a coronal view perpendicular to the optic nerve. The single slice was to go through the landmark of where the corpus callosum and third ventricle appear to meet. The conventional spin-echo diffusion-weighted scan was then collected with a FOV of 22.5 x 22.5 mm^2, 0.8 mm thickness, TR = 1500 ms, and maximum b-value= 2441.9.(Lin et al., 2017)

Diffusion Basis Spectrum Imaging (DBSI)

DBSI analysis uses the linear combination of the anisotropic components derived from traditional DTI analysis with an isotropic component that includes the calculation of a hindered, restricted, and water fraction. Details are presented in Chapter 2. The mouse imaging data was processed using a DBSI processing package from Song et al. to generate FA, RD, and AD maps, along with fraction maps for fiber (anisotropic) (FF), restricted (RF), hindered (HF), and water (WF) components.

The white matter of each mouse was individually segmented using the b0 images. The white matter consisted of just an ROI of the optic nerve for the optic nerve specific imaging. The whole brain images were segmented into the following regions: corpus callosum (medial), corpus callosum (lateral), optic tract, internal capsule, external capsule, cerebral peduncle, fimbria, arbor vitae, middle cerebellar peduncle, and medullar white matter. Whole brain regions were filtered with an FA threshold > 0.4. Averages of the FA, RD, AD, FF, RF, HF, and WF were found for each region and student's t-tests were used to assess statistical significance.

4.3 Results

The *Wfs1*$^{-/-}$ and control mice were housed together. However, the groups of mice could be distinguished from a distance. The *Wfs1*$^{-/-}$ mice were significantly smaller than the control mice (Batch 2: *Wfs1*$^{-/-}$: 17.4 ± 3.02 g, controls: 25.25 ± 2.63g, p = 0.0023). Their back showed distinct kyphosis. Younger Wfs1$^{-/-}$ mice showed exophthalmos, while older mice appeared to have squinty eyes. The Wfs1$^{-/-}$ mice also had a significantly smaller brain, though this decreased pertains to the entire brain and is not regionally specific.

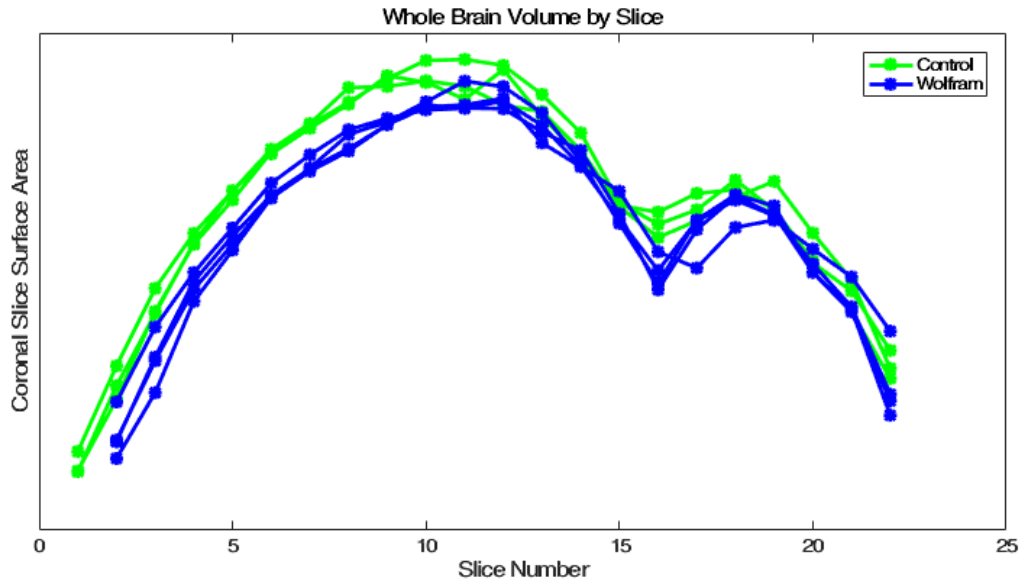

Figure 4.1: Whole brain volume by slice. Wfs1$^{-/-}$ *mice have a consistently smaller brain throughout all regions.*

Optic Nerve

The optic nerves of the Wolfram mice were significantly smaller (Figure 4.2C). The effect is so drastic that many of the mice can be easily distinguished by this feature alone (Figure 2.XA-B, optic nerves highlighted with a red box).

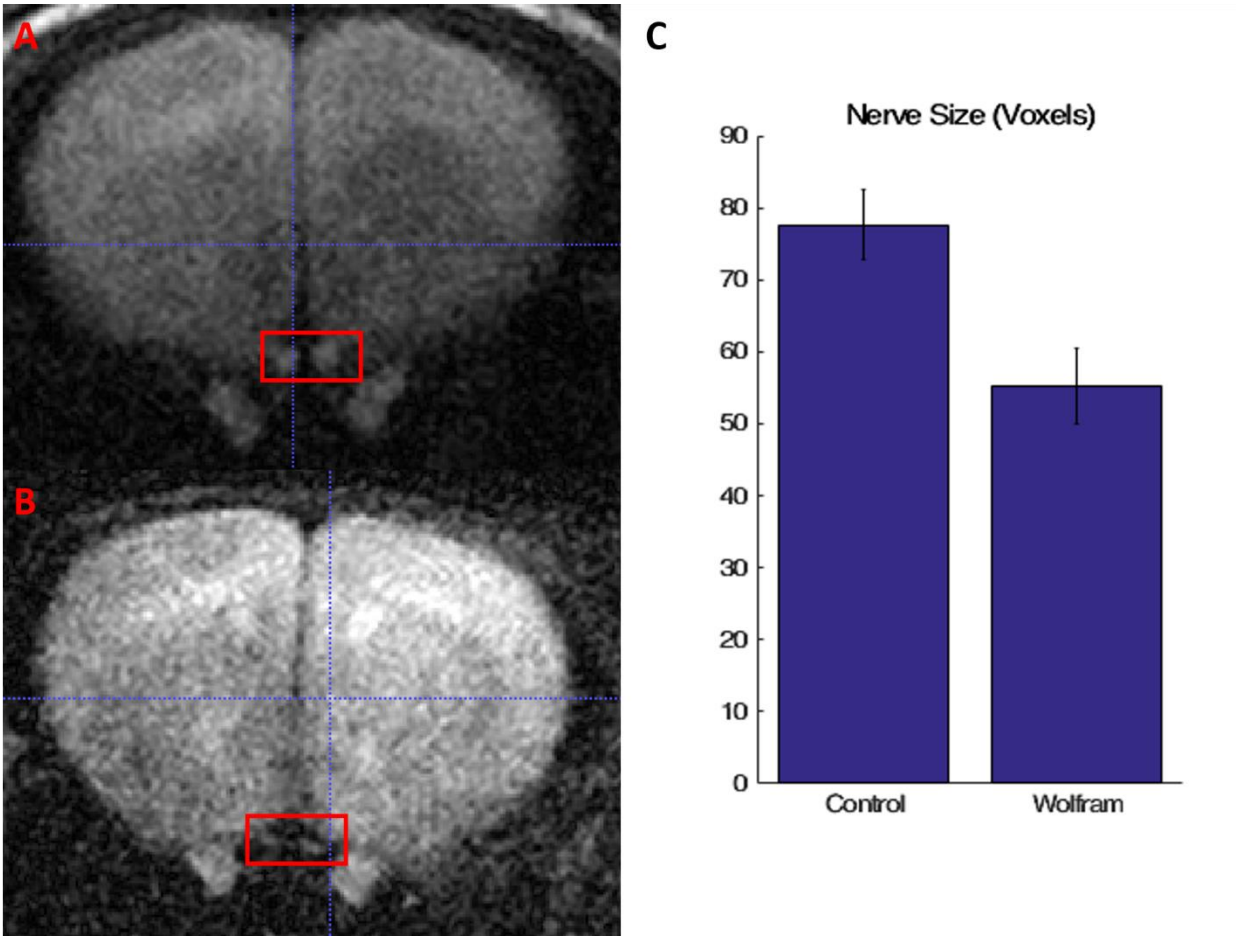

Figure 4.2 Optic nerve size in Wfs1$^{-/-}$ mice. A) Optic nerve in a control mouse. B) Optic Nerve in a Wfs1$^{-/-}$ mouse *C) Comparison of cross-sectional area in optic nerve. P<0.05.*

The anisotropic metrics of FA, RD, and AD along with the isotropic metric of FF were evaluated in the optic nerves of the two groups (Figure 4.3). The Wolfram mice has a significantly lower FF than the control mice. While not significant, the Wolfram mice had a decreased FA and AD along with an increased RD, which would be consistent with demyelination.

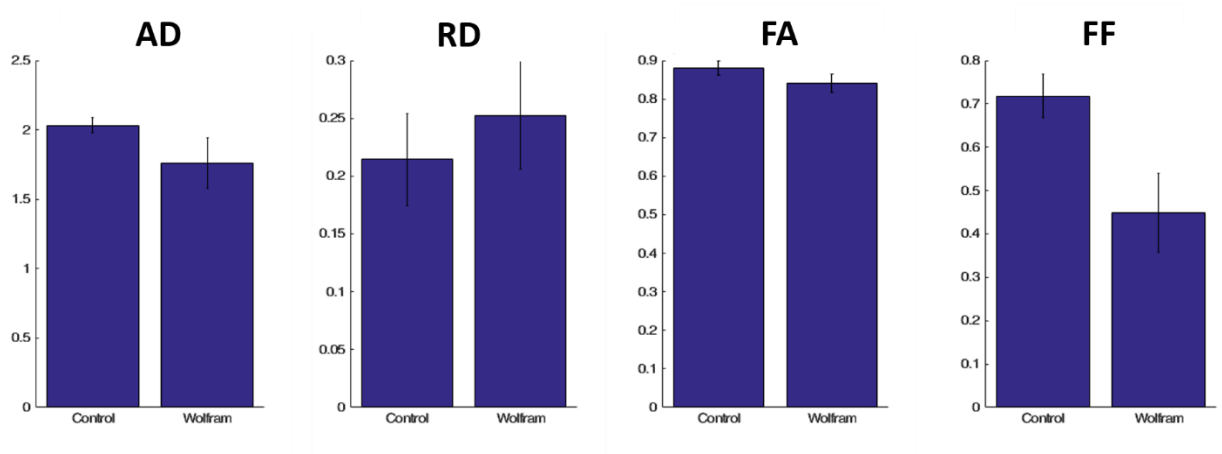

Figure 4.15 Myelin integrity metrics in the optic nerves. Fiber fraction is significantly smaller in the Wolfram mice

Representative examples of the anisotropic maps in a Wolfram and control mouse are shown below. A Wolfram mouse with a relatively large optic nerve was chosen here. The AD and RD of the Wolfram mouse are patchier, showing a greater variance. The extreme highs in the AD and lows of the RD in the Wolfram mouse appear mostly in the periphery vs centrum of the nerve.

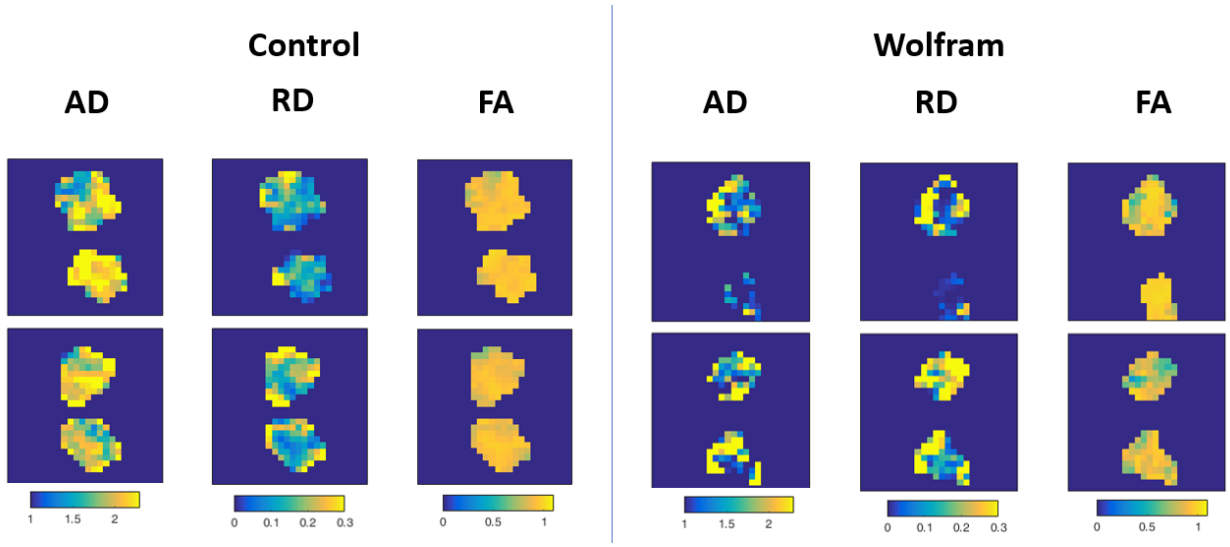

Figure 4.4 Topographic distribution of myelin integrity metrics in an example Wolfram and control optic nerve

Whole Brain

Averages for anisotropic and isotropic metrics were found in a collection of white matter regions within the mouse brains, shown in Figure 4.5 and 4.6 below. After multiple comparison correction, no differences were found to be significant. Without accounting for multiple comparisons, the optic tract showed decreased AD and FA, and increased RD in Wolfram mice as compared to controls. The RD in the external capsule trended toward an increase in Wolfram. The corpus callosum appeared to trend in the opposite direction, with a potential increase in RD in Wolfram. FF shows remarkably little difference between the two groups. The Wolfram group trends toward an increase of RF in the optic tract and trends toward an increase in HR in the middle cerebellar peduncle in the Wolfram group, though potential trends go in either direction across the brain in the HR.

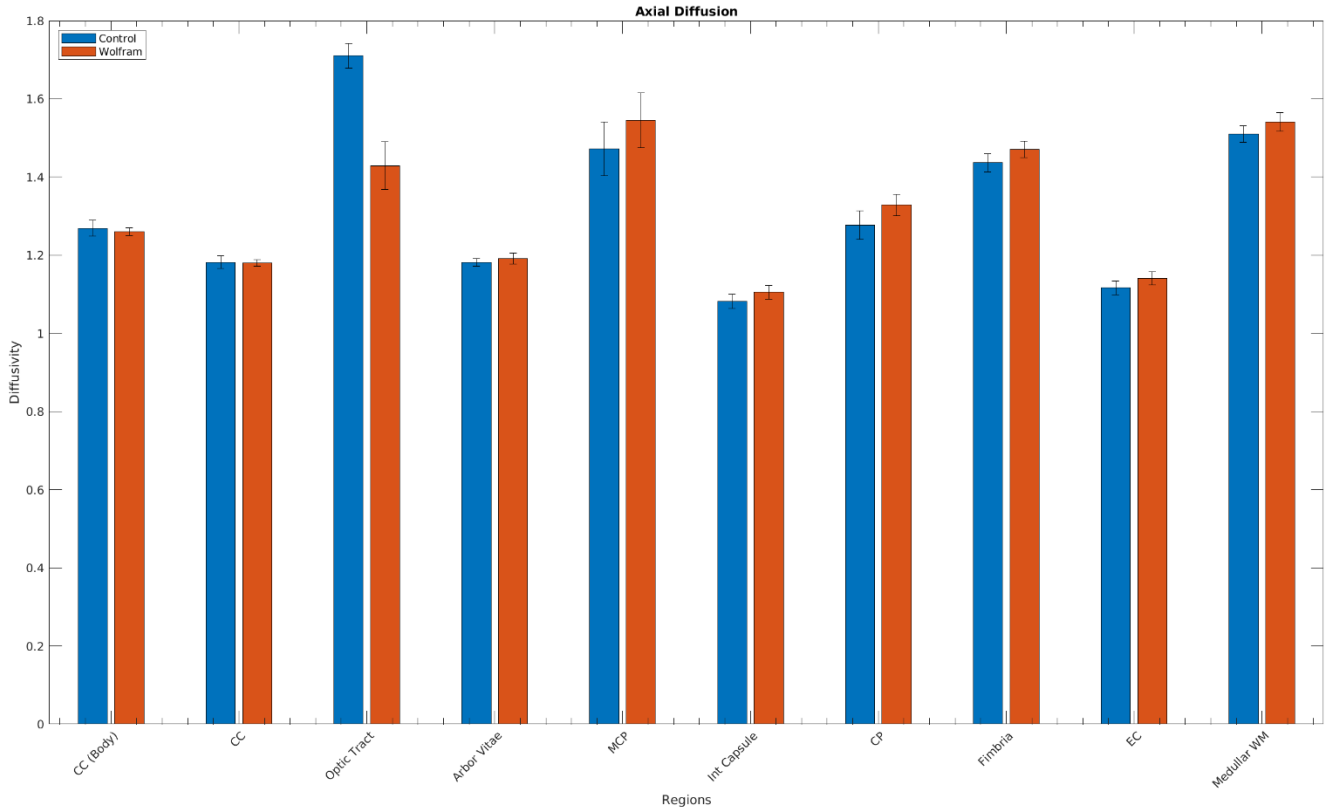
Axial Diffusion
Control
Wolfram
Diffusivity
1.8
1.6
1.4
1.2
1
0.8
0.6
0.4
0.2
0
CC (Body)
CC
Optic Tract
Arbor Vitae
MCP
Int Capsule
CP
Fimbria
EC
Medullar WM
Regions

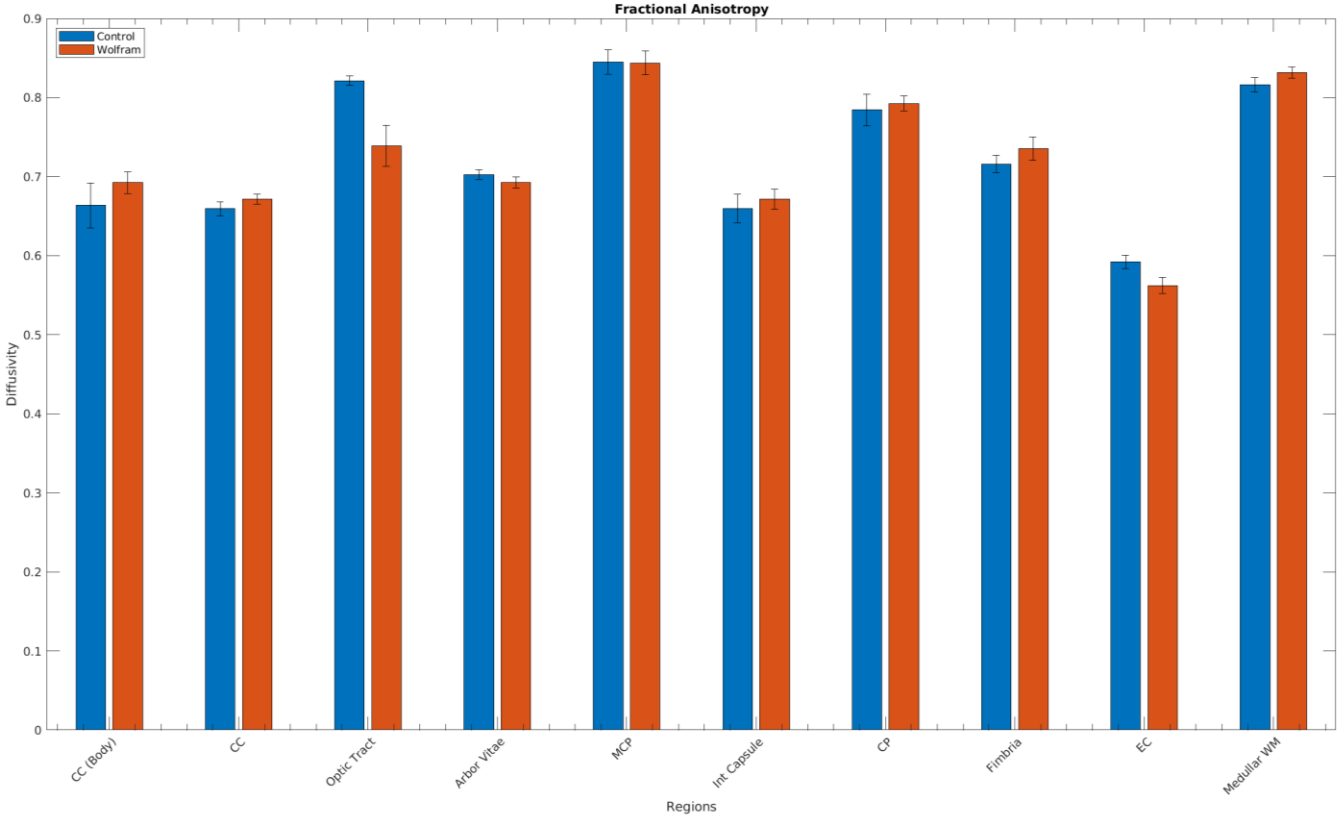
Fractional Anisotropy
Control
Wolfram
Diffusivity
0.9
0.8
0.7
0.6
0.5
0.4
0.3
0.2
0.1
0
CC (Body)
CC
Optic Tract
Arbor Vitae
MCP
Int Capsule
CP
Fimbria
EC
Medullar WM
Regions

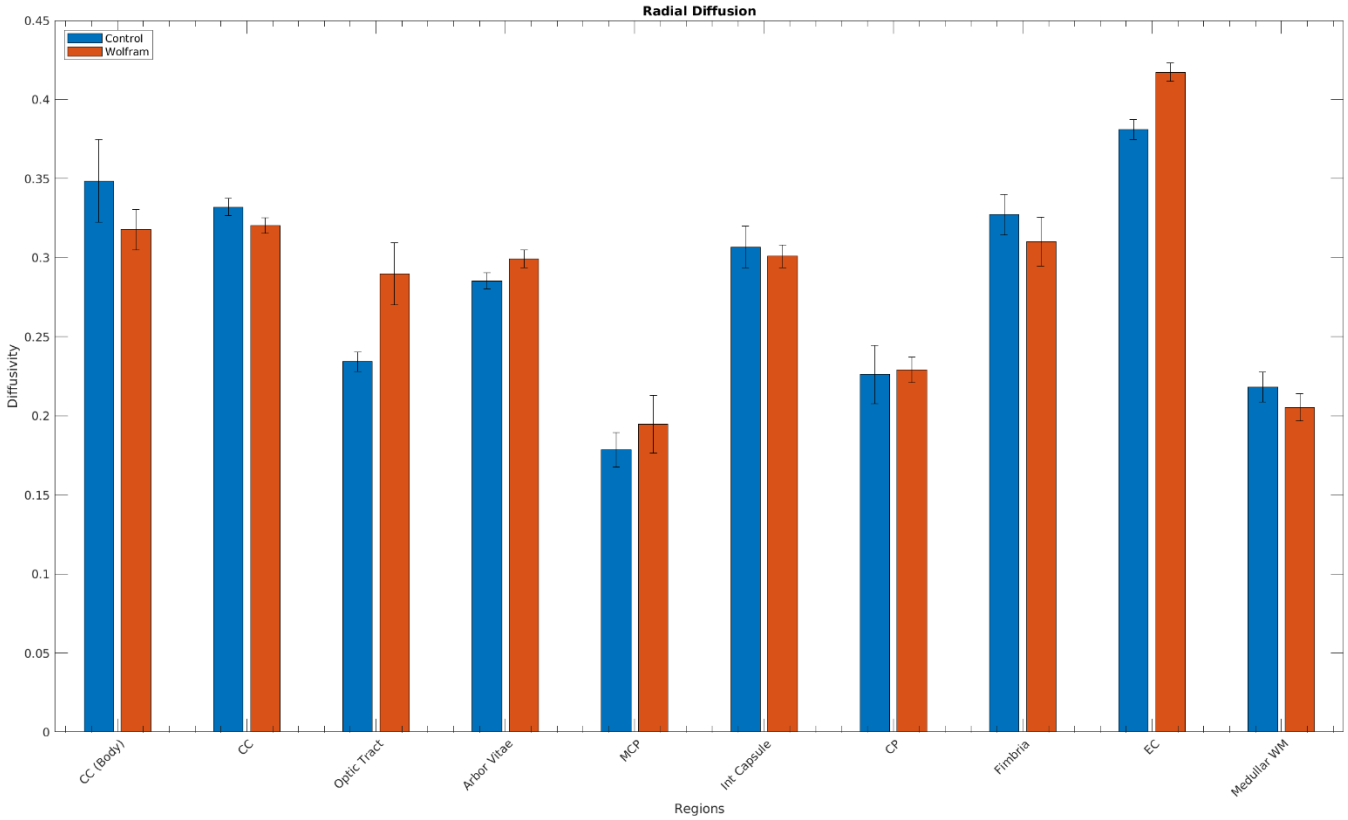

Figure 4.5 Anisotropic integrity metrics across a selection of white matter tracts

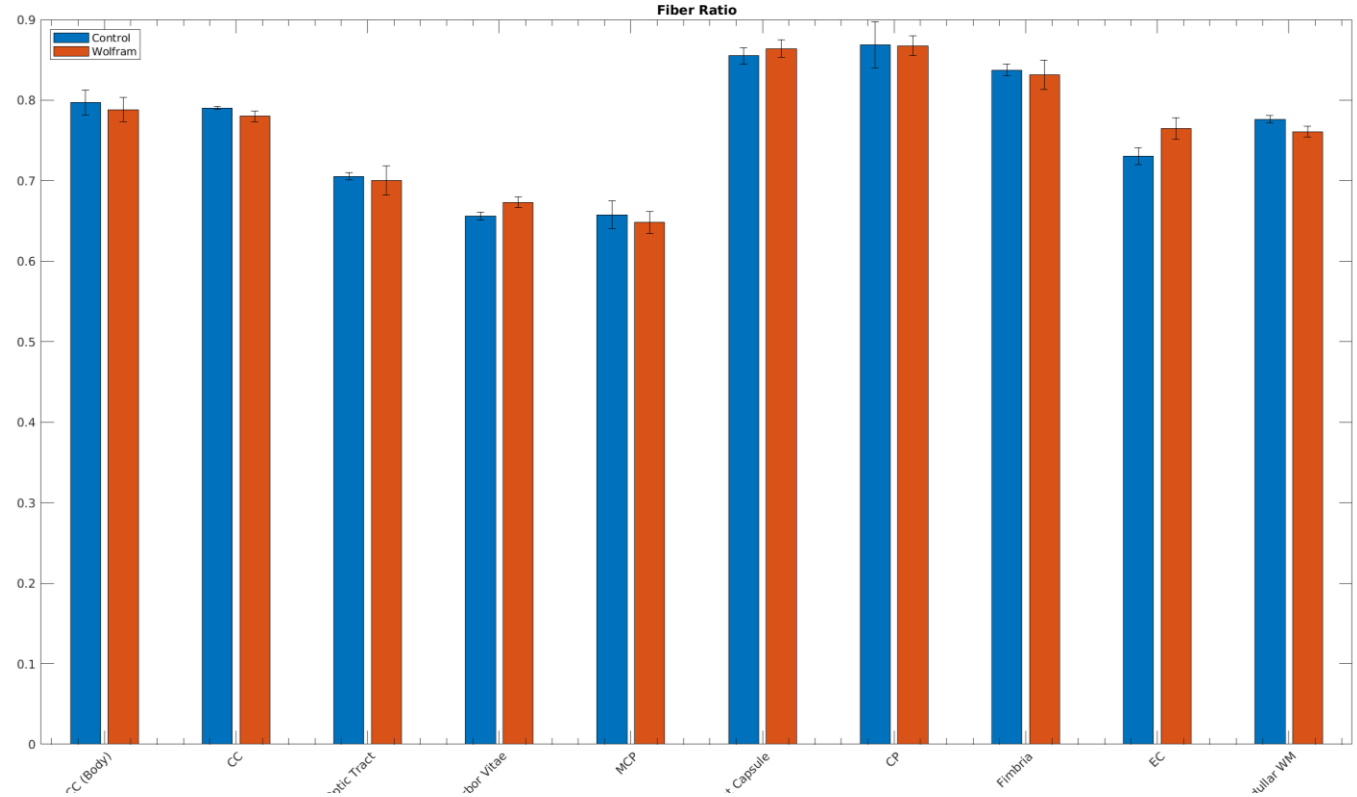
Fiber Ratio
Control
Wolfram
0.9
0.8
0.7
0.6
0.5
0.4
0.3
0.2
0.1
0
CC
CP
Fimbria
EC

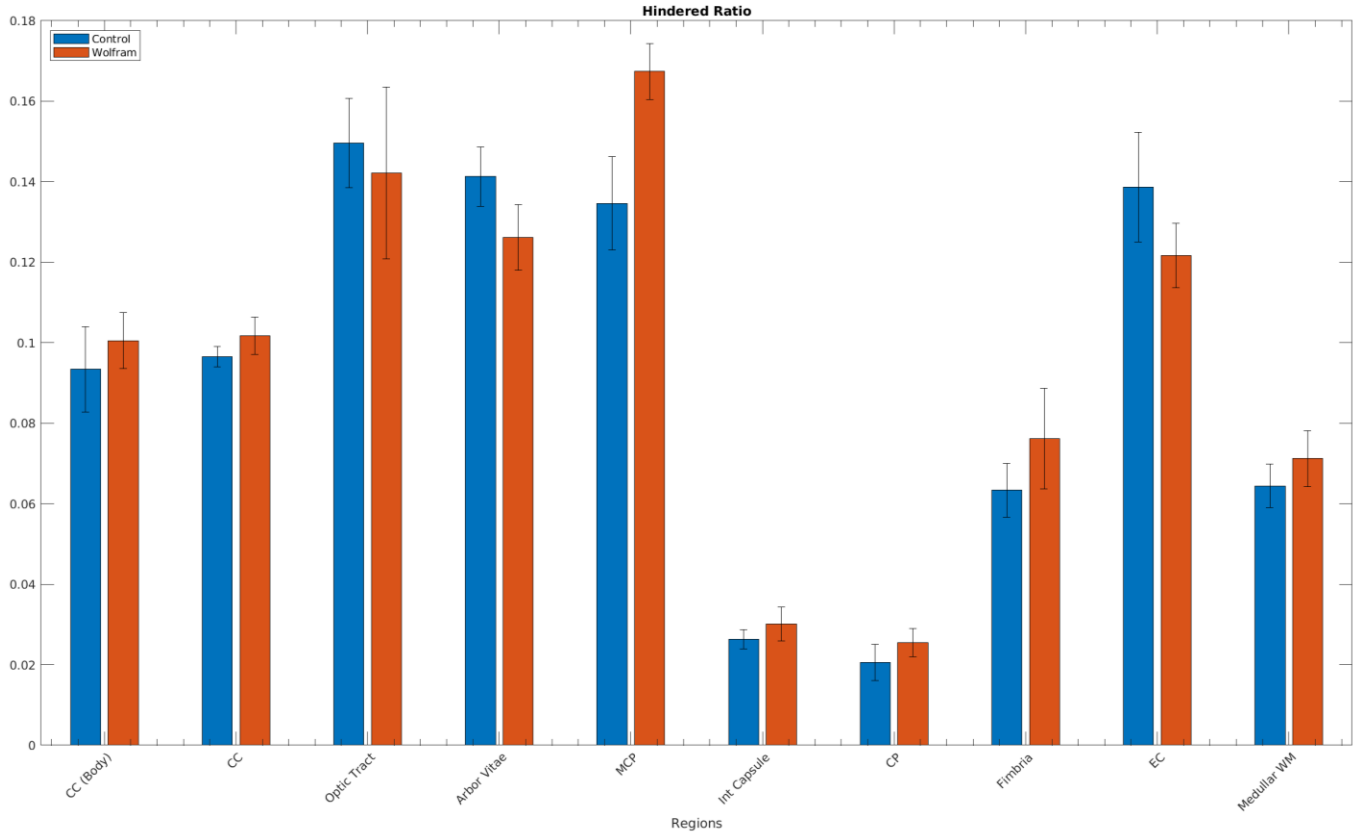
Hindered Ratio
Control
Wolfram
0.18
0.16
0.14
0.12
0.1
0.08
0.06
0.04
0.02
0
CC (Body)
CC
Optic Tract
Arbor Vitae
MCP
Int Capsule
CP
Fimbria
EC
Medullar WM
Regions

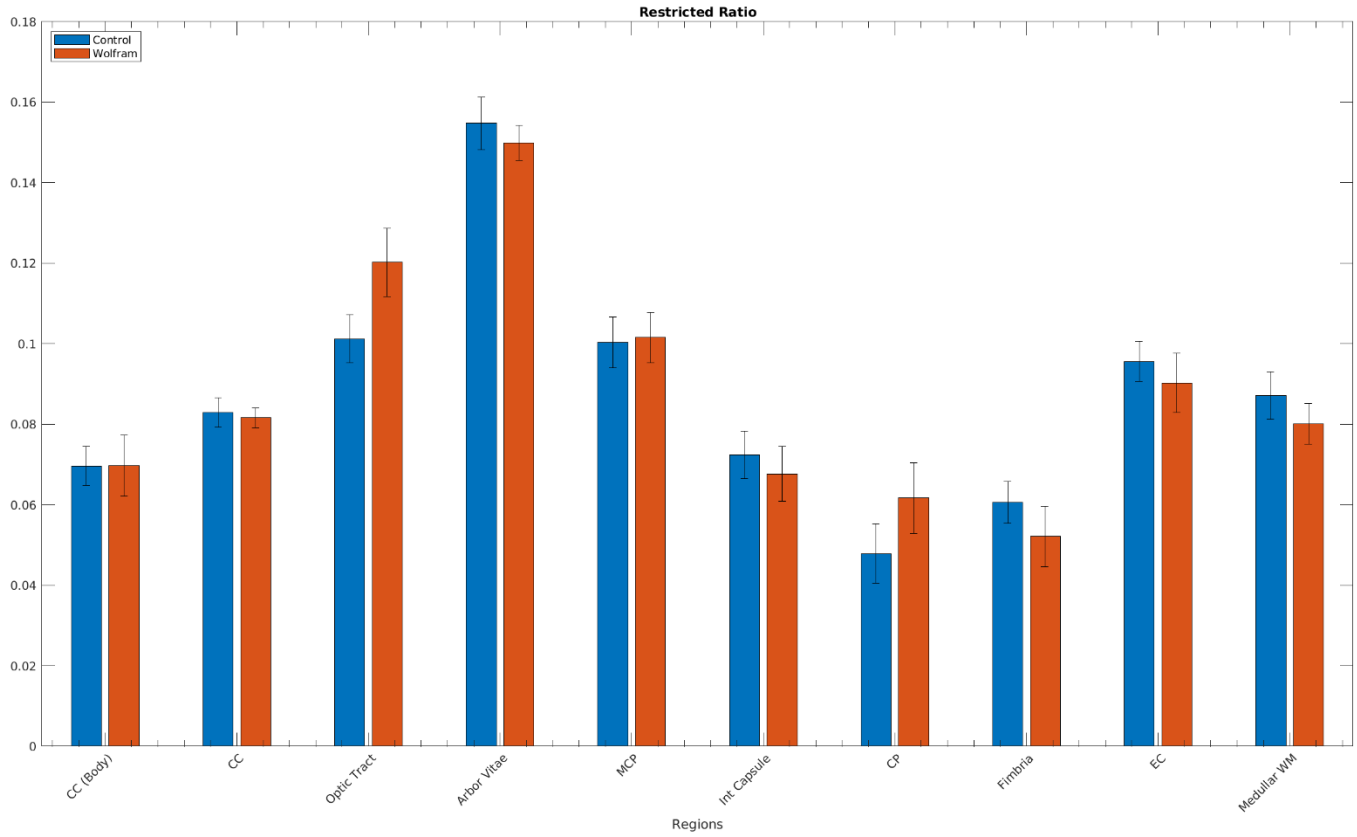

Figure 4.6 Distribution of component fractions across a selection of white matter tracts across the brain

4.4 Discussion

The primary goal of the Wolfram mouse imaging experiments was to examine how congruous the mouse model was to the human phenotype. When we first acquired this model mouse, very little was known about the neural phenotype. We were initially interested in the optic nerve, as measurements pertaining to myelin metrics and vision are most robust in humans, with all of our patients experiencing some level of optic atrophy and most of them showing a decline in vision over the human study period. Initial experiments on the mouse vision also seemed promising, and our own optic nerve data initially appeared to support the use of the model. Several of the mice showed grossly smaller nerves and correspondent myelin metrics, namely, decreased FA and AD and increased RD.

On closer examination, it was realized that the squinty eye phenotype was the result of burst eyeballs. The mice were experiencing progressively higher intraocular pressure, as evidenced by the exophthalmos in the younger mice, until the eyeballs were no longer present. This is a major confounding variable for the study of the optic nerve and entire visual system. Upon closer examination of the data, the significant results of the imaging and size of the optic nerve data were driven by the two mice that presented with the squinty eye phenotype. The lack of visual stimulus caused, if at least contributed, to the severe atrophy of the optic nerve. This difference can be seen when comparing the optic nerves shown in Figures 2 and 4, where the former mouse has become enucleated while the latter still has its eyeballs. This confound is problematic when there is no evidence of enucleation or even increased ocular pressure in the human phenotype.

With the optic nerve eliminated as a valid mediator between the human and mouse phenotype, we proceeded to acquire a second group of mice which were studied at 6 months of age, prior to enucleation. We also expanded our study to the rest of the white matter in mouse brain. Unlike in the human, where differences in myelin integrity are apparent throughout most of the brain, differences in the mice did not reach true statistical significance. It is of note that the largest differences – like in the humans – were seen in the optic tract. However, due to the increased intraocular pressure, one cannot deduce whether this is caused by the same mechanism as in the human. Furthermore, differences in the myelin integrity appear to be driven by AD, the metric of axonal damage, unlike the RD, the metric of demyelination, as in humans. The fiber fraction is remarkably similar across all regions, suggesting myelin is less vulnerable in this model than in humans. It is possible that the sample size is too small to find significant differences, especially for areas outside of the visual tract, as those differences are of smaller

magnitude in humans. The mice may also be too young. Differences in humans outside the visual system were not present in early childhood. We chose to use younger mice in order to minimize the impact of the ocular pressure, and while six month old mice are adult, the trajectory of the disease may follow a delayed timeline in the mice.

The restricted fraction was somewhat increased in the optic tracts and cerebral peduncles in the Wolfram mice. This is completely inconsistent with humans which show an increase of the restricted fraction across the brain in healthy controls and one that increases with age. The mechanism behind this in humans remains a conundrum, but unfortunately histology of this model would not provide a possible explanation.

Overall, the exon 5 deletion Wolfram mouse model is not a sufficiently good model of the neuronal phenotype of Wolfram syndrome. Volume differences are not specific to the regions that are seen to be smaller in humans. Some differences in the myelin metrics of the optic tracts are irrelevant on the background of mouse ocular enucleation, and there is no evidence to suggest that one could learn more about the etiology of the differences in the restricted fraction that are present in humans. The use of this model with respect to Wolfram syndrome should be restricted to metabolic concerns outside the brain.

4.5 References

Batchelor, P. G., Atkinson, D., Hill, D. L. G., Calamante, F., & Connelly, A. (2003). Anisotropic noise propagation in diffusion tensor MRI sampling schemes. *Magnetic Resonance in Medicine*, *49*(6), 1143–1151. https://doi.org/10.1002/mrm.10491

Cagalinec, M., Liiv, M., Hodurova, Z., Hickey, M. A., Vaarmann, A., Mandel, M., … Kaasik, A.

(2016). Role of Mitochondrial Dynamics in Neuronal Development: Mechanism for Wolfram Syndrome. *PLoS Biology*, *14*(7). https://doi.org/10.1371/journal.pbio.1002511

Delettre, C., Hamel, C. P., Koks, S., Seveno, M., Lenaers, G., & Wersinger, D. M. B. (2014). Visual phenotyping of Wfs1 mutant mice, models of Wolfram syndrome neuronal and diabetic symptoms. *Investigative Ophthalmology & Visual Science*, *55*(13), 6177–6177.

Lin, T.-H., Chiang, C.-W., Perez-Torres, C. J., Sun, P., Wallendorf, M., Tsen-Hsuan Lin, A., … Song, S.-K. (2017). Diffusion MRI quantifies early axonal loss in the presence of nerve swelling Recommended Citation Diffusion MRI quantifies early axonal loss in the presence of nerve swelling. *Journal of Neuroinflammation*, *14*. https://doi.org/10.1186/s12974-017-0852-3

Lin, T.-H., Sun, P., Hallman, M., Hwang, F. C., Wallendorf, M., Ray, W. Z., … Song, S.-K. (2019). Noninvasive Quantification of Axonal Loss in the Presence of Tissue Swelling in Traumatic Spinal Cord Injury Mice. *Journal of Neurotrauma*, *36*(15), 2308–2315. https://doi.org/10.1089/neu.2018.6016

Chapter 5: Conclusion

5.1 Summary of Results and Commentary

Wolfram syndrome is a complex, rare neurodegenerative disease with significant white matter involvement. In this work, we have explored when these white matter deficits develop and how they progress with time. We have shown that the divergence from normal development falls broadly into two patterns. One pattern applies to white matter tracts related to the visual system. From the earliest ages studied, these tracts in the patients with Wolfram already have lower levels of myelination as compared to controls. Despite the initial lower levels of myelin, the tracts appear to myelinate at the same rate as healthy controls. That the difference in myelin integrity is already visible in early childhood suggests that these tracts may have never myelinated correctly. The average magnitude of the difference in FA between the Wolfram and control groups is also notable as being particularly large. The effect is not subtle, even in a small sample size, underscoring the severity of the deficits. The second pattern appears to be present throughout most of the rest of the white matter tracts in the brain, where a divergence in myelin development is not seen until the adolescence, with lower levels of myelination seen in the brains with Wolfram. This may be caused by either a slowing of the myelination process, degradation of myelin, or a combination of the two.

The two patterns suggest that Wolfram syndrome has aspects of both of a neurodegenerative and neurodevelopmental disorder. It can be hypothesized that the tracts following the first pattern, with the large deficits from the earliest of ages, were never myelinated to the expected level. A potential explanation of this could be the phenomenon that the proliferation of oligodendrocyte precursor cells depends on the electrical activity in axons (Barres & Raff, n.d.), so for an instance delayed eye opening will delay myelination of the optic nerve. It is known that the retinal nerve fiber layer in Wolfram is exceptionally thin from the

earliest ages we have examined (Hoekel et al., 2018), and decreased levels of myelination could be a downstream effect. Pattern two on the other hand suggests a neurodegenerative component. It is particularly interesting that the myelination trajectory of the patients with Wolfram falls off in adolescence. Though the specific role of *WFS1* in oligodendrocytes is still unknown, we have examined *WFS1* gene expression in across different developmental age spans in healthy brains using BrainSpan Atlas of the Developing Human Brain (Samara et al., 2019). This has shown us that *WFS1* expression is greatest during late childhood-early adulthood (8-15 years of age), the second half of which correlates with the split in trajectories.

Due to the vulnerability of myelin in white matters in Wolfram, we also explored whether myelin in gray matter may be similarly affected. In the cortical gray matter, a couple regions showed a significant group X time interaction, in the temporal and parahippocampal areas. Larger effects were seen in subcortical regions, particularly in the cerebellum and brainstem. The methodology used for estimating myelin is not the gold standard of the field, but was the only modality available for this dataset. Correlations between the myelin index and FA in the white matter tracts were high, lending credence to the method, though analyzing the white matter tracts through the myelin index underreports the differences between the groups. It is thus possible that the myelin in gray matter in Wolfram syndrome is affected, but to a lesser degree as well as only being affected later in the disease progression.

Correlations between lesions and symptom presentation are always of interest. As in many other conditions, the correlations between pathology and expected effect were minimal. It would have been expected that deficits in microstructure of the optic radiations and ILF would correlate to visual acuity or that deficits in the acoustic radiations would correlate to auditory acuity, but this did not appear to be the case. This is not particularly surprising when one takes

into account the lack of change in, for example, FA in the optic radiations over age, even though most of the Wolfram patients experienced annual worsening visual acuity over this same time period. Instead, examining FA and FF averages over the entire white matter skeleton were more reliable indicators of disease severity. It might thus be suggested that white matter metrics can use used a general biomarkers to judge the severity of neurodegeneration. However, noise in the data precludes this biomarker from being a reliable choice for a drug efficacy trial. Furthermore, the lack of relationship between myelin integrity neuroimaging metrics in particular tracts and changes in the symptoms of the patient suggests that the myelin deficits are not driving the symptoms themselves.

Animal models are frequently used in science as a bridge between studying a disease on a cellular level and studying a disease in a living human. We had hoped the newest Wolfram mouse model would be a tool to better elucidate the changes in the brain caused by the disease and to this end we tested whether the same differences in white matter tracts would also be seen in the mouse model. Little evidence outside the visual tracts were found, and this effect was confounded with the previously unknown symptom of globe rupture.

5.2 Future Directions

Many questions still remain unanswered with respect to the role of myelin in Wolfram syndrome. As with any longitudinal imaging study, the sequences used to collect this data are dated. The current DTI imaging standard uses over three times as many directions, which would certainly improve the quality of the data. Such improvements would hopefully decrease the intrasubject variance and allow for a better estimate of the progression of the disease in the white matter tracts. Due to the noise in the present set, conclusions were limited to comparisons

between ages rather than actual analysis over time. This distinction is particularly important in Wolfram syndrome due to the heterogenous presentation of disease. While age does loosely correlate with disease severity, it is not uncommon to see older patients with milder symptoms or younger patients with more severe ones.

Myelin mapping was the only available modality to probe the integrity of myelin outside the white matter tracts, and while a promising relationship between myelin mapping and standard DTI metrics has been shown here, more precise modalities are available. Studying myelin water fraction through advanced analysis – such as with a Bayesian application – of mcDESPOT generated signals could better distinguish group differences (Bouhrara & Spencer, 2016). While it too is a surrogate marker for myelin, as it measures the water between layers of myelin, it is still a more direct measure than myelin mapping.

In this work, we tested the newest, most promising animal model available – an exon 5 knock out mouse model. This model has shown itself to be unsatisfactory for studying the neurophenotype of Wolfram syndrome. Recently, a newer animal has been developed – an exon 5 knockout in a rat (Plaas et al., 2017). The rat appears to have many of the expected symptoms, including reduced beta cell mass, ER stress in the pancreas, cataracts, retinal gliosis, ER stress in the retina, optic atrophy, and reduced medullary volume. Importantly, there does not appear to be increased intraocular pressure or any evidence of global rupture. It would thus be important to examine if the mouse also presents other aspects of the neurological phenotype such as ataxia and dysphagia, as well as showing similar temporal and topographic patterns of myelin deficiencies and differences in volumes of regions such as the cerebellum and thalamus. Current literature suggests the model may only encompass the neurodegenerative aspects of disease, without the neurodevelopment components (Toots et al., 2018). Nevertheless, there is potential

for the study of the progression of neurodegeneration in Wolfram syndrome on a cellular level. A strong disease model also allows for research into potential treatments, and indeed, studies on the efficacy of liraglutide are currently being conducted (Seppa et al., 2019; Toots et al., 2018). Whether this or any other treatment translates to humans remains to be seen.

Another promising avenue of research is through the use of human induced pluripotent stem cells (hiPSCs) and oligodendrocytes derived from them. The methodology was applied in Pelizaues-Merzbacher, a disease that faces many of the same challenges as Wolfram syndrome with respect to research. It is also a rare, genetic disease where myelin has been implicated, caused by single gene but by hundreds different mutations. Nevin et al. were able to use hiPSC-derived oligodendrocytes from several individuals with different mutations to identify individual and shared defects in mRNA expression, oligodendrocyte progenitor development, oligodendrocyte morphology, and oligodendrocyte capacity for myelination. This in turn led to the classification of presentations of the disease into sub-groups (Nevin et al., 2017). A similar approach could likely be applied to Wolfram syndrome.

5.3 Concluding Thoughts

This work has greatly advanced the field's understanding of how and where Wolfram syndrome impacts myelin, particularly highlighting the variability of myelin vulnerability across regions. These findings are crucial for the betterment of our understanding of this severe disease and will facilitate the identification of therapeutic targets and biomarkers to evaluate the efficacy of potential treatments.

5.4 References

Barres, B. A., & Raff, M. C. (n.d.). Proliferation of oligodendrocyte precursor cells depends on electrical activity in axons. In *J. l. J. Phys,a/ .. Land* (Vol. 25). University of Chicago Press.

Bouhrara, M., & Spencer, R. G. (2016). Improved determination of the myelin water fraction in human brain using magnetic resonance imaging through Bayesian analysis of mcDESPOT. *NeuroImage*, *127*, 456–471. https://doi.org/10.1016/j.neuroimage.2015.10.034

Hoekel, J., Narayanan, A., Rutlin, J., Lugar, H., Al-Lozi, A., Hershey, T., & Tychsen, L. (2018). Visual pathway function and structure in Wolfram syndrome: Patient age, variation and progression. *BMJ Open Ophthalmology*, *3*(1). https://doi.org/10.1136/bmjophth-2017-000081

Nevin, Z. S., Factor, D. C., Karl, R. T., Douvaras, P., Laukka, J., Windrem, M. S., … Tesar, P. J. (2017). Modeling the Mutational and Phenotypic Landscapes of Pelizaeus-Merzbacher Disease with Human iPSC-Derived Oligodendrocytes. *American Journal of Human Genetics*, *100*(4), 617–634. https://doi.org/10.1016/j.ajhg.2017.03.005

Plaas, M., Seppa, K., Reimets, R., Jagomäe, T., Toots, M., Koppel, T., … Vasar, E. (2017). Wfs1-deficient rats develop primary symptoms of Wolfram syndrome: Insulin-dependent diabetes, optic nerve atrophy and medullary degeneration. *Scientific Reports*, *7*(1). https://doi.org/10.1038/s41598-017-09392-x

Samara, A., Rahn, R., Neyman, O., Park, K. Y., Samara, A., Marshall, B., … Hershey, T. (2019, December 3). Developmental hypomyelination in Wolfram syndrome: New insights from neuroimaging and gene expression analyses. *Orphanet Journal of Rare Diseases*, Vol. 14. https://doi.org/10.1186/s13023-019-1260-9

Seppa, K., Toots, M., Reimets, R., Jagomäe, T., Koppel, T., Pallase, M., … Plaas, M. (2019). GLP-1 receptor agonist liraglutide has a neuroprotective effect on an aged rat model of Wolfram syndrome. *Scientific Reports*, *9*(1), 1–13. https://doi.org/10.1038/s41598-019-52295-2

Toots, M., Seppa, K., Jagomäe, T., Koppel, T., Pallase, M., Heinla, I., … Vasar, E. (2018). Preventive treatment with liraglutide protects against development of glucose intolerance in a rat model of Wolfram syndrome. *Scientific Reports*, *8*(1), 1–10. https://doi.org/10.1038/s41598-018-28314-z